2-A

07461-51-T

THE UNIVERSITY OF MICHIGAN

COLLEGE OF ENGINEERING
DEPARTMENT OF MECHANICAL ENGINEERING
HEAT TRANSFER LABORATORY

Technical Report No. 7

Incipient and Steady Boiling of Liquid Nitrogen and Liquid Hydrogen Under Reduced Gravity

HERMAN MERTE, JR.

Under contract with:

National Aeronautics and Space Administration
George C. Marshall Space Flight Center
Contract No. NAS-8-20228
Huntsville, Alabama

Administered through:

November 1970

OFFICE OF RESEARCH ADMINISTRATION - ANN ARBOR

THE UNIVERSITY OF MICHIGAN

COLLEGE OF ENGINEERING
Department of Mechanical Engineering

Technical Report No. 7

INCIPIENT AND STEADY BOILING OF LIQUID NITROGEN AND LIQUID HYDROGEN UNDER REDUCED GRAVITY

Herman Merte, Jr.

ORA Project 07461

under contract with:

NATIONAL AERONAUTICS AND SPACE ADMINISTRATION
GEORGE C. MARSHALL SPACE FLIGHT CENTER
CONTRACT NO. NAS-8-20228
HUNTSVILLE, ALABAMA

administered through:

OFFICE OF RESEARCH ADMINISTRATION ANN ARBOR

November 1970

TABLE OF CONTENTS

LIST OF TABLES

LIST OF FIGURES

LIST OF FIGURES (Continued)

LIST OF FIGURES (Continued)

LIST OF FIGURES (Concluded)

NOMENCLATURE

English Letters

a = acceleration, or thermal diffusivity

A = area

A_o = constant

C_P = specific heat

g = acceleration due to earth gravity

h = enthalpy, or heat transfer coefficient

m = mass, or constant

n = index

Nu = Nusselt number

q/A = heat flux

R = electrical resistance

R_a^1 = modified Rayleigh number

t = time

T = temperature

ΔT_{sat} = $T_{surface} - T_{saturation}$ = heater surface superheat

ΔT_{max} = maximum heater surface superheat

ΔT_{ss} = steady state heater surface superheat (= ΔT_{sat})

V = Volume

Greek Letters

α = defined by Eq. (4)

β = defined by Eq. (4)

Greek Letters (Concluded)

δ = defined by Eq. (4)

ρ = density

τ = delay times—defined locally

ABSTRACT

This report presents the recent results of incipient and steady boiling of cryogenic liquids, both LN_2 and LH_2, under reduced gravity conditions. The parameters varied included the fluid used, heater surface temperature, geometry, orientation, and a/g.

Reduced gravity was obtained with a drop tower designed for liquid hydrogen applications which has 32 ft free fall distance, giving 1.34 sec of free fall. A transient calorimeter technique was used with a variety of geometries. This technique provides results readily in all of the boiling regimes.

Results are presented for a 1 in. dia sphere in LH_2 at a/g = 1 and a/g = 0, which are similar in character to the results obtained earlier with LN_2.

The results for a 2-1/4 in. dia sphere in both LN_2 and LH_2 at a/g = 1 are presented, to ascertain the effect of size. The only difference between the 1 in. dia and 2-1/4 in. dia spheres appears to be in the $(q/A)_{min}$ and transition regions.

The transient calorimeter technique was adapted to flat surfaces to determine the influence of geometry and orientation on boiling of LN_2 and LH_2 at a/g = 1 and reduced gravities. A vertical cylinder was used to simulate a vertical flat plate at a/g = 1. A 3 in. dia disc, of which the center 1 in. square section constituted the measuring section, was used to determine the influence of orientation in LN_2 at a/g = 1 and a/g = 0. It was observed that in nucleate boiling, for a given ΔT_{sat}, the heat flux is greater for the horizontal down orientation, less for the horizontal up, with the vertical orientation heat flux in between. In reduced gravity the geometry becomes influential in the way in which the liquid momentum is retained during the short time "zero" g. This indicates the importance of long time reduced gravity tests in determining the true nature of "zero" gravity boiling heat transfer. Tests with the disc in liquid hydrogen were conducted only at a/g = 1, and the results were qualitatively similar to those with LN_2.

The results of incipient boiling of LN_2 on polished aluminum at a/g = 1 are presented, along with incipient boiling of LH_2 on a fiber glass surface similar to that used in the LH_2 tank of the Saturn S-IVB. These supplement data for incipient boiling on stainless steel and copper surfaces presented earlier.

Measurements of incipient boiling at a/g = 1 and a/g = 0 were made in both LN_2 and LH_2, using a transient technique with a platinum wire. A step increase in power was applied, and from the transient wire temperature measurements it was possible to observe when nucleate boiling began. It was observed, in both LN_2 and LH_2, that the maximum heater superheat at nucleation was independent of the body forces present.

I. INTRODUCTION

This technical report is the seventh of a series under Contract No. NAS-8-20228, through Mod No. 9, reporting results obtained upon the completion of certain specific identifiable phases of research. For convenience the six prior reports are listed below and the abstracts are contained in the Appendix.

Technical Report No. 1., "The Dynamics of Moving Bubbles in Single- and Binary-Component Systems," ORA Report 07461-14-T, by N. Tokuda, W. J. Yang, J. A. Clark, and H. Merte, Jr., December, 1966.

Technical Report No. 2., "Boiling of Liquid Nitrogen in Reduced Gravity Fields with Subcooling," ORA Report 07461-20-T, by E. W. Lewis, J. A. Clark, and H. Merte, Jr., May 1967.

Technical Report No. 3., "Incipient Boiling of Cryogenic Liquids," ORA Report 07461-28-T, by K. J. Coeling, J. A. Clark, H. Merte, Jr., and E. R. Lady, December, 1967.

Technical Report No. 4., "Finite Difference Solution of Stratification and Pressure Rise in Containers," ORA Report 07461-30-T, by H. Merte, Jr., J. A. Clark, and H. Z. Barakat, January, 1968.

Technical Report No. 5., "Finite Difference Calculation of Pressure Rise in Saturn S-IVB Fuel Tank," ORA Report 07461-39-T, by H. Merte, Jr., C. C. Suh, E. R. Lady, and J. A. Clark, April, 1969.

Technical Report No. 6., "Film Boiling on Vertical Surfaces in Turbulent Regime," ORA Report 07461-50-T, by N. V. Suryanarayana, and H. Merte, Jr., September 1970.

The various personnel who have been involved with and made contributions to different facets of the research described in these seven reports include the following:

Prof. J. A. Clark	Mr. W. Kidder
Prof. E. R. Lady	Mr. J. Dembinski
Prof. H. Merte, Jr.	Mr. A. Brunsvold
Prof. W. J. Yang	Mr. S. A. Korpela
Dr. H. Z. Barakat	Mr. C. C. Suh
Dr. E. W. Lewis	Mr. R. H. Marshall
Dr. N. Tokuda	Mr. E. Oker
Dr. K. Coeling	Mr. P. Vaishnav
Dr. N. V. Suryanarayana	Mr. L. Mohan
Mr. H. Morihara	Mr. E. Klosterhaus

The purpose of this technical report is to bring together the recent results of incipient and steady boiling of cryogenic liquids, both LN_2 and LH_2, under reduced gravity conditions. The parameters varied included the fluid used, heater surface temperature, geometry, orientation, and a/g.

Incipient and nucleate boiling have significance in the long-term storage of cryogenic liquids, as is described in Ref. 1. It is important to know, for a given material, the heater surface superheat and related heat flux for the initiation of a vapor bubble, as well as the heater surface—heat flux relationship for well-established boiling, for the various conditions of heater surface geometry, orientation and gravity levels encountered in space storage of cryogenic liquids. The results presented here are directed toward achieving this end.

Current efforts are commencing to incorporate photographic data with thermal measurements to obtain more detailed information about the mechanism of incipient and nucleate boiling. This research will simultaneously measure the active nucleating site population density, the frequency of bubble formation, the maximum departure size, the heat flux, and heater surface superheat. These results would be reported in a future technical report.

A research space on the roof of the G. G. Brown Laboratory on the North Campus was designed expressly for research involving liquid hydrogen. This facility was constructed with funds provided jointly by the National Science Foundation and The University of Michigan. A drop tower for use with liquid hydrogen is located immediately beneath this structure. The facility will now be described.

II. DROP TOWER AND INSTRUMENTATION DESCRIPTION

An elevation view of the drop tower and research space is shown in Figure 1. A 4-ft^2 chute enclosed by sheet aluminum is located beneath the research space, giving approximately 32 ft of free-fall distance, corresponding to a free-fall time of about 1.34 sec. An explosion proof ventilating fan located on the roof provides a minimum of two air changes per minute in the space in which hydrogen is used. Additional facilities for safety include a four-station hydrogen gas alarm, provision for flooding the research space with CO_2, and lead covered nonspark floors with electrical grounding of personnel.

Figure 2 is a plan view of the research space, and shows an air lock room adjacent to the drop tower shaft head chamber which is also well ventilated and used for research with hydrogen at $a/g = 1$. The space adjacent to these ventilated areas houses the instrumentation, drawing boards, and workshop space.

Figure 3 is a sectional view of the drop package and shows the deceleration method used. The piston assembly on the left side serves also to contain the particular test vessel being used for a specific purpose. It is able to accommodate a vessel or system having a maximum size of 19 in. dia by 36 in. long. Prior to release the piston is extended as shown. At the completion of the drop the cone and spike on the right penetrate into a sand box to decelerate the cylinder. The piston keeps moving, compressing the air to a predetermined pressure giving the maximum desired deceleration level, in this case 12 psi and 20 g's, respectively. At this point the metering pin, which is attached to the bottom of the piston assembly and constitutes a variable area orifice, vents the air at a suitable rate to prevent a further pressure build-up. At the appropriate position the metering pin closes to provide the final cushion of air. Theoretically the pressure within the cylinder was to remain constant to complete deceleration, but this was not quite achieved in practice. A piezoelectric crystal accelerometer and pressure gage were mounted on the drop package to monitor these values, and the results are shown in Figure 4. As is seen the maximum values of pressure and acceleration were 15 psi and 25 g's, respectively, which were deemed acceptable.

For fractional gravity operation two counterweights attached to the drop package with cables and pulleys were installed in opposite corners of the chute. A Kistler Model 303 servo-accelerometer was used to measure the body forces on the test package during both free-fall and fractional gravity. With the recording system used the maximum sensitivity possible was ± 0.001 g.

Figure 5 shows the results with fractional gravity. The mean value of effective body force present on the test package is $a/g = 0.23$ with an oscillation of amplitude $a/g = \pm 0.03$, arising from the action of the counterweight cable as a spring. The natural frequency of the two-mass-spring system appears to be about 9.5 cps. Using the measured value of $a/g = 0.23$, the calculated elapsed drop time is 1.52 sec as compared to 1.54 sec measured.

Figure 6 shows acceleration measurements made with free-fall. The accelerometer was mounted directly on the top cover of the outer vessel, from which the entire assembly is initially supported by a rod at the center. The accelerometer thus picks up the vibration of the cover-rod system, which is about 45 cps. The mean readings of two different tests are plotted in Figure 7. The increase of the body force due to drag is noted-being a maximum of $a/g = 0.008$. The frontal area of the test package is a large disc. An abrupt decrease in a/g occurs near the end, in Figure 7, and corresponds to the point where the test package emerges from the chute into the lower chamber after falling 27 ft. The elapsed time computed for the free-fall of 28 ft 7 in. in a vacuum is 1.335 sec, as compared to the experimental value of 1.345 sec. The "calibrated" zero shown arises from computing the mean output signal between $a/g = 1$ and $a/g = -1$, which assumes a perfectly linear output from the servo-accelerometer.

All electrical signal connections to the drop package were made with a drop cable. Since the drop package weighed over 500 lbs, it is presumed that the effect of the bending resistance of the cable on the fall characteristics is quite small. In any case the resulting resistance is accounted for in the a/g measurement shown in Figure 7. To avoid interference from the earth's magnetic field as the cable is falling, double shielding was provided.

The thermoelectric power of the copper-constantan thermocouples, used because of their stability, varied from approximately 9 $\mu v/^\circ R$ at liquid nitrogen temperatures to 3.3 $\mu v/^\circ R$ at liquid hydrogen temperatures. It was thus necessary that the instrumentation used have appropriate high sensitivities. For the steady state readings and for calibration of the recorder a Honeywell potentiometer Model 2768 with a Rubicon Model 3550 photoelectric galvanometer was used. This unit has a least reading of 0.01μv, and the measured temperature uncertainly is estimated to be $\pm 0.05^\circ R$ and $\pm 0.14^\circ R$ in liquid nitrogen and liquid hydrogen, respectively.

For the transient measurements, an 8-channel Sanborn Model 358 system was used, with Lo-Level preamplifiers for the thermocouple recordings. The maximum sensitivity is 1 μv/division, where the division is 0.8 mm. The recorder system is calibrated with the potentiometer immediately prior to each test. The maximum chart speed is 100 mm/sec, and the manufacturer's specifications state that with a step change input covering the entire channel width of 4 cm., the system is capable of following from 10% to 90% of the change in 4 msec. This was confirmed by experiment. With a sensitivity of 2 μv/division used the system can follow a rate of 20,000 μv/sec, entirely adequate for the processes encountered here.

Figure 8 is a section through the superinsulated cryostat test vessel installed in the drop package for obtaining measurements of boiling with LH_2. The inner Dewar vessel is 8 in. dia by 12 in. deep with a neck opening of 4 in. dia. To the top of the Dewar is attached a heating chamber into which the test piece can be drawn and electrically heated. A reservoir for liquid nitrogen is provided at the top of the Dewar, which serves to precool the Dewar before filling it with liquid hydrogen.

A double-walled fill line, three thermocouples—two at different heights in the test liquid and one in the vapor space—a tube carrying two liquid level indicating sensors—one high level and one low level—pass through the lower flange of the heating chamber. Two more thermocouples and the electrical leads for the heater pass through the top flange of the heating chamber. A gland through which the tube carrying the test piece slides is mounted on this top flange. By raising or lowering this tube the test piece is removed or immersed from the test liquid. Two liquid level indicating sensors are mounted in the reservoir on the top of the Dewar.

The Dewar itself is suspended from the cover plate of the drop package by stainless steel rods. Appropriate fittings for the fill lines, vent line, pressure release, etc., are mounted on the cover plate. After filling the Dewar with the test liquid, two pressure relief valves were attached to the fill lines, to regulate the pressure in the Dewar. A small lecture bottle mounted on the drop package provides helium for pressurizing the system for studies in subcooled liquids.

The thermocouple wires from the test pieces pass through the 1/4 in. dia supporting tube. The thermocouple outputs are connected to a recorder via a drop cable, consisting of eight 24-gauge copper wires and 24-gauge constantan wires. Double shielding of this cable was necessary to minimize noise pickup, particularly when operating at high sensitivities. The constantan wires served to make the reference junctions in ice. The liquid level sensors consist of carbon resistors, using the difference between the self-heating temperature when in liquid or vapor for detection purposes.

The superinsulated Dewar described above was also used to calibrate the thermocouples to an accuracy of $\pm 0.1^{\circ}R$, with the vapor-pressure technique described in Ref. 2.

To obtain boiling data at $a/g = 1$ for large surfaces that could not be introduced in the fractional gravity Dewar of Figure 8, the Pyrex glass Dewar shown in Figure 9 was used for LH_2 where a closed system is necessary. This was originally obtained for the incipient boiling work of Reg. 2 with LH_2. The inner Dewar is vacuum insulated with the upper part terminating in a single wall attached to a metal flange via a Kovar intermediate flange. The inner Dewar is surrounded by a second Dewar, filled with LN_2 to act as a heat shield. The inner Dewar has an I.D. of 10 cm., a height of 65 cm., and a capacity of 5 liters. Two diametrically opposed 1-in. wide unsilvered strips in both Dewars permit visual observation of the interior.

III. BOILING DATA

For obtaining the heat transfer data in the various boiling regions the transient technique was adopted, as described in detail in Ref. 3. If the rate of temperature change through an object is uniform, then it may be treated as a lumped system, and the heat flux evaluated from the transient temperature measurements using the first law analysis:

$$q/A = \frac{m}{A}\frac{dh}{dt} = \frac{\rho v}{A} C_p(T) \frac{dT}{dt} \qquad (1)$$

Thus, the heat flux is calculated from the slope of the cooling curve and the known body properties.

A considerable amount of data with boiling LN_2 from a 1-in. dia/sphere is reported in Ref. 3. Corresponding data obtained with LH_2 is presented below, both for sperical and flat surface geometries. It was hoped to be able to obtain visual data on the cessation of nucleate boiling with the transient cooling of the sphere in LH_2. However, the sphere passes through the transition peak heat flux and nucleate boiling requires so rapidly; in about 1/5 sec with the 1 in. dia sphere, that it was not possible to observe this point. It was not deemed worthwhile to pursue this further with the use of a high speed camera when superior data on incipient boiling is available with a steady technique.[2] The cooling transient in the transition and nucleate boiling regions is rapid in LH_2 because of the low C_p of copper at these temperatures. This is both an advantage and a disadvantage. It is possible to pass through the complete transition-to-nucleate boiling region with free fall in a single drop period when the test package release is synchronized with the onset of transition boiling. This was not possible with LN_2.

With C_p being small, it is important that the values used in Eq. 1 be known with precision, since it varies considerably with temperature near the LH_2 temperatures. Values from various sources for 99.999% pure copper are listed in Table I. The copper used in the test specimens was OFHC commercial copper, with 99.92% copper minimum. Since the specific heat of metals is not extremely sensitive to impurities, the values for the special high purity copper were deemed applicable. The values of C_p listed in the fourth column of Table I (C_p [7]) were used in reducing the data.

With a rapid transient occurring with LH_2 in the vicinity of the peak heat flux it is necessary to establish that the lumped system analysis of Eq. 1 is acceptable. To test this a computational experiment was conducted using a sphere. The sphere is subjected to a step change in temperature of the environment starting from the experimental ΔT_{sat} corresponding to the maximum heat flux. The heat transfer coefficient is assumed constant at a value 50% higher than the maximum experimental value obtained with LH_2. The analytic solution

TABLE I

SPECIFIC HEAT OF COPPER

($Btu/lbm\ ^\circ R \times 10^3$)

°K	°R	C_p [4]*	C_p [5]	% Diff. [4]-[5]	C_p [6]	% Diff. [4]-[6]	C_p[7]	% Diff. [4]-[7]	C_p[8]	% Diff. [4]-[8]
20	36	1.78	.177	+0.56			1.78	0	1.74	+ 2.25
25	45	3.55	3.59	-1.13			3.64	-2.54	3.62	- 1.97
30	54	6.10	6.31	-3.44	6.27	-2.79	6.44	-5.57	6.37	- 4.43
35	63	9.4	9.91	-5.41	9.82	-4.47	9.96	-5.96	9.97	- 5.53
40	72	13.0	13.96	-7.38	14.07	-8.23	14.08	-8.31	14.07	- 8.23
45	81	17.2	18.48	-7.44	18.57	-7.97	18.62	-8.26	18.54	- 7.79
50	90	21.80	22.93	-5.18	23.27	-6.74	23.34	-7.06	23.15	- 6.19
70	126	38.50	40.47	-5.12	40.75	-5.84	40.87	-6.16	40.86	- 6.10
100	180	56.80	59.80	-5.28	59.83	-5.33	60.13	-5.86	60.23	- 6.04
150	270	70.00	76.63	-9.47	76.65	-9.50	76.65	-9.5	77.16	-10.23
200	360						85.12			
260	468						91.20			
300	540						91.99			

*Numbers in brackets indicate the literature references.

to this problem is available and was used to compute the surface heat flux as a function of time. This is plotted in Figure 10 as the exact solution. At the same time the temperature of the sphere at the centerline and at a radius of 7/8 R_o are computed. The latter corresponds to the physical location of the thermocouple in the real experiment. The sphere is then assumed lumped at the temperature corresponding to each of these locations, and the heat flux is computed from the first law. These two results are included in Figure 10. It is noted that after an initial time of 3 msec, the error in assuming the system lumped corresponding to a radius of 7/8 R_o is less than 1%, and a lumped system assumption is justified. Figure 10 indicates that the location of the thermocouple in the experiment is important. Figure 11 is a representative sample of data for LH_2 at atmospheric pressure and a/g = 1. Three thermocouples are located at different points in the sphere, and their comparable behavior verifies the lumped behavior of the sphere.

With a rapid transient occurring with LH_2 in the vicinity of the peak heat flux it is important that the thermocouple be capable of following this change. A delay in the response of the thermocouple is possible due to the effect of the solder used to attach the junction to the bottom of the hole drilled in the test surfaces. The construction of the thermocouple is shown in the upper part of Figure 12. The lumped behavior of the sphere means that the temperature drop across distance D can be neglected. The thermocouple, however, generates a net EMF corresponding to the mean temperature of the solder in length L. It was considered possible that with a transient temperature change taking place, the decreased thermal diffusity of the solder, compared to copper, could result in a source of error. To assess this a mathematical model was solved, shown on the bottom of Figure 12 and approximating in a conservative way the physical system. The solder is considered as an infinite slab, neglecting curvature and insulated on one side. The temperature response of the solder at the mid-point in the hole will be more rapid than that of the slab, since heat transfer actually takes place on the lateral surfaces of the hole. The variation of the surface temperature of the slab is represented by an exponential function which approximates the transient temperature of the lumped copper sphere. The problem was solved by the method of Laplace transform, the solution for T_c is given by Eq. 2. A_o and m are given constants obtained from approximating the transient analytical temperature of the sphere.

$$T_c = T(L/2, t) = T_\infty + A_o \frac{\cos\left(\sqrt{m/a}\, L/2\right)}{\cos\left(\sqrt{m/a}\, L\right)} e^{-mt}$$

$$+ \sum_{n=1}^{\infty} (-1)^{n-1} \left[\frac{A_o \pi (2n-1)}{\left\{\left[(2n-1)\frac{\pi}{2}\right]^2 - L^2 m/a\right\}} - \frac{4(T_o - T_\infty)}{(2n-1)\pi} \right] e^{-\left[(2n-1)\frac{\pi}{2}\right]^2 \frac{at}{L^2}} \cos \frac{\pi}{4}(2n-1) \qquad (2)$$

T_c represents the temperature sensed by the thermocouple in the solder, and q_c is the heat flux computed from $\partial T_c/\partial t$, assuming that T_c represents the temperature of the sphere. The percent error resulting from the effect of the solder is represented in Figure 13 as $(q_s - q_c)/q_s$, where q_s is the heat flux computed using T_s as the sphere temperature. Two different thichness L are used, .02 in. and .04 in, which cover the range attempted in the construction of the junction. A range of thermal conductivities are included, since some uncertainty exists in the value of this property near liquid hydrogen temperatures. Using the maximum value of L = 0.04 in. and the best estimate of K = 34 Btu/hr-ft-°R, the maximum possible error in heat flux due to the effect of the solder is about 12%. Owing to heat transfer between the solder and the sides of the hole, which is .045 in. in diameter, the actual error is most likely less than one half of this, or less than 6%, since the lateral area is four times the end area of contact. It is thus concluded that the solder contributes a relatively small uncertainty to the heat flux measurement.

To confirm that the recorder imposes no limitation on the ability of the thermocouple to follow the temperature transient, an equivalent heat flux was computed using the maximum response capability of the recorder system, which was found to be 20,000 μv/sec at a sensitivity of 2 μv/division. With a 1 in. dia copper sphere in the vicinity of the peak heat flux in LH_2, this would correspond to a heat flux of q/A = 518,000 Btu/hr ft^2, which is 20 times greater than that observed. Thus no limitation is imposed by the recorder.

The data are presented below in groups corresponding to the different geometries covered.

A. SPHERE

A sphere had been used as a dynamic calorimeter in previous work [3] because of its inherent simplicity and symmetry, and because its geometry minimizes undesired heat losses (or gains). The results in Ref. 9 were used to define a reference curve for boiling in LN_2. This makes comparison between various changes in parameters quite convenient. A corresponding reference curve is defined below for LH_2. Results were presented in Ref 3 for sphere sizes down to 1/4 in. dia in LN_2. This has been extended to a sphere 2-1/4 in. dia in both LN_2 and LH_2.

1. 1 Inch Diameter

a. LN_2

With the new drop package and instrumentation systems, tests were conducted with LN_2 for checking purposes and confirmed further the results presented in Refs. 3 and 9. The results are not presented here. Figure 14 is a view of the sphere used for both LN_2 and LH_2.

b. LH_2

In the early trial runs, while becoming familiar with the use of LH_2, a number of runs gave strange results. An example is shown in Figure 15, with the open circles representing these results. It was subsequently confirmed that this was due to the introduction of small quantities of moisture into the vapor space by condensed moisture adhering to the sliding tube as the test vessel is immersed. This occurred only after an initial test had taken place such that the support tube was cooled, and when the sphere had not been subsequently heated above the dew point. The presence of solid condensed moisture on the surface of the sphere evidently permits the premature onset of transition boiling because of the change in surface properties, the ice acting as a thin coating having a low thermal diffusivity. The ice coating problem was eliminated by adopting the procedure of heating the test surface above the dew point prior to each test.

Data at a/g = 1 and at atmospheric pressure for the saturated liquid case are shown in Figure 16 for the entire boiling region covered. This is used to define what is called a "Reference Curve." Based on past experience it was found to be desirable to define such a curve when comparing the influences of several different parameters. All subsequent plots will include this reference curve, which acts as an anchor point. It also serves as a check on reproducibility of subsequent results obtained under reduced gravity, since data at a/g = 1 are also obtained each time immediately prior to release of the test package. The results of boiling under various pressures, reduced gravities and with subcooling are presented below as Figures 17-23, each of which will be briefly discussed.

Figure 17. Effect of pressure at a/g = 1, saturated LH_2.

This indicates the influence of increasing pressure, with saturated liquids over the various boiling regimes. For given values of ΔT_{sat} ($T_{surface} - T_{saturation}$), increasing the pressure results in increased heat flux with film boiling, in the minimum and maximum heat flux regions, and with nucleate boiling, all of which are qualitatively consistent with observations made with other fluids and predicated by the correlations.[3]

At low levels of ΔT_{sat} as is present in the nucleate boiling region the sensitivity and accuracy of the temperature measuring system become significant in assessing reproducibility and trends between different tests. The thermo-electric power of copper-constantan thermocouples at liquid hydrogen temperature is 3.3 μv/°R. Owing to the presence of A.C. pickup in the signal, it was necessary to record the signals at the somewhat reduced attenuation of 2 μv/division. This results in an uncertainty on the order of ± 0.5°R in the level of the temperature between different tests.

Figure 18. Effect of a/g at P = 14.7 psia, saturated LH_2.

The influence of reduced gravity under free-fall conditions is shown here for the case of a saturated liquid at atmospheric pressure. As is noted in Figure 7, the measured body force level on the test package varies from $a/g = 0$ at the instant of release to a maximum value of $a/g = 0.008$ just prior to impact. The body force present during all free-fall tests thus far conducted should be considered to be within the range $0 \leq a/g \leq 0.008$.

The data points at $a/g = 1$ immediately preceding the test package release are included, and attached to the corresponding free-fall data point by a dashed line. Each connected point corresponds to an individual test. Data points not connected by dashed lines are continuations, in the same test, of the data points immediately to their right. This results from the relatively rapid rate of change of temperature of the sphere as compared to the free-fall time of approximately 1.4 sec. The heat flux is higher in the nucleate boiling region and the specific heat of the copper becomes quite small, so the entire transition-peak and nucleate-boiling region is covered during the free-fall period. The data for free-fall appear to form a continuous curve, which would indicate that the body force present during free-fall is quite reproducible. At this lowest pressure used, atmospheric, a reduction in g results in a significant decrease in heat flux with nucleate boiling. This effect seems to decrease as pressure increases, as may be noted by comparing Figures 18, 19, and 20, and is believed to be a consequence of partial vapor blanketing occurring, more so at lower pressures where the specific volumes are significantly higher. These changes with a/g in the nucleate boiling region were not observed with LN_2. This is believed to reflect differences in the properties, most likely those related to the body forces, surface tension forces, viscous forces, and inertia forces.

Figure 19. Effect of a/g at P = 23.3 psia, saturated LH_2.

The influence of reduced gravity under free-fall conditions is shown here for the case of a saturated liquid at a pressure p = 23.3 psia. The changes observed with free-fall appear consistent with those at atmospheric pressure, except in the nucleate boiling region. This could be attributed to the uncertainty in temperature level of $\pm$ 0.5°R referred to earlier.

Figure 20. Effect of a/g at P = 37 psia, saturated LH_2.

The influence of reduced gravity under free-fall conditions and $a/g = 0.2$ is shown for the case of a saturated liquid at the highest pressure used, p = 37 psia. The peak heat flux and the film boiling regions appear to behave in an orderly fashion, but the variations in the nucleate boiling region are somewhat larger than had been previously observed. It is possible that the net behavior with nucleate boiling during reduced gravity will depend to some extent on the point on the cooling curve at which release of the test package takes place. Because of the rapid rate at which the temperature of the sphere is changing in the vicinity of the transition region, it is difficult to repeat the test package release at the same sphere temperature. Any variation desired would have to arise almost from pure chance. Unfortunately, at the time the tests were being conducted the possibility of the release time influencing the

nucleate boiling behavior was not known.

It appears from examining Figures 18, 19, and 20 in the vicinity where the test package release takes place in the minimum heat flux region, that the transition phenomena between film and nucleate boiling is independent of the body forces, and is governed by the ΔT_{sat} alone. The only requirement is that liquid be available and able to make contact with the heating surface, implying that disturbing forces of some magnitude ($a/g < .008$ in this case) must be present.

In all three figures, a minimum heat flux is quite well defined, even at $a/g = 0.008$. It is believed that the violent action of the vapor bubbles in this region provides the agitation necessary to produce a maximum heat flux, being in a sense self-perpetuating. Although speculative at this point, it is believed that an unstable transition region would also be observed at very low acceleration, $a/g < 10^{-5}$. This should be confirmed by experiment. If so, this could be significant in the long-term storage of cryogenics in space flight. If a region of the inner wall became dried out and heated to a temperature between the maximum and minimum heat flux region, and momentary contact was then made with the liquid owing to some small forces, it would be important to know whether a stable vapor film would be formed, or if the agitation set up would "quench" the wall, producing large quantities of vapor.

Figure 21. Effect of pressure at $a/g = 0.008$.

The free-fall portions of Figures 18, 19, and 20 are combined to demonstrate the influence of pressure for saturated liquids. Comparing Figure 17 with Figure 21, the relative effect of pressure in the film boiling region is about the same for both $a/g = 1$ and $a/g = 0.008$, with heat flux increasing with pressure for given levels of ΔT_{sat}. $(q/A)_{max}$ also increases with pressure in both cases. However, a distinct difference in behavior with pressure occurs in the nucleate boiling region, with large increases in heat flux with pressure taking place at low gravities, as compared to $a/g = 1$. At very low body forces, large changes in vapor density relative to latent heat can significantly influence the ability of the liquid to reach the heating surface. This is indicated in Table II, in which the volume change per Btu of heat transfer, $\Delta v/h_{fg}$, is computed for the three pressures used in Figure 21. It

is noted that the vapor generation at 14.7 psia is over twice as large in magnitude as that at 37 psia, for a given heat flux. Thus, at the low body force of a/g = 0.008 this greater amount of vapor will impede the motion of liquid toward the heating surface, and require a greater ΔT_{sat} for a given heat flux, as is the case in Figure 21.

TABLE II

CHANGE IN RELATIVE VAPOR GENERATION
WITH PRESSURE FOR LIQUID HYDROGEN

Pressure, psia	v_v, ft^3/lbm	v_L, ft^3/lbm	h_{fg}, Btu/lbm	$\Delta v/h_{fg}$, ft^3/Btu	$\frac{(\Delta v/h_{fg})_P}{(\Delta v/h_{fg})_{P=37}}$
14.7	13.37	0.23	192.0	0.0685	2.08
23.3	9.10	0.23	188.2	.0471	1.43
37	6.25	0.25	182.0	.0330	1.00

Figure 22. Effect of subcooling at a/g = 1 with p = 37 psia.

Data for saturated liquid hydrogen at p = 37 psia are compared with that for a subcooled liquid. The results are quite reproducible, as several different tests are represented. It appears that subcooling increases $(q/A)_{min}$ and decreases $(q/A)_{max}$, while otherwise having relatively little effect. With LN_2, it had been observed that $(q/A)_{min}$ also increases with subcooling, but $(q/A)_{max}$ also increased.

Figure 23. Effect of a/g with subcooling at p = 37 psia.

The behavior of film boiling with reduced gravity and subcooling is quite similar to the saturated liquid case. This would be anticipated, provided the film boiling process is limited or controlled by diffusion taking place across the vapor film rather than within the liquid. This is apparently the present case.

It is also noted in Figure 23 that for a/g = 0.008 the heat flux at $(q/A)_{min}$ appears greater than the lowest heat flux with film boiling at a/g = .008. It is possible that the ΔT_{sat} corresponding to $(q/A)_{min}$ has been

increased considerably. Even at a/g = 1 subcooling appears to have introduced a plateau for $(q/A)_{min}$. At a/g = 0.008, it is possible that the violent agitation associated with transition boiling, compared to film boiling, served to mix the liquid more effectively, bringing the subcooled liquid closer to the heating surface.

c. Comparison with correlations

All of the film boiling data presented in Figures 16-23 for the 1 in. dia sphere in saturated liquid hydrogen have been placed in dimensionless form and are plotted in Figure 24. Also included is the correlation which compared favorably with film boiling in liquid nitrogen,

$$Nu = 0.15\ (Ra')^{1/3} \qquad (3)$$

along with the correlation of Bromley. These were presented in Ref. 9.

It should also be noted that the data in Figure 24 appear to parallel the correlation of Bromley, which has a 1/4 power on the modified Rayleigh number. In comparing this with Figure 9 of Ref. 9, the hydrogen data extend the total data available to Ra' below 10^9, which was the lower limit for LN_2, and the departure from Eq. 3 begins at this level. It is possible that a transition from a type of turbulent to laminar film boiling takes place in the region of Ra' 10^8 - 10^9, as was suggested in Ref. 9. In spite of some uncertainty in the measurement of the acceleration during free-fall, it appears from Figure 24 that the data obtained with free-fall, are in line with that for other body forces.

In Table III the experimental results for the maximum and minimum heat flux with LH_2 boiling on the 1 in. sphere are tabulated, as taken from Figures 16-23, and are compared with the predicted values using the same correlations as used in the earlier work with LN_2[9], the correlation of Noyes[10] for $(q/A)_{max}$ and that of Berenson[11] for $(q/A)_{min}$. These were reasonably successful in correlating the behavior with LN_2, but from Table III it is observed that the predicted values are considerably higher than those observed. Experimental values of $(q/A)_{max}$ less than that predicted by a correlation similar to that of Ref. 10 was observed by Astruc.[13] Using a platinum wire 0.05 mm diameter as a heating element and resistance thermometer, a $(q/A)_{max}$

= 16,500 Btu/hr ft^2 with ΔT_{sat} = 3.6°R was measured in liquid hydrogen at atmospheric pressure. Although the ΔT_{sat} at the peak heat flux is considerably less than that with the 1 in. dia sphere, as noted from Figure 16, the peak heat fluxes are comparable. On the other hand, an experimental study of boiling of hydrogen at atmospheric pressure from a horizontal copper surface[14] produced $(q/A)_{max}$ = 31,600Btu/hr ft^2, considerably higher than the value of $(q/A)_{max}$ = 18,000 Btu/hr ft^2 in Table III for the corresponding condition. It should be mentioned that the heat flux in Ref. 14 was computed from a measured temperature gradient in the copper surface. The thermal conductivity of copper is very sensitive to both the temperature level and the impurity content at liquid hydrogen temperature levels, and the accuracy of a heat flux computation based on this is subject to question.

TABLE III

COMPARISON OF THEORETICAL AND EXPERIMENTAL RESULTS FOR $(q/A)_{max}$ AND $(q/A)_{min}$

(Liquid hydrogen - 1 in. dia sphere)

Pressure, psia	a/g	$(q/A)_{max}$, Btu/hr ft^2		$(q/A)_{min}$, Btu/hr ft^2	
		Correlation, Noyes[10]	Experimental	Correlation, Berenson[11]	Experimental
14.7	1.0	28,250	18,000	2,218	900
	0.235	19,800	11,000	1,550	1,020
	0.008	8,450	7,800	663	440
23.3	1.0	32,000	20,000	3,030	1,070
	0.235	22,200		2,120	
	0.008	9,550	8,000	905	605
37.0	1.0	38,000	23,000 (17,700-6.5°R)	4,540	1,250 (2,500-6.5°R)
	0.235	26,600	13,000 (12,000-6.5°R)	3,160	1,500
	0.008	11,380	10,000 (9,600-6.5°R)	1,358	540 (1,600-6.5°R)

Note: Experimental values in parentheses apply for subcooled case with degree of bulk subcooling indicated.

2. 2-1/4 Inch Diameter

Earlier work with boiling of LN_2 from the sphere indicated[3] that the 1 in. and 1/2 in. dia spheres behaved similarly, while the 1/4 in. dia sphere departed

somewhat in the film boiling region. This has been demonstrated to be related to the increasing role of surface tension as size is reduced.[15] It was desired to explore the influence of a size larger than 1 in. dia. This has been accomplished for both LN_2 and LH_2 at a/g = 1, using a copper sphere 2-1/4 in. dia. Operation under reduced gravity was not possible because of the limitation in size imposed by the drop package Dewar.

a. LN_2

Figure 25 shows the results of operation with LN_2 at atmospheric pressure, and may be compared with the behavior of the 1 in. dia sphere, as indicated by the reference curve. Two thermocouples were installed, one at the center and one near the surface. The heat flux was computed independently from each thermocouple, assuming that the sphere was lumped corresponding to each measurement. As is noted in Figure 25, the two reproduce each other quite well.

After each run, in which the sphere was cooled to the liquid nitrogen temperature, the sphere was drawn up into the vapor space until it became heated just above the $(q/A)_{min}$ region, and then reinserted into the liquid. This is designated as a rerun. In both cases the only difference is that the transition region curve is shifted somewhat to the left, giving a lower heat flux for a given ΔT_{sat}. The same phenomena was observed with the 1 in. dia sphere and in the 3 in. dia disc data, to be presented later. This is believed due to the higher velocities induced in the liquid by the normal runs. If the onset of the transition boiling, the minimum heat flux, is characterized by a Helmholtz instability, a higher velocity will cause an early breakdown of film boiling, as occurs in Figure 25.

The film boiling is the same as with the 1 in. sphere and the $(q/A)_{max}$ is also unchanged. The $(q/A)_{min}$ is somewhat higher, and the heat flux is nucleate boiling is also somewhat higher, for a given ΔT_{sat}. The transition boiling curve is shifted to the right of that for the 1 in. dia sphere.

b. LH_2

The relative behavior between the 2-1/4 in. and the 1 in. dia sphere with LH_2 in Figure 26, is quite similar to that with LN_2: film boiling is unchanged, the $(q/A)_{min}$ is higher, the transition region is shifted to the right, the $(q/A)_{max}$ is about the same, and the nucleate boiling behavior appears unchanged. In both separate runs of Figure 26, the thermocouple recordings exhibited considerable noise. This was later found to be due to faulty insulation on the wires, but no liquid hydrogen was then available to repeat the tests. The only part of the data that might be questionable is in the lower end of nucleate boiling, where high sensitivity in the amplifiers was necessary.

B. FLAT SURFACES

The geometry of a sphere, while desirable from the point of symmetry, may

produce questionable results when the results are extrapolated to flat surfaces. Flat surfaces introduce the variable of orientation, while a sphere includes all orientations. A program to obtain boiling data with flat surfaces was initiated to explore the influence of orientation simultaneously with reduced gravity. To obtain data with the short time (1.35 sec) near-zero gravity condition available, it was necessary to adopt the transient technique used with the sphere to the flat surface configuration. This introduces the problem of edge effects, not present with the sphere. A vertical cylinder large enough so that surface tension effects are negligible simulates a vertical flat plate, and eliminates part of the edge effects. A flat circular disc, insulated on the back side, minimizes the edge effects and permits the convenient variation of orientation. These two independent sets of tests are described below.

1. Vertical Cylinder (Vertical Flat Plate)

Figure 27 shows the section of a typical calorimeter assembly used for the vertical cylindrical surface. The test sections, whose locations can be varied along the axis of the cylinder, each contain a thermocouple for measuring the cooling rate of the isolated test section, thus permitting the determination of the localized heat flux. It was desired to specify an isothermal condition along the vertical surface. If the cylinder has been continuous, an isothermal state would have been assured throughout the boiling range, but only a mean value of heat flux could have been measured. To measure local values of heat flux the 1/4 in. thick test sections were isolated from the adjacent sections with Teflon spacers .005 in. thick. If the local heat fluxes vary along the cylinder, then the isothermal condition will be present only upon initially plunging the cylinder into the liquid hydrogen (assuming that the cylinder is initially isothermal).

For film boiling data this presents no problem, since the desired data is obtained shortly after immersing the cylinder, while temperature differences between adjacent sections are still quite small. The various temperature levels with film boiling are achieved by precooling the cylinder to the desired level prior to immersion in the LH_2. Film boiling results with the vertical cylinders are presented in detail in Reference 16.

For data in the transition and nucleate boiling region, the cylinder was precooled to a temperature just above the minimum heat flux region and then immersed in the liquid hydrogen. It appeared, from the time-temperature data, that the test sections and spacer sections successively went through the minimum and maximum heat flux regions from bottom to top in order. This meant that when a section below the test section went through the peak heat flux, a large temperature difference was quickly established across the 0.005 in. Teflon spacer, serving as a heat leak and hence a possible source of error in computing the heat flux.

a. LH_2

The results are shown in Figures 28a-c, with the boiling of LH_2 from the 1 in. dia vertical cylinder. Because of the uncertainties in the nucleate boiling results associated with the heat leaks, the data were not reduced over the entire nucleate boiling region. Each of the figures represents tests conducted on different days with different charges of liquid hydrogen. The various values of "X" are indicated, representing the local values of heat flux at that height along the heated surface. Included for purposes of comparison are the results for film boiling obtained independently and taken from Ref. 16.

In all three figures the data for the minimum heat flux near the leading edge appear reasonably consistent in that the levels of heat flux are greater than those for distances farther from the leading edge, both in the minimum heat flux and film boiling regions. However, consistency does not appear for the other points in the minimum heat flux region, nor in the peak heat flux region.

This may be attributed in part to the axial conduction losses, mentioned before, associated with the fact that the various sections pass sequentially through the transition region. An example is shown quite clearly in Figure 28a, by the points marked "A" and "B". These are in the test section 3 in. from the leading edge. Both "A" and "B" are in the film boiling region, but with "A" the spacer section below is still in film boiling, whereas with "B" the spacer section below has already passed through the transition and nucleate boiling region, resulting in an increased heat loss and an apparent increase in heat flux.

Although it has not been verified, it is possible that the discrepancies in the minimum and maximum heat flux in Figures 28a-c are due to minute quantities of solid H_2O, CO_2, N_2, or O_2, deposited on the heating surface owing to the technique followed, similar to that observed with the sphere and presented in Figure 15. In that case, the problem of the formation of ice on the surface was overcome by always immersing the sphere at a temperature above the freezing point of water and permitting it to cool continuously to the transition region. However, in the present case with the vertical cylinder this would result in a large nonuniform axial temperature distribution. The following technique of precooling was adopted; by removing the cylinder from the liquid periodically as it moved down the cooling curve and selectively heating portions of it with radiation, a uniform temperature at all sections could be attained. The ingress of water vapor observed with the sphere was believed to occur at the sliding "O" ring seal on the vertical support rod. With the cylinder a lowering mechanism was designed which involved only a rotating "O" ring seal. However, it is possible that this was still insufficient to maintain a perfect seal, and permitted a minute quantity of water vapor to enter.

Since additional data for a vertical surface in the maximum and minimum heat flux region will be presented with the circular disc tests, it was decided

to abandon further explorations with the vertical cylinder. The potential problem of icing does not exist with the disc since the disc is immersed in the liquid hydrogen above the freezing point of water.

b. LN_2

Data for transition region boiling in LN_2 from local sections of a vertical cylinder are shown in Figures 29a-c. These correspond to the data presented for LH_2 in Figures 28a-c. As discussed earlier, even though beginning with an isothermal test surface just above the $(q/A)_{min}$ region, the sections nearer the leading edge will pass through the minimum heat flux earlier, resulting in a large ΔT between adjacent sections, since the film boiling heat transfer varies with height, as shown in Ref. 16. This would decrease the percentage accuracy of the heat flux computations significantly in those regions where the heat flux is relatively low, i.e., the minimum heat flux and lower ΔT nucleate boiling regions. In spite of this possibility, the $(q/A)_{min}$ points in Figures 29a,b appear reasonably consistent. Figures 29a,b apply for a cylinder 2-1/4 in. in diameter, while Figure 29c is for a cylinder 1 in. in diameter. In the vertical orientation these differences in diameter do not affect the boiling process. Data in the nucleate boiling region, however, were affected considerably by the heat transfer from adjacent sections, and hence are not given here. Data with nucleate boiling on a vertical surface has been obtained with the circular disc and is presented below.

Results for boiling in the peak heat flux region for the vertical cylinder should not be significantly affected by the heat loss to adjacent sections. However, it may be that the $(q/A)_{max}$ at a particular section is influenced by the flow of vapor from a section below. If a section below is going through $(q/A)_{max}$ at the same time, the section of interest may become "liquid starved." It is possible that the discrepancies of $(q/A)_{max}$ in Figures 28a-c for LH_2 result from this effect. The results for LN_2 appear more internally reproducible in Figures 29a-c. The ranges of $(q/A)_{max}$ over ranges of height from the leading edge are given in Table IV, taken from Figures 29a-c. It is noted that the data near the leading edge are quite reproducible, most likely because no source of vapor exists below that part.

TABLE IV

$(q/A)_{max}$ ON VERTICAL SURFACE—LN_2

Height, in.	$(q/A)_{max}$, Btu/hr ft^2
0-2	48,000-52,000
2-4	42,000-60,000
4-6	54,000-64,000

2. 3 Inch Diameter Flat Plate

Figure 30 shows a section through one half of the disc used here. The central "test section" piece 1 in.^{2} is used to compute the heat flux. This is isolated from the edge of the disc by a series of slits 0.030 in. wide, leaving only a piece of metal 0.030 in. thick for structural purposes. Each piece adjacent to the test section thus acts as a guard heater, its thermal capacity helping to isolate the test section from the edge effects. An identical piece is attached to this section such that an "air gap" exists to reduce thermal communication between the two pieces. Direct contact still remains via the 1/4 in. land on the periphery. The disc is supported by two stainless screws. Initial tests in LN_2 were conducted with the perimeter of the disc bare, and the joint coated with a small bead of RTV rubber cement. This had the effect of increasing the effective heat transfer area, and the RTV tended to produce nucleate boiling prematurely on the perimeter, both of which result in errors.

The results of these preliminary tests are shown in Figure 31. It must be kept in mind that in the horizontal orientation the results are based on the temperature measurements in the particular section of the disc indicated by an "X" on the sketch included. Presumably the other section is performing as would be measured for that particular orientation.

The $(q/A)_{min}$ is about the same for all three orientations, as is to be expected since the disc is behaving similar to a lumped system at this point. The ΔT_{min} is somewhat higher than normal, as will be seen in Figure 36, since the uninsulated perimeter tends to produce transition boiling prematurely. Film boiling is also similar for all three orientations except at the early point where the disc was plunged into the LN_2. The variation is a result of the edge effect and thermal interaction between the two halves. The values of $(q/A)_{max}$ are about the same for the vertical and horizontal up (HU), but lower for the horizontal down (HD), since the large amount of vapor generated has difficulty in being removed from the underside vicinity of the heating surface. In nucleate boiling the HD orientation has the highest heat flux, while the HU has the lowest, with the vertical between. These are qualitatively the same as the improved results summarized in Figure 36, to be discussed later.

Figure 32 shows the results of further preliminary tests intended to demonstrate qualitatively the effect of thermal interaction between the two halves of the disc. The perimeter and one side of the disc were covered with approximately 1/4 in. thick Styrofoam insulation. Comparing this data with the vertical orientation data in Figure 31 it is noted that the heat flux is considerably lower for all levels of ΔT_{sat}. This can be viewed as resulting from either a decrease in the effective heat transfer surface area, or an increase in the effective heat capacity. In the $(q/A)_{min}$ and film boiling regions the heat flux is almost 1/2 that where symmetry is maintained, as in Figure 33. This indicates that as long as the heat flux from the central portion is relatively low, the disc halves are effectively in good thermal communication. The influence of the insulated section on $(q/A)_{max}$ is not so

great, since the surface passes through this region so rapidly that sufficient time does not exist for appreciable heat transfer from adjacent sections to take place. The darkened points in Figure 32, and subsequent Figures 33-35, are transition reruns. Data over all the boiling regimes are first obtained on cool-down. Then the disc is taken out of the LN_2 and heated to just above the ΔT_{min} point, and then reinserted in the LN_2, repeating just the transition and nucleate boiling portion of the curves. Two complete sets of data are obtained for each condition. It is noted, in Figure 32, that the reproducibility between the two sets of data in the nucleate boiling region is not good. Noise in the recorded signal was present at the low levels of attenuation, in the nucleate boiling region, and was found to be due to a frayed shielded cable between the test vessel and the recorder. This was replaced between tests D-033 and D-034 in Figure 33, and from test D-034 on no difficulties occurred.

With the completion of the preliminary tests, in all of the subsequent tests Styrofoam insulation existed only on the perimeter of the disc, as indicated in Figure 33.

a. LN_2

Figure 33 presents the results for the vertical orientation. The two sets of data are not reproducible, as mentioned above, but as will be seen in Figures 34 and 35, once the frayed cable was replaced the data became reproducible.

Figure 34 presents results for the orientation where the heating surface was facing upward (HU). The results are quite close to those for the 1 in. dia sphere. Also, the results in the nucleate boiling region duplicate quite closely corresponding results obtained with a steady state technique, as indicated in Figure 8 of Ref. 9. The levels of $(q/A)_{max}$ and $(q/A)_{min}$ fall reasonably well within predictions for this orientation, also given in Ref. 9.

Figure 35 presents results for the orientation where the heating surface is facing downward (HD). The $(q/A)_{max}$ is quite similar to that for the sphere at $a/g \approx 0$. Under zero gravity the only agitation possible is that due to the action of the bubbles, and the behavior resembles that for the horizontal surface facing downward since buoyant forces would tend to keep the vapor against the solid heating surface. With film boiling the behavior is similar to the sphere at $a/g = 1$; the heat flux is not as high as with the vertical surface in Figure 33 because the vapor flow is somewhat impeded. The heat flux in nucleate boiling is considerably higher.

It may be observed in Figures 33-35, that in all cases on the transition rerun the data shifted to the left in the transition region. This means that the vapor film becomes unstable at a lower ΔT when film boiling is initiated from a lower ΔT. This was discussed earlier in connection with Figure 25, and is believed related to the lower velocity associated with the reruns.

Figure 36 is a composite of Figures 33-35 for purposes of comparison. In the nucleate boiling region, the HD orientation results in the largest heat flux, while the HU gives the lowest, with vertical in between. This is consistent with the qualitative results of Ref. 17, which refers to the importance of the liquid microlayer entrapped beneath the vapor bubble as it forms and grows. The HD orientation provides more microlayer area beneath a given bubble. The HU data agree with the steady state data given in Ref. 9 and provides the smallest microlayer area. It might be speculated that the zero gravity data will fall between the HD and HU, or resemble the vertical data.

In the critical heat flux region, the HD has the lowest heat flux while the other two orientations are about the same, and hence a crossover takes place within the nucleate boiling region.

In film boiling, the vertical orientation has the highest levels of heat flux because the vapor flow path is parallel to the body force direction. The HD has the lowest heat flux since the vapor can be removed only by flowing to the edge of the disc. It might be anticipated that film boiling in the HD orientation is size dependent. When comparing film boiling with the disc (Figure 33) with that obtained with the vertical cylinder (Figures 29a-c) it is noted that the heat flux is about 50% greater for the disc. This is believed to be a consequence of the unusual starting edge associated with a vertical circular disc, which influences the interfacial oscillations, which itself greatly influences the heat flux with film boiling as shown in Ref. 16.

Although $(q/A)_{min}$ follows the trends of film boiling, Δt_{min} remains essentially unchanged with the various orientations, with transition boiling beginning at ΔT = 50-60°F.

To obtain free-fall tests in the drop tower it was necessary to modify the drop package for the disc, since the disc was too large in size for the superinsulated cryostat. The superinsulated cryostat was removed from the drop package and a container insulated with Styrofoam installed, shown schematically in Figure 37. The complications of pressure regulation were avoided by operating with an open vessel. However, this necessitated certain precautions to avoid contamination of the LN_2 by CO_2 and H_2O in the air. This was accomplished with loose fitting lids, as shown in Figure 37. The off-gassing of the LN_2 was sufficient to oppose the diffusion in the air. It was found necessary to refill the container with LN_2 after each drop, since the heat capacity of the disc is large relative to the LN_2 container capacity. The procedure followed in conducting the tests was to insert the disc into the LN_2 while at room temperature, and release the test package when the disc temperature reached the desired point on the cooling curve.

Figures 38, 39, and 40 present the results obtained immediately preceding and during the free-fall, corresponding to $a/g \cong 0.008$, for the three orientations used; vertical, horizontal up and horizontal down, respectively.

Included on each is a dotted line representing the data for $a/g = 1$ from the corresponding orientations in Figures 33, 34, and 35.

Each darkened symbol on Figures 38-40 is a data point immediately preceding a free-fall. Comparison of these with the dotted lines reveals the degree of reproducibility possible. Since the heat capacity of the disc is large relative to the sphere, the temperature change during free-fall is considerably smaller, even in the regions of high heat flux. Consequently, a large number of drop tests were necessary to cover the entire boiling curve. Each drop test in Figures 38-40 is represented by a number alongside the data point. The open points are measurements during free-fall. In some cases changes occurred during the fall, which are designated by the accompanying symbols E or L to indicate the early or late part of the free-fall period. In several instances an intermediate point M is included.

Figure 38 shows results for the vertical orientation. In film boiling the heat flux continues to decrease to the end of the free-fall period. This would serve to indicate that viscous decay of the liquid momentum set up during operation at $a/g = 1$ is taking place. The liquid velocity serves to continue the vapor removal process after the onset of reduced gravity. The reproducibility between two different drops, 14 and 18, should be noted. The heat flux in drop 16 at $(q/A)_{min}$ first decreases and then increases during the fall, owing to the breakdown of the stable vapor film which leads to the onset of transition boiling. Releases during established transition boiling continues to result in decreased heat flux, again indicating a viscous decay in the liquid which is inhibiting somewhat the continuing breakdown of the vapor film which characterizes transition boiling. With release of the test package at the peak heat flux region, the results with free-fall follow those for $a/g = 1$.

Figure 39 shows results for the horizontal surface heating upward. The regular decrease of heat flux in the film boiling region as well as in the transition, peak heat flux and nucleate boiling regions upon release all indicate that a well directed liquid motion does not exist with this orientation, as did with the vertical surface. Rather, at $a/g = 1$ it is most likely that the liquid motion in the vicinity of the upper surface takes place in the form of cells, which cannot store significant amounts of momentum. Thus the process of viscous decay of the liquid momentum does not take place.

Figure 40 shows results for the horizontal surface heating downward. In the film boiling region virtually no changes take place upon release to free-fall. At $a/g = 1$ the body forces tend to keep the vapor against the heating surface. Also, if any liquid momentum is established by operation at $a/g = 1$, it is most likely directed upward toward the heating surface and outward toward the edges. In film boiling at $a/g \approx 0$ this liquid motion would also tend to keep the vapor adjacent to the heating surface. Thus one would expect little change upon release of the test package. The heat flux also remains fairly high when release takes place in the vicinity of the peak heat flux region. In fact, in the transition region the heat flux increases, indicating that liquid momentum is again a factor serving to bring the liquid into contact with the heating surface and continuing the progressive breakdown of the vapor

film. On the lower ΔT side of nucleate boiling, this same liquid momentum appears to keep the vapor in the vicinity of the heating surface, resulting in a decrease in heat flux with reduced gravity below that for $a/g = 1$ with the same orientation.

These results together indicate that the prior history has an important bearing on what will take place during low gravity boiling, and thus indicates the importance of long term reduced gravity testing to adequately predict the steady behavior of boiling in very low gravity fields.

b. LH_2

Data was obtained for boiling of LH_2 at $a/g = 1$ from the disc of Figure 30 in the various orientations. The disc was too large for the free-fall cryostat shown in Figure 8, which would be necessary for use with LH_2. Hence data with the disc in LH_2 were restricted to $a/g = 1$, using the glass cryostat in Figure 9. The results are shown in Figures 41-44 and are quite similar to those obtained with LN_2, in a relative sense.

Figure 41 shows the results for the vertical orientation. The darkened points represent the transition reruns as described earlier for LN_2. The data for Run D-040 must be discounted to some extent in the transition and nucleate boiling regions, since the pressure in the Dewar rose from 2-5 psi during the run owing to inadequate venting capacity for this first run in LH_2. Additional openings were then provided in the vessel to maintain near atmospheric pressure. Similar to the behavior with LN_2 the heat flux increased appreciably over that for the 1 in. dia sphere in the minimum heat flux and film boiling regions. The nucleate boiling and peak heat fluxes increased slightly.

Figure 42 presents results for the orientation where the heating surface was facing upward (HU). The heat flux at the lower end of the nucleate boiling region is lower than that with the sphere, again similar to the behavior with LN_2.

Figure 43 presents results for the orientation where the heating surface is facing downward (HD). The $(q/A)_{max}$ is reduced below that for the sphere, whereas the heat flux in nucleate boiling is considerably higher, for a given ΔT_{sat}, again similar to the behavior with LN_2. In Run D-044 the disc was tilted approximately 25-30° from the horizontal, so these results are not representative.

Figure 44 is a composite of Figures 41-43 for purposes of comparison. The differences in behavior with the various orientations are not as pronounced as with LN_2. This is possibly related to the differences in the acceleration of the vapor bubbles as they detach from the vicinity of the heating surface. This acceleration is proportional to

$$a \propto \frac{\rho_l - \rho_v}{\rho_v} = \rho_l/\rho_v - 1$$

$\rho_l/\rho_v - 1$ has a value of 54 for LH_2 and 175 for LN_2 at atmospheric pressure, three times as great for LN_2 as for LH_2.

C. COMPARISONS OF LH_2 DATA FOR NUCLEATE BOILING

Comparisons of nucleate pool boiling of LH_2 at atmospheric pressure and $a/g = 1$ are made in Figure 45 with data from a number of different external sources. It was desired to use data obtained only with horizontal copper heating surfaces, but only three such sets existed, from Refs. 2 and 14 plus this present work as indicated in Figure 45. It is noted that the results of Refs. 2 and 14 are quite complementary, while the disc data from Figure 42 is parallel to these but displaced by 1.5-2.0°R. It was shown in Ref. 2 that by varying the surface roughness of a horizontal stainless steel surface the nucleate boiling curve can be shifted by as much as 3.6°R. In Figure 23 of Ref. 2, it was shown that varying the surface roughness of a horizontal copper surface changes the slope as well. Surface preparation of the 1 in. dia copper sphere and the horizontal disc were similar, but no attempts had been made to make it the same as that of Ref. 2. It might have been desirable to vary the surface finish of the copper disc used for the various orientations, in Figures 41-44. Reference 2 also showed that for stainless steel with LH_2, changing from a horizontal to vertical orientation shifts the results to a higher heat flux by 1°R. Similar behavior occurred with copper in LH_2, as is noted in Figure 44.

Data for a thin lead film deposited on glass,[18] a horizontal platinum wire,[13] and a vertical brass cylinder[12] are included in Figure 45 for the sake of additional comparisons.

IV. INCIPIENT BOILING

A. STEADY STATE

Results of measuring the onset of nucleate boiling (incipient boiling) from stainless steel and copper surfaces obtained with the electrical heating steady state technique are presented in detail in Ref. 2. Efforts were continued since that time to obtain the corresponding data with aluminum surfaces, with various degrees of roughness and after being anodized. Owing to the anticipated difficulty of soldering stainless steel to aluminum, a non-soldered construction of the heater surface was used as shown on the left side of Figure 46. This was inserted in the glass cryostat of Figure 9.

1. LN_2

Figure 47 shows the results of two tests made with this configuration, heating upward in LN_2. Included on the Figure 47 are the results from Ref. 2 for the natural convection, incipient and nucleate boiling for LN_2 from polished stainless and copper surfaces. The natural convection results from the aluminum surface follow that obtained in Ref. 2 quite well, which indicates that the measurements of heat flux and temperature have acceptable accuracy. As the heat flux was increased the first bubbles began forming at the junction of the aluminum and the Teflon holder. A further increase in the power caused more sites to become active at the edge until a continuous ring of bubbles was formed. These sites on the edge then seem to feed and trigger new sites across the aluminum surface. It was not desired that the edges serve as the initial nucleating sites, since the incipient boiling then becomes a function of geometry. A further disadvantage of this system was due to the creeping of the Teflon holder. After the initial test it was not possible to maintain a vacuum on the back sides of the heater, which was necessary to keep the heat losses at a minimum.

To overcome these handicaps, attention then was directed back to the design shown on the right side of Figure 46, the same technique used in Ref. 2, in which a stainless steel foil 0.001 in. thick was soldered to the main heater body, then lapped away with lapping compound until the substrate material appeared. If a sound solder joint was present, the parent metal—solder fillet—stainless foil formed a continuous surface at which no preferential nucleation took place.

The difficulty in accomplishing this was due to the difficulty in soft soldering aluminum to stainless steel, each of which are difficult to solder in themselves. After a considerable number of trials, a procedure which was found to produce a satisfactory system at least part of the time was to "tin" the stainless foil with a stainless steel solder, "tin" the aluminum with an

aluminum solder, and then fuse the solders together. Then the stainless foil was lapped away to expose the aluminum underside, with a solder fillet holding the foil to the edge of the aluminum disc. About one out of every four trials was successful. However, owing to the difficulties in soldering, the fillet remaining was about four times as large as those obtained between the stainless steel fin and the copper surface used in Ref. 2. As a consequence the heat loss correction from the fin amounted to approximately 40% of the power input. This correction has been applied to all of the data presented.

The data obtained with two different polished aluminum surfaces in LN_2, designated as Runs 171 and 172, are presented in Figure 48. The data in the non-boiling region are observed to conform quite well with the normal natural convection correlation, and was also shown in Ref. 2 to be valid for the present configuration. This agreement demonstrates the adequacy and accuracy of the measurements made. Run 171-B was a repeat of 171-A, the same sample, for purposes of rechecking the point of formation of the initial vapor. Several points were obtained with a decreasing heat flux, which reproduced the results for increasing heat flux well. This is similar to the behavior observed with polished stainless steel and copper in liquid hydrogen, reported in Ref. 2. A difference in behavior between the two different polished surfaces did exist, indicating that some parameter, as yet unknown, was not the same in the preparation of the two surfaces.

In Figure 49 the results of incipient and nucleate boiling from the aluminum surfaces roughened with 600 grit emery powder are presented. Good comparison with the non-boiling convection correlation is again noted. The three tests were conducted successively with the identical surface. For test No. 173-A, the first of the series, a higher degree of surface superheat was achieved before nucleation took place than for the subsequent tests, indicating that once boiling had taken place, vapor of sufficient sizes became entrapped in the surface to serve as active nuclei at lower levels of surface temperature. The reproducibility of the succeeding two tests is good. Similar behavior with other materials in liquid hydrogen was reported in Ref. 2. The data in test No. 173-A are nearly vertical with increasing heat flux until the surface became completely covered with nucleating sites, at which point interaction between the bubbles results in a shift to the right. The vertical behavior of the data indicates a uniform distribution of potential nucleating sites. The data with decreasing heat flux is opposite to that observed with liquid hydrogen (i.e., the shift is to higher ΔT's rather than lower ones).

The nucleate boiling curves for the polished and roughened aluminum surfaces are superimposed on one another in Figure 50, and include data obtained with copper and stainless steel as reported in Ref. 2. The effect of roughness with aluminum is to decrease significantly the heater surface superheat for a given level of heat flux. The effect of roughness with stainless steel is not nearly so pronounced. Also, the behavior of the polished aluminum, copper, and stainless steel in liquid nitrogen are not significantly different, whereas the differences between polished copper and stainless steel

in liquid hydrogen were quite dramatic, as reported in Ref. 2. These results indicate that both the surface topographical features of the solid and the surface energies of the solid, liquid, and vapor are important elements in incipient boiling and must be takin into consideration.

Continuing difficulties in soldering the stainless steel fin to the aluminum heater surface prevented tests of aluminum surfaces with liquid hydrogen. Attempts were made to anodize the aluminum surface, but the chemical solution attacked the soldered joint. A different type of construction would be necessary to work with anodized aluminum.

The points at which the initial vapor formation occurs with LN_2 are plotted in Figure 51 on the natural convection line, where they must lie. Points 3-5 for copper and stainless steel are reprcduced from Figure 32 of Ref. 2. The general effect of roughening is to reduce the heater surface superheat at which incipient boiling takes place.

2. LH_2

A sample of the internal insulation for the S-IVB vehicle LH_2 tank was furnished by NASA Huntsville, and consisted of polyurethane foam with glass fibers and glass cloth, bonded to aluminum on one side and sealed with some type of resin on the glass cloth side. The properties given were:

Density: Approx. 10 lbm/ft^3
Mean thickness: 1 in.
C_p: 35 Btu/lbm°F
k: 0.2 - 0.4 Btu-in./hr-ft^2-°F } at mean temperature of 200°R

The fiber glass coating on the interior of the insulation material was carefully removed from its backing and glued onto a copper surface in an arrangement similar to that on the left side of Figure 46. The fiber glass extended far enough over the Teflon holder to eliminate the edge effect. The copper surface was then used as a heater for the fiber glass and the temperature of the copper was measured. In order to account for the temperature drop through the fiber glass-glue combination, an estimate of its "average" thermal resistance was made by comparing the non-boiling convection controlled portion of the q/A vs. ΔT_{sat} curve with data recorded previously. It was assumed that at a given convective heat flux, the ΔT_s will not depend on the surface material and that the difference between the two sets of readings is due to the temperature drop between the copper and the fiber glass-liquid interface.

One site on the surface tested was active at very close to zero heat flux and superheat. It is felt that this was a natural site in the material and not caused by damage to it during preparation. The points where the next two sites first became active are indicated on Figure 52. It is interesting to note that up to 3°K superheat, the curve does not have the sharp break upwards

that were obtained with the polished stainless and polished copper surfaces. The difference is most likely that the copper has a large number of cavities or a relatively uniform size that all tend to become active at about the same value of superheat. Here the surface is rough on a macroscopic scale but smooth on a microscopic scale except for a few active sites. Over the entire range tested, the boiling was not exceedingly vigorous. Data is not reported at higher heat fluxes as the thermal resistance of the fiber glass and glue changes with temperature and the temperature drop through it cannot be accurately calculated. Also included in Figure 52 is the natural convection correlation from Ref. 2.

The surface superheat in Figure 52 is an "average" value, and because of the possible variations in thichness and composition of the surface, there may be spots considerably warmer and cooler. The temperature drop across the fiber glass surface constitutes a relatively large fraction of the total temperature difference between the copper surface and the liquid. This increases the uncertainty in the "average" surface temperature, particularly as the heat flux is increased. The heat flux is based on a projected area and also has uncertainties due to difficulties in calculating losses because of unknown thermal properties. It was not possible to consider the effect of the changes with temperature of the thermal properties of the fiber glass and glue.

B. TRANSIENT

The objective of this research is to obtain experimental information on the significance of body forces on the inception of boiling of LN_2 and LH_2, particularly incipient boiling under zero gravity. Zero gravity was simulated with LN_2 in Ref. 2 by inverting the horizontal heater and contraining the natural convection at the edges. This work indicated that the heat flux at the incipience of nucleate boiling is reduced significantly, but the heater surface superheat remains essentially the same. Physically, the nucleation tendency should be influenced by body forces only insofar that natural convection is influenced. The analysis of Hsu[19] shows the dependence of the incipient boiling point on convective effects.

It was desired to provide a more direct verification of the role of body forces on nucleating behavior by subjecting a heating surface to both standard and reduced gravity, and measuring the heat flux and surface superheat directly. It would have been desirable to observe the nucleation visually as well, but limitations in the experimental apparatus did not permit this at the time. It was thus necessary to make these observations relying solely on thermal measurements. Further, since a free fall time of only 1.4 sec was available, it was necessary that the heat capacity of the heater surface be low, and the response to a change be rapid. This dictated direct electrical heating of a thin ribbon or film. If a suitable step change in power generation takes place, the temperature rises smoothly until nucleate boiling begins, at which time the surface temperature will decrease because of the more effective heat transfer due to the boiling. By selecting a material whose electrical resistance is a

reasonable function of temperature, such as platinum, both heat flux and temperature can be determined with the measurement of the heater current and voltage.

Thus, the delay time to initiate nucleation, and the heater surface superheat and heat flux at nucleation can be determined. These can be related to the normal steady values at a/g = 1 by making steady measurements of temperature and heat flux at a/g = 1, then making the transient measurements at a/g = 1. The role of the body force is then observed by comparing the transient measurements at a/g = 1 with those obtained under free fall conditions.

It was anticipated that a platinum ribbon that would be used for this work. Because of the low resistivity, currents between 50-100 amps would be necessary for reasonable widths of the ribbon. This is no problem at a/g = 1 but would entail difficulties with free fall because special electrical cables would be necessary. It was thus decided to work with a platinum wire 0.0053 in. in diameter, where the current would not be expected to exceed 5 amps.

Figure 53 is a schematic view of the holder for the 2 in. long platinum wire. Two brass strips are attached to the ends of a Teflon block, and the platinum is carefully soldered into holes in the brass in such a way that preferential nucleation does not take place at the brass strip. Potential leads are soldered to the platinum wire on the outside of the brass strips, since no IR drop takes place between the solder joint and the brass strip. Initially, the potential leads were welded to the wire between the brass strips in order to avoid the end effects, but nucleation always began at the welded junction. Since the wire is 2 in. long, it is felt that whatever small end effects are present will be negligible for the purposes of this investigation. The platinum wire holder shown is used in the glass dewar of Figure 9 for measurement at a/g = 1, and in the dewar of Figure 8 for the free-fall measurements.

Figure 54 shows the D.C. power supply used. No adjustable resistors were used in the circuit. Based on past experience with platinum wires used as resistance thermometers, wiping contacts of adjustable resistors are a source of noise, and do not permit the precise measurements of voltage and current necessary. A bank of small ceramic resistors shunted by knife switches serve to control the current. These were selected to provide fine increments of current. For the steady case with the wire measurements of current, voltage and liquid temperature were made with the potentiometer described in section II, while for the transient case with a step increase in power these measurements were recorded on the Sanborn recorder.

For precision determination of the platinum wire temperature, it is necessary that the wire be calibrated. Reference grade wire was obtained, for which the polynomial Callender-Van Dusen equation, Eq. (4) is commonly used[20]

$$T = \frac{R_t - R_o}{R_o} + \delta\left(\frac{T}{100} - 1\right)\left(\frac{T}{100}\right) + \beta\left(\frac{T}{100} - 1\right)\left(\frac{T}{100}\right)^3 \qquad (4)$$

Equation (4) was used for the work presented here using the coefficients listed below in Table V:

TABLE V

TYPICAL COEFFICIENTS FOR THE CALLENDER - VAN DUSEN EQUATION FOR PURE ANNEALED STRAIN FREE PLATINUM

α = 0.00392506
δ = 1.4927
β = 0.11035
T = °C
R_o = Resistance at 0°C
R_t = Resistance at T°C

R_o in Equation (4) was determined immediately prior to each test by calibration in the LN_2 or LH_2 used. Thus, R_t and T are both measured, and R_o computed. To insure that the current used for these calibration did not introduce self-heating errors, a number of initial tests were conducted in which the current was varied. These are shown in Figure 55, and no self-heating effects are evident. The value of I = 40 ma was generally used thereafter. With this calibration, the maximum uncertainty in the level of temperature is estimated to be $\pm$ 0.13°C, this maximum occurring at the higher levels of wire current under test conditions.

Figure 56a shows a typical result of a transient test with a step increase in power to the wire. Based on this, it was necessary to define the various time "delay" intervals, as indicated in Figure 56b. Three segments are defined as below:

τ_1: The transient delay time for the wire to reach the new "steady" temperature.

τ_2: The dwell time during which the fluid surrounding the wire is heated and natural convection occurs. This is sustained until nucleate boiling begins. Sometimes $\tau_2 = 0$.

τ_3: The propagation time for the nucleation to spread across the entire length of the wire.

E_{max}: The maximum voltage drop across the platinum wire during the process. Corresponds to ΔT_{max}.

E_{ss}: The new steady voltage drop across the platinum wire. Corresponds to ΔT_{ss}.

Since the resistance of the platinum wire is a small portion of the circuit resistance, the voltage across the platinum wire is a direct function of its resistance and hence its temperature. ΔT_{max} is not necessarily the incipient ΔT_{sat} obtained with steady techniques, since a transient diffusional process

is taking place in the liquid during τ_2. It should be possible to compute the temperature distribution in the liquid at the end of period τ_2, and then relate this to the condition for the activation of a nucleating site.

Visual observation at a/g = 1 has confirmed that nucleating sites spread across the wire during period τ_3, when nucleate boiling causes the wire temperature to drop. The rate at which it drops depends on the level of the imposed heat flux.

The procedure for the transient tests at a/g = 1 was to repeat the step change in power level a number to times for each power level to determine the reproducibility. The time intervals between tests was varied in regular patterms to observe if this had any influence on the delay times. This was observed not to be the case. For the transient tests at $a/g \approx 0$, the tests were repeated 3-4 times at a/g = 1, then again immediately following the release of the test package. This sequence was then repeated several times before increasing the level of the current.

1. LN_2

Figure 57 shows data in the natural convection and nucleate boiling regions obtained with the platinum wire in liquid nitrogen under steady conditions. The non-boiling convection compares quite well with a correlation obtained for the comparable geometry.[21] The nucleate boiling portion of the curve is steep, indicating that the nucleation cavities are quite uniform in size. Upon decreasing the heat flux, nucleate boiling persisted for a ΔT_{sat} below that necessary to initiate boiling. Also included for the sake of a reference point are the results for flat horizontal surfaces, and two other materials. It should be noted that the incipient boiling point occurs at about the same ΔT_{sat} for the platinum wire as for the horizontal surfaces, but at a considerably higher heat flux. The latter is a consequence of the difference in geometry.

Also included in Figure 57 are the levels of heat flux applied in the step changes of power input—the transient process. Heat flux levels lower than those shown resulted in no boiling at all, while those levels higher than shown reverted to film boiling. At a/g = 1, film boiling occurred at q/A = 3.26 watts/cm^2, considerably below the heat flux levels obtained with nucleate boiling under steady conditions. For a large surface the burnout or peak heat flux with LN_2 is $(q/A)_{max}$ = 15.2 watts/cm^2 at a/g = 1.[9] Owing to the rapid transient, combined with the small size of wire, the liquid attains a high degree of super-heat with no natural convection being induced yet. Once the first site becomes active, the remaining superheated liquid probably flashes into vapor, which surrounds the wire. Since the imposed heat flux is above the minimum for stable film boiling, the film boiling condition remains. This indicates the desirability of using the transient technique with larger sized surfaces, which would not be so prone to pass into film boiling as readily as

the smaller surfaces. Nevertheless, even though the wire passes into film boiling, it was possible in some cases to detect the point at which this occurs, which constitutes the initial nucleation point. Figure 58 shows two examples of this for $q/A = 3.26$ watts/cm^2, one passing directly into film boiling and the other passing into film boiling after a slight delay.

In order to assess the reproducibility of results obtained, a number of tests were repeated consecutively. Figure 59 shows one typical set at $a/g = 1$. While ΔT_{ss}, ΔT_{max} and τ_1 are fairly reprodicible, τ_2 and τ_3 are not. This means that it may not be possible to utilize the latter two parameters as indicators in assessing the influence of a/g on the incipient boiling process. Note that the ΔT_{ss} value in Figure 59 falls on the steady value plotted in Figure 57, and serves as a continual check on the experimental measurements. All tests were repeated a sufficient number of times so that a statistically meaningful sample was obtained. The results to be presented represent mean values for each case. Each free fall point is the mean of at least four tests, and each point at $a/g = 1$ prior to the free fall point is the mean of 16 tests.

The initiation and establishment of nucleate boiling under free-fall conditions appeared to be an unstable phenomena, as noted in Figure 60. The free-fall test immediately followed the one at $a/g = 1$. The ΔT_{max} under free-fall is the same as that at $a/g = 1$, and is defined as that point where the wire temperature has a momentary decrease. It then increases to a maximum value, then decreases in a somewhat irregular fashion to a steady value at $a/g = .008$. After impact the wire reaches a temperature equal to that of the prior test at $a/g = 1$.

Figure 61 is a plot of the delay time τ_1 versus heat flux for the initial tests conducted at $a/g = 1$, and for the free-fall tests along with the tests at $a/g = 1$ immediately preceeding the drop. The heat flux is not the actual heat flux at the surface of the wire, but rather the equivalent power input to the wire, since a transient process is taking place. Where the rate of change of wire temperature is zero, then this parameter is the steady heat flux. Although some scatter is present there does appear to be a trend of a decrease in τ_1 as heat flux increases, but with no particular effect of a/g. τ_1 is defined as the time taken for the wire to reach a new steady operating temperature or for nucleation to begin. If this is governed solely by the transient conduction process in both the wire and the surrounding stagnant liquid, then it is reasonable that τ_1 decrease as the power generation in the wire increase, and that it be independent of a/g, as appears to be the case.

No consistancy appeared in the behavior of delay time τ_2, as was observed in Figure 59 at $a/g = 1$. Nor was any pattern of behavior obvious at $a/g \approx 0$. τ_2 is the delay time between the point where the wire reaches its steady or maximum temperature, and where nucleate boiling is initiated. Since at the end of period τ_1 little or no further changes in temperature of the wire are taking place, the equivalent of an imposed heat flux on the liquid domain is present, and the temperature distribution in the liquid could be computed. If

specific cavities in the surface are activated in accordance with the theory based on the work of Hsu[19] then the temperature at certain locations in the liquid must reach a specific value for this activation to take place. To determine the sensitivity of the temperature distribution in the liquid to the delay period τ_2, it will be necessary to solve the diffusion equation in the liquid surrounding the wire. This remains as a future task.

Figure 62 shows the transient delay time τ_3 as a function of the equivalent steady heat flux for both a/g = 1 and a/g ≈ 0. τ_3 represents the period of time for the initial nucleation sites to spread to cover the entire surface. As pointed out in connection with Figure 57, there exists only a certain range of heat flux at a/g = 1 within which it is possible to obtain nucleate boiling with the process of the step change in heat flux. Below this value nucleation does not occur, while above this value the process reverts directly to film boiling. These are indicated in Figure 62. It appears that under free-fall conditions (a/g = .008) that this range of heat flux is reduced. Using the value of the burnout heat flux for a large surface in LN_2 at atmospheric pressure of $(q/A)_{max}$ = 15.2 watts/cm^2 at a/g = 1, this is reduced to $(q/A)_{max}$ = 4.5 watts/cm^2 at a/g = 0.008, using the proportionality of $(q/A)_{max}$ on $(a/g)^{1/4}$. This latter value is about 50% higher than the maximum attainable nucleate boiling heat flux in Figure 62. The comparison is not unreasonable considering the effects of differences in size and the transient procedure used.

It is also interesting to note in Figure 62 that with free fall, as the heat flux is increased the delay time τ_3 also increases. The rate at which nucleation spreads across the wire is believed to be related to the rate at which the disturbances caused by the bubbles spreads across the surface. The disturbances in this case would be the result of seeding of potential nucleation sites from adjacent active sites. Increasing the power level would increase the liquid superheat and hence supposedly increase the effectiveness of the seeding process. This evidently is not the case.

Figure 63 shows the plot of the maximum transient superheat ΔT_{max} as a function of the heat flux. This is the maximum superheat of the wire before nucleation takes place. The values of ΔT_{max} are considerably higher than the steady state values of Figure 57. Also included in Figure 63 are the steady natural convection and steady nucleate boiling curves for the platinum wire as taken from Figure 57. It should be noted that the values of ΔT_{max} vary linearly with the steady heat flux along an extension of the steady state natural convection curve. This is representative of a diffusion limited process, which most likely is the case because of the small size of wire used. One might postulate the following process taking place after the step increase in power: a thin thermal boundary layer is established very rapidly before nucleation takes place. For nucleation to begin, the temperature at some location outside this boundary layer must reach some specific value. With the transient power input, the wire temperature must be higher than that obtained in a steady process in order that the liquid temperature reach this specfic value.

Since the behavior of ΔT_{max} in Figure 63 is independent of the body force, this would indicate that the initial nucleation process is governed by the temperature at some location in the liquid, and independent of gravity. With steady techniques and under circumstances such that convective effects would be small, this temperature is approximated by the heater surface temperature, as was demonstrated in Ref. 2. The level of heat flux at which nucleation takes place, however, is very sensitive to convective effects and geometrical effects as well.

2. LH_2

The general procedures described in the preceding section were repeated using liquid hydrogen at atmospheric pressure. Since the electrical resistance of the wire is reduced considerably at LH_2 temperatures it was necessary to operate at relatively higher levels of current to obtain a given heat flux. This resulted in limitations in the heat flux with free-fall because of the small size of wire in the flexible drop cables.

Figure 64 shows the data in the natural convection and nucleate boiling regions obtained with the platinum wire in liquid hydrogen under steady conditions. The non-boiling results do not compare well with the correlation for small wires,[21] whereas with LN_2 the comparison was quite good. The nucleate boiling data also does not compare well with the results of others[13] for the same geometry. It appears as if the results in Figure 64 are shifted to lower ΔT's, which most likely is due to errors in the relative level of temperature. These errors of relative temperature are of minor consequence in the present investigation, where the differences in behavior at $a/g = 1$ and $a/g \approx 0$ are sought.

Included in Figure 64 for the sake of a reference point are the results of natural convection and nucleate boiling for a large horizontal surface in LH_2. It should be noted that the initial incipient boiling points differ by 0.4°K, for these two different systems, whereas the comparison in LN_2 was good (Figure 57). Also included in Figure 64 are the levels of heat flux applied in the transient process for both the tests at $a/g = 1$ and $a/g \approx 0$. Heat flux levels around 0.3 watts/cm^2 resulted in no boiling at $a/g = 1$, whereas boiling took place at $a/g = 0$. No film boiling occured in any of the tests with LH_2.

Reproducibility tests were conducted in LH_2 similar to those presented in Figure 59, with similar results. The delay time defined as τ_2 did not appear in any of the tests, or at the most was very small as on the left side of Figure 65. Either nucleation occurs immediately when the wire temperature reaches a certain value, or it does not occur at all, again unlike the behavior in LN_2. This difference cannot be related to differences in the temperature distribution in the liquid since the thermal diffusivity of LH_2 is only about twice that of LN_2 at atmospheric pressure. This behavior therefore is most likely a consequence of interfacial energy differences.

Figure 65 shows typical differences of τ_1, τ_3, and ΔT_{max} at a/g = 1 associated with variations in heat flux. In general τ_1 decreased and ΔT_{max} increased as heat flux was increased, τ_3 was somewhat irregular.

Figure 66 is an example of the data obtained when the heat flux is initiated during free-fall. The effect of the impact of the test package on the wire temperature, due to liquid sloshing, etc., is indicated by the lower trace on the right.

Figure 67 is the plot of the delay time τ_1 versus heat flux for the independent tests conducted at a/g = 1, and for the free-fall tests and the tests at a/g = 1 immediately preceding the drop. The distinct decrease in τ_1 as heat flux increases is similar to the behavior with LN_2, and the absence of any effect of a/g again indicates that the process taking place is governed by conduction only.

Figure 68 shows the transient delay time τ_3, which decreases as heat flux increases. Some irregularity is noted between the two sets of tests at a/g = 1. Under reduced gravity the delay time τ_3 decreases, for a given heat flux, which is opposite to the observations noted with LN_2 in Figure 62. Also noteworthy in Figure 68 is the relatively large magnitude of τ_3 with LH_2 when compared to LN_2.

Figure 69 is a plot of the maximum transient superheat ΔT_{max} as a function of heat flux, which is the maximum superheat of the wire immediately prior to nucleation. Also included are the steady natural convection and the steady nucleate boiling results of Figure 64. The irregularity in the data between the two sets of data similar to that in Figure 68, is to be noted. The two processes represented in the figures, τ_3 and ΔT_{max}, are related; an increase in ΔT_{max}, for a given heat flux, corresponds to a decrease in τ_3, since a higher ΔT_{max} corresponds to a higher superheat in the liquid immediately adjacent to the heater surface.

The lack of any change in ΔT_{max} in reducing the body forces from a/g = 1 to a/g = 0.008 again indicates that the initial nucleation process is independent of gravity. The rate at which this nucleation spreads, once having started, does appear to be gravity sensitive, as manifested in Figure 68 by τ_3. As mentioned earlier, the level of heat flux at which nucleation takes place is sensitive to convective effects, and hence gravity.

In Ref. 22 zero gravity pool boiling was simulated by the use of a magnetic-colloidal suspension in the presence of a magnetic field to counter the body force due to gravity. The simulated zero-gravity appeared to result in a decrease in the initial incipient boiling point by about 5°F for the system used. As the authors point out, the simulation of zero gravity by the colloid suspension is not complete since the vapor phase is still subjected to the earth gravity. It should also be emphasized that the liquid phase also is always subjected to earth gravity, and it is only the viscous interaction between the liquid and solid particles that can result in an effective decrease

in the buoyant forces. Since at the initial incipient boiling point the vapor phase is not yet present, it appears more likely that the decrease in the incipient boiling point observed by the authors is a result of the solid particles acting as nucleation sites, as suggested by the authors. This possibility was first suggested in work reported with nucleate boiling of water at high pressures,[23] in order to explain an observed change in ΔT_{sat} with changes in concentration of suspended solid particles.

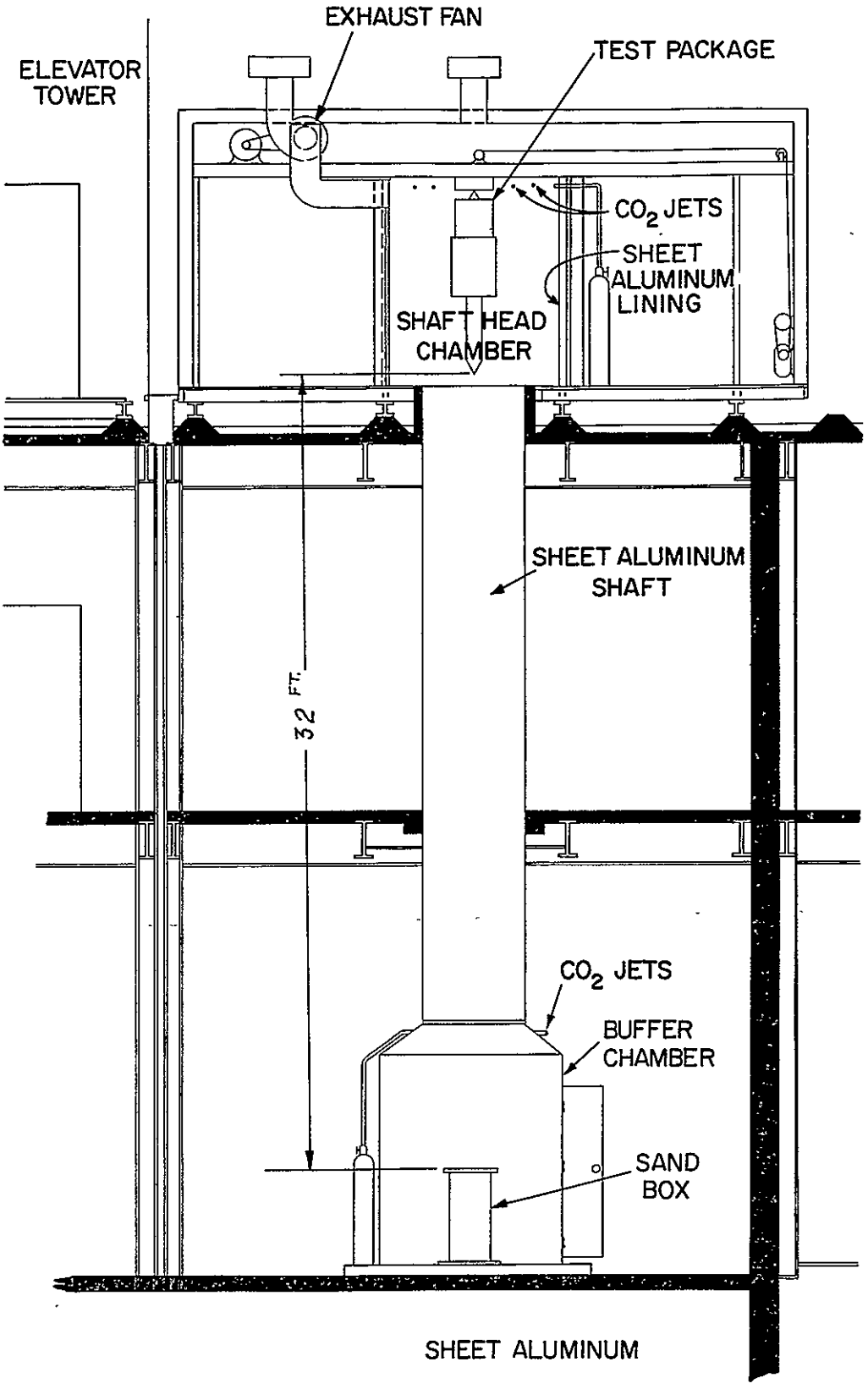

Figure 1. Drop tower—elevation.

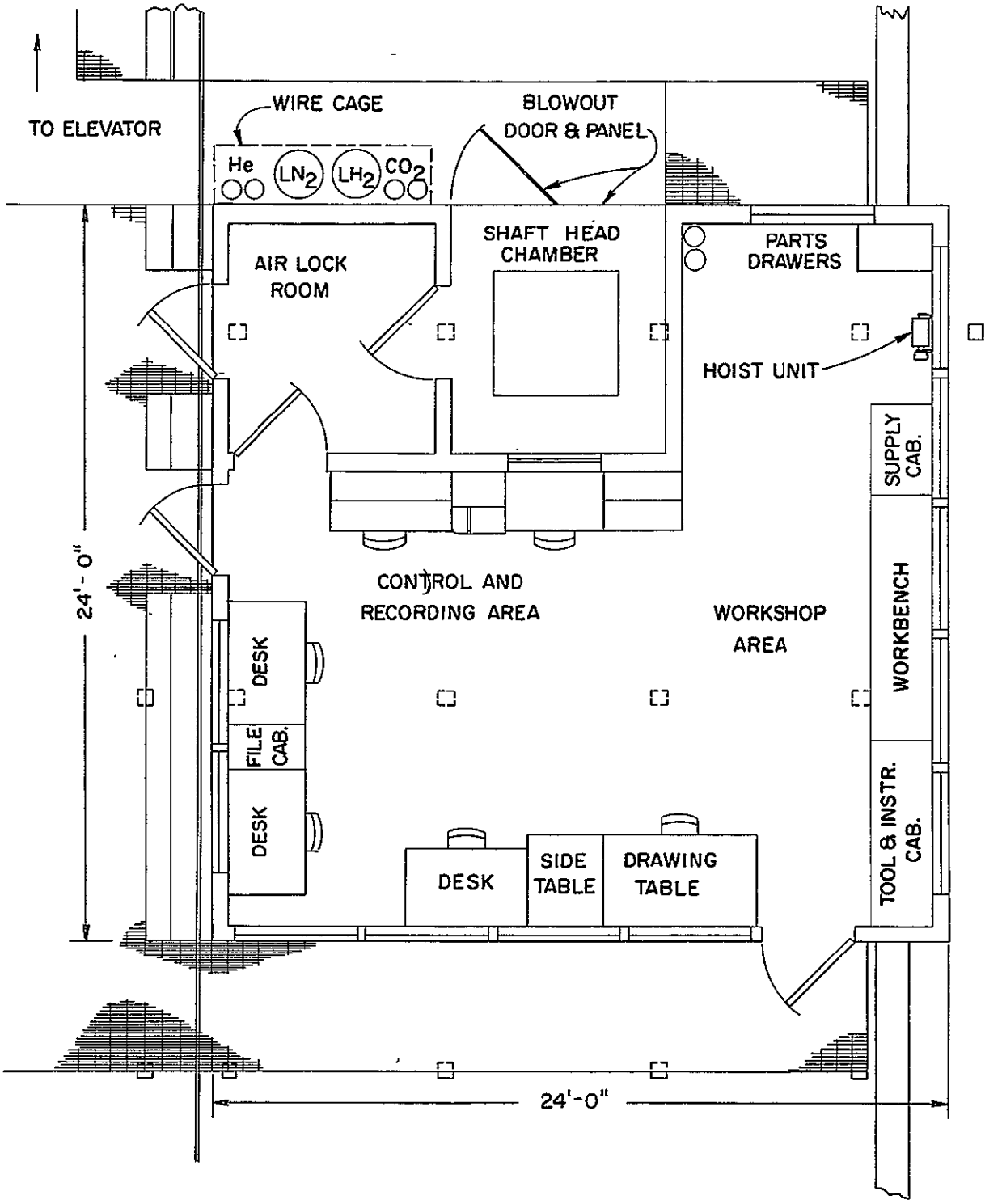

Figure 2. Drop tower—plan on third floor.

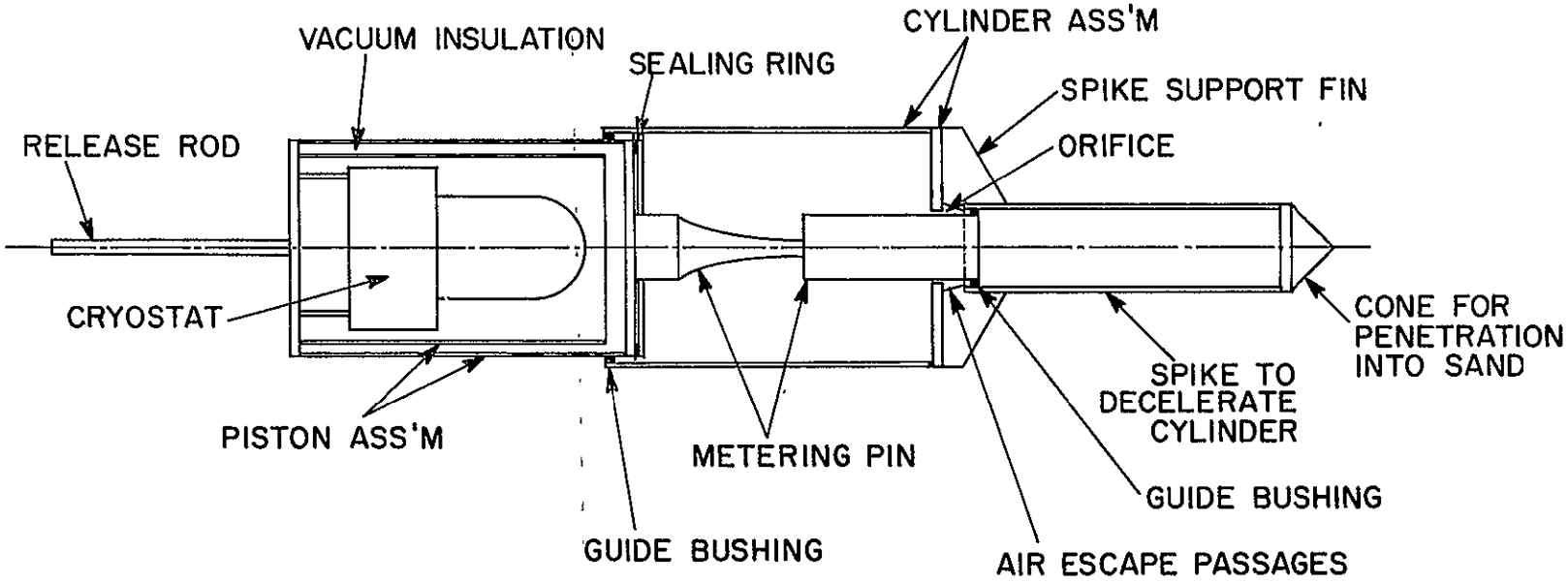

Figure 3. Drop package.

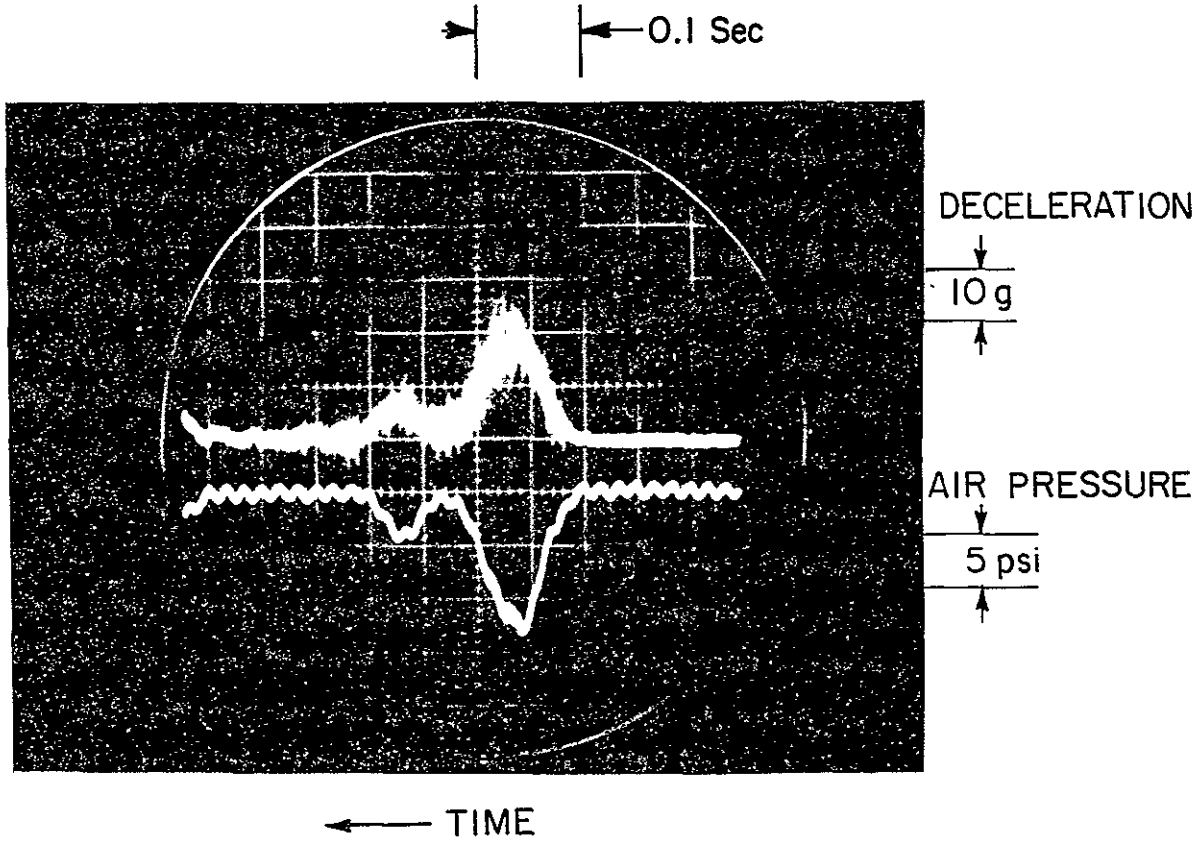

Figure 4. Drop package deceleration--inner cylinder; oscilloscope trace.

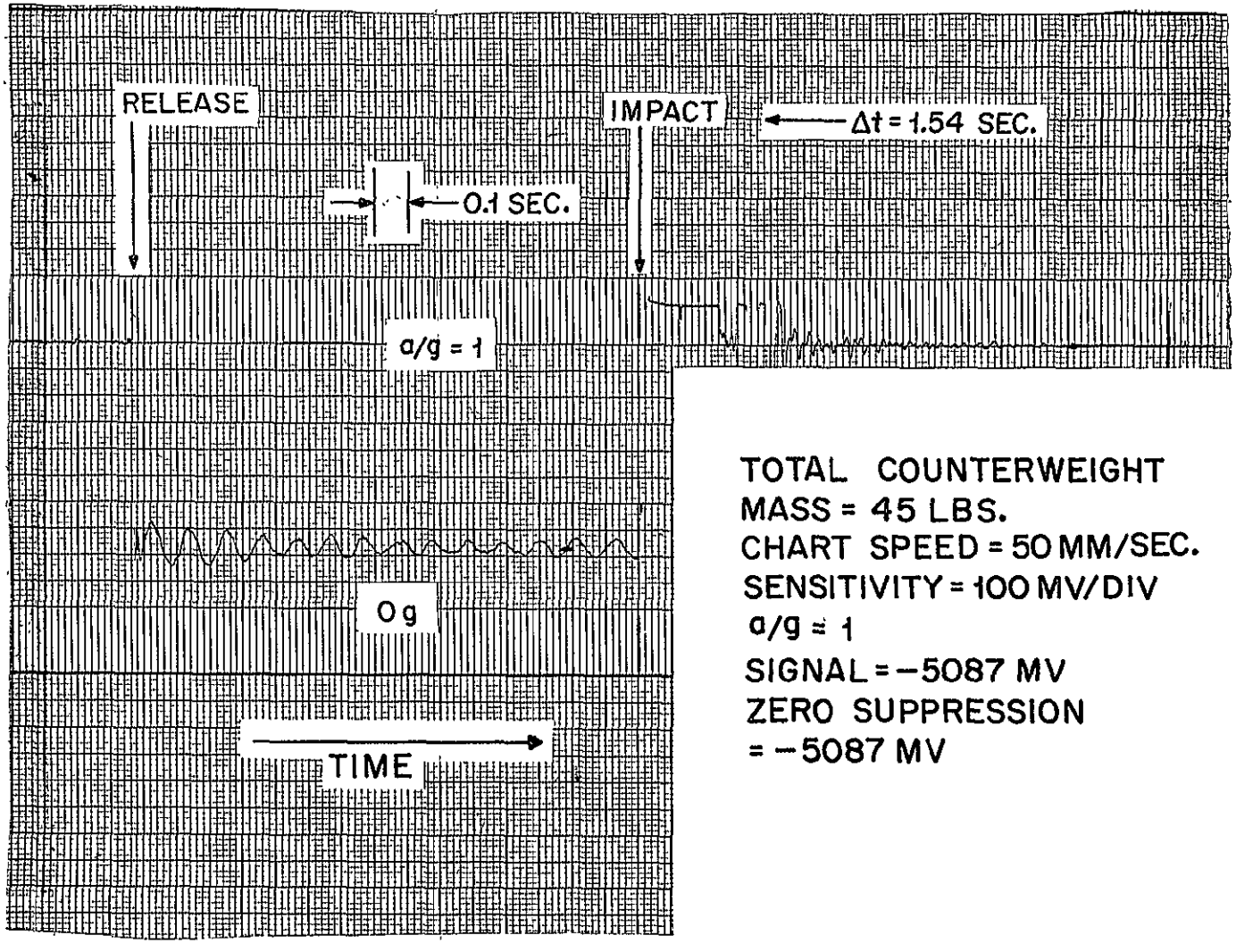

Figure 5. Accelerometer measurement with fractional gravity.

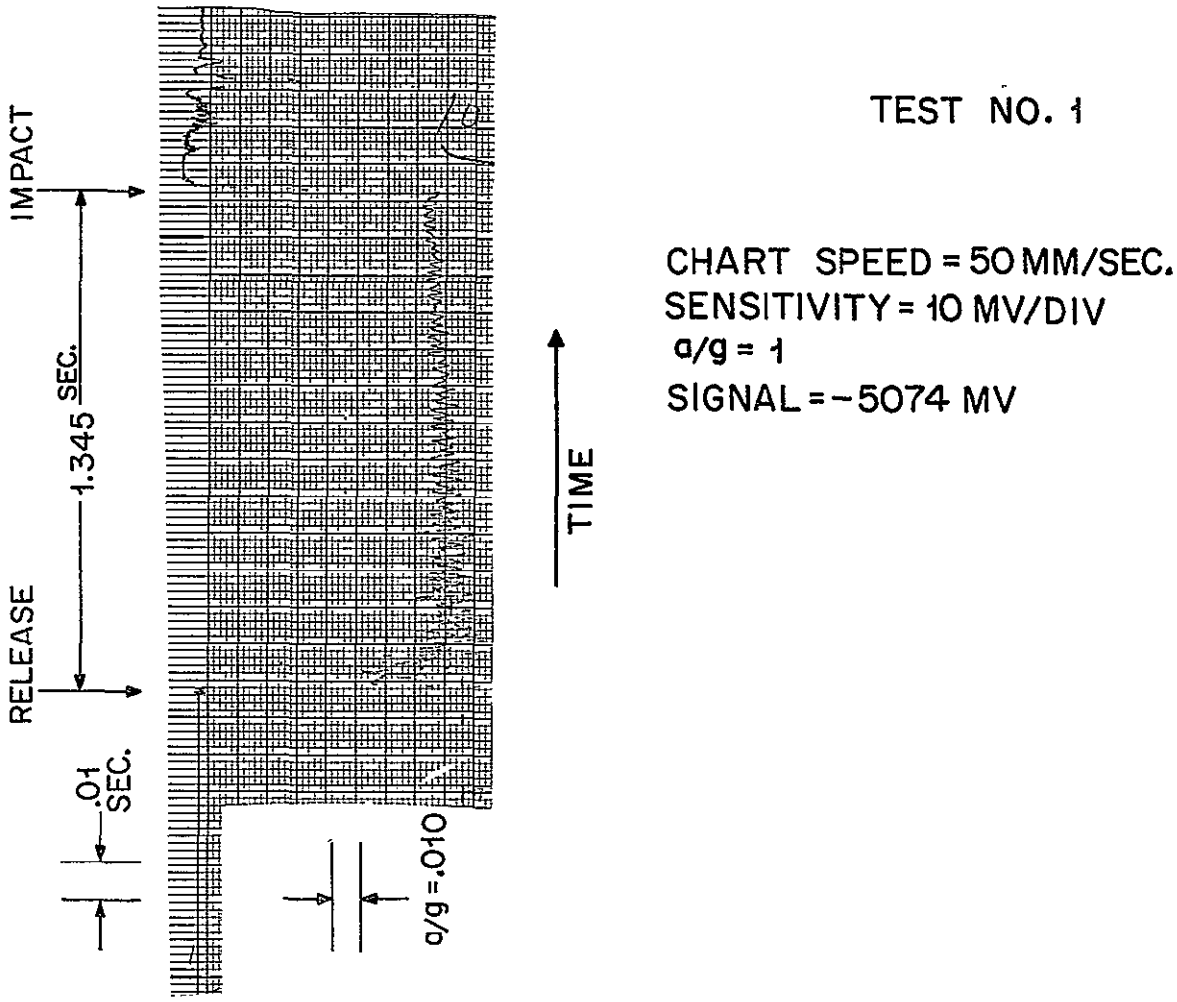

Figure 6. Accelerometer measurements with free fall.

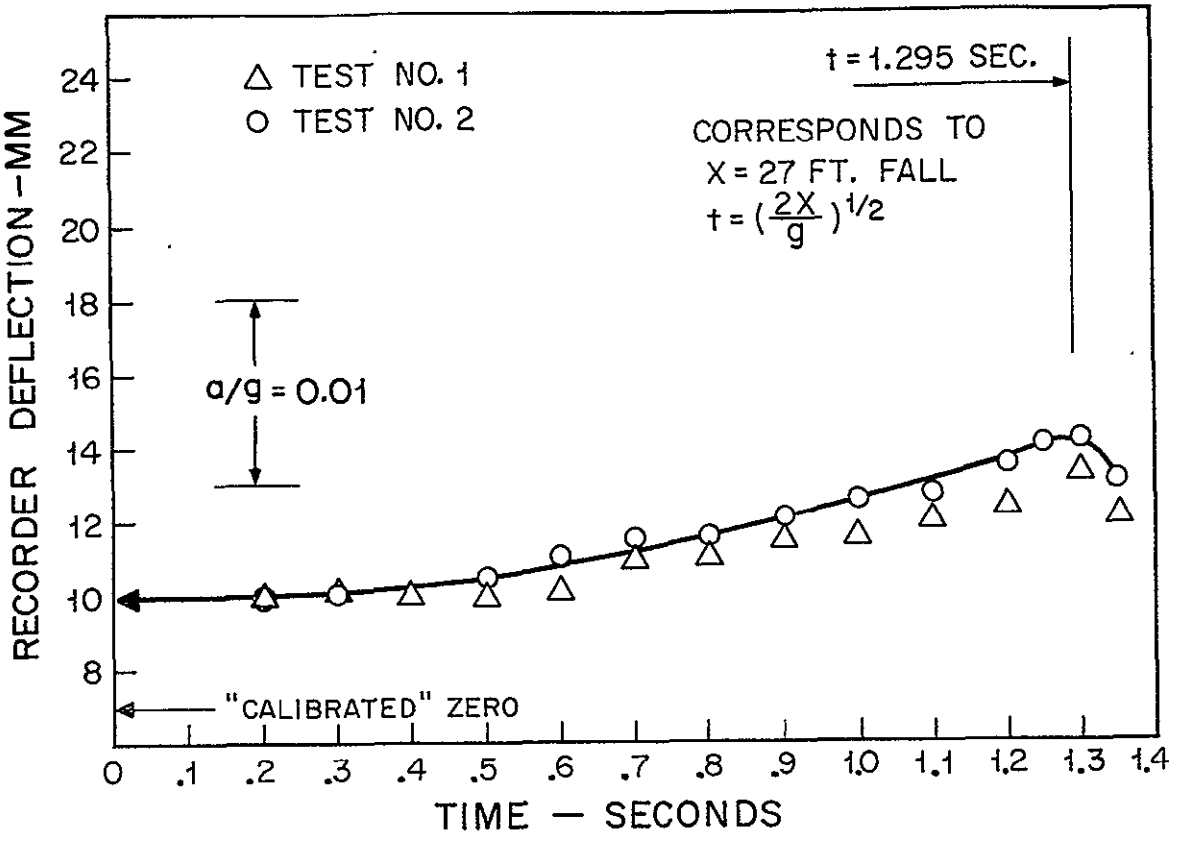

Figure 7. Smoothed plot of free fall acceleration measurement.

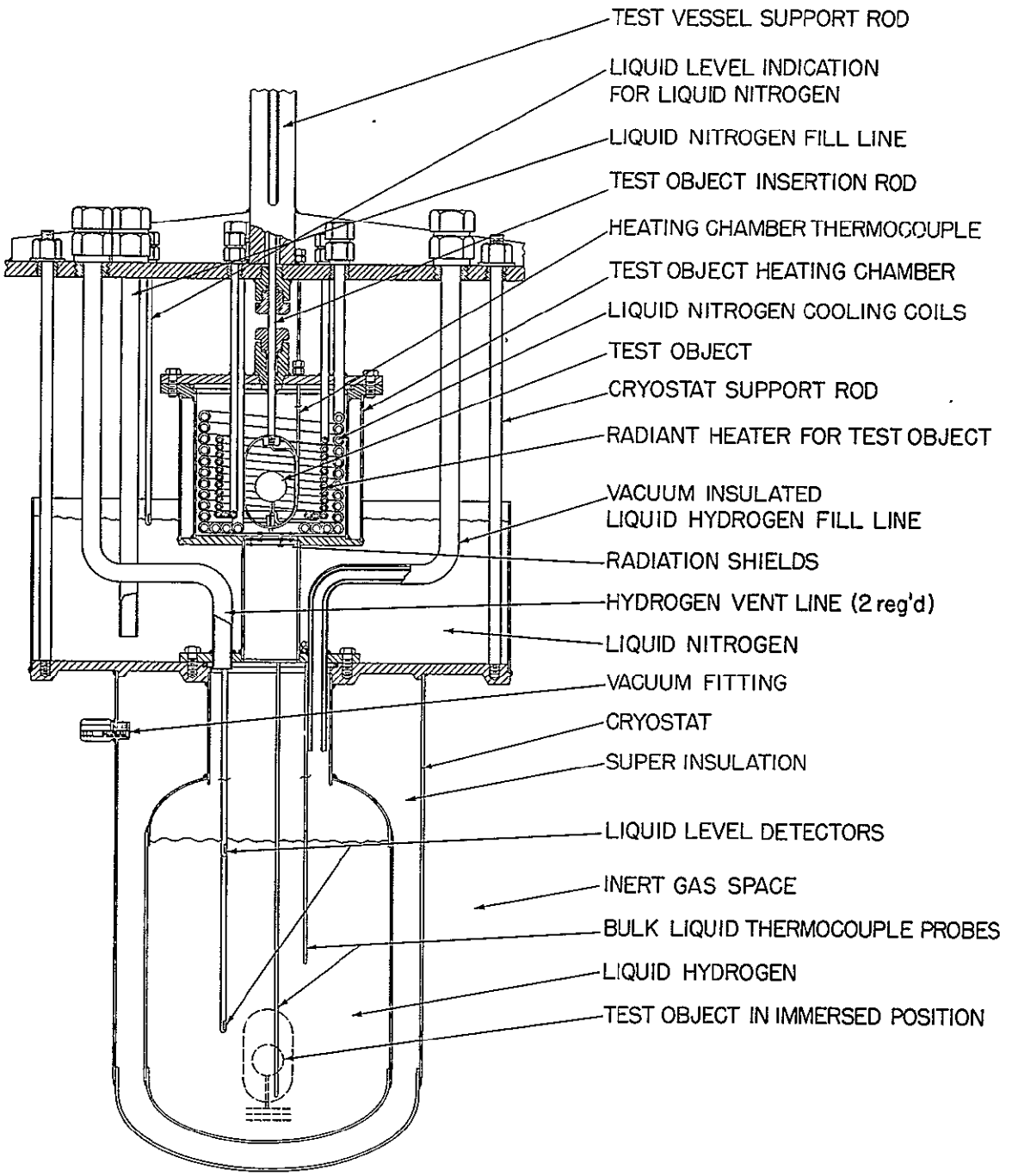

Figure 8. Cryostat test vessel for fractional gravity.

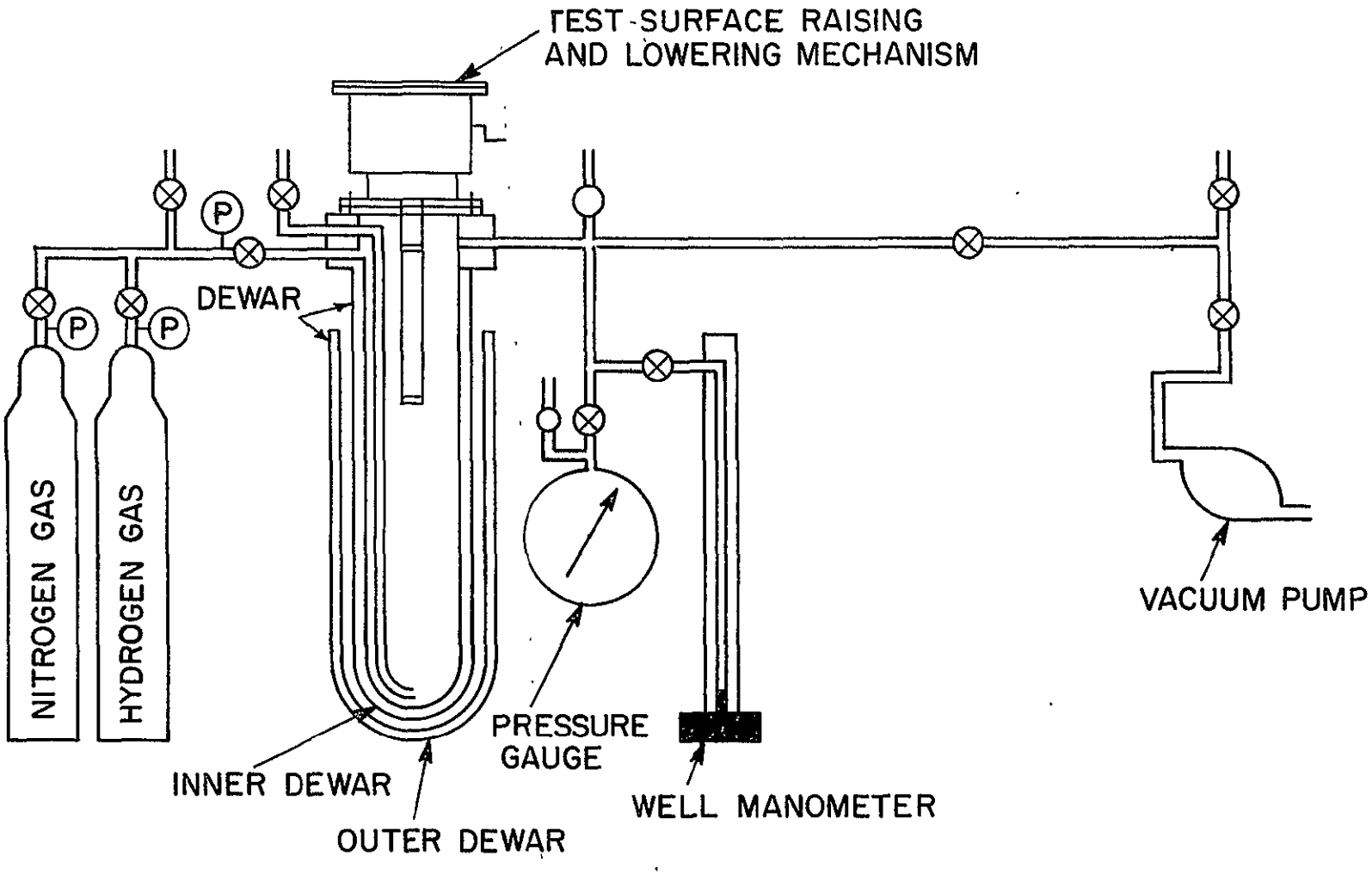

Figure 9. Cryostat test vessel for a/g = 1.

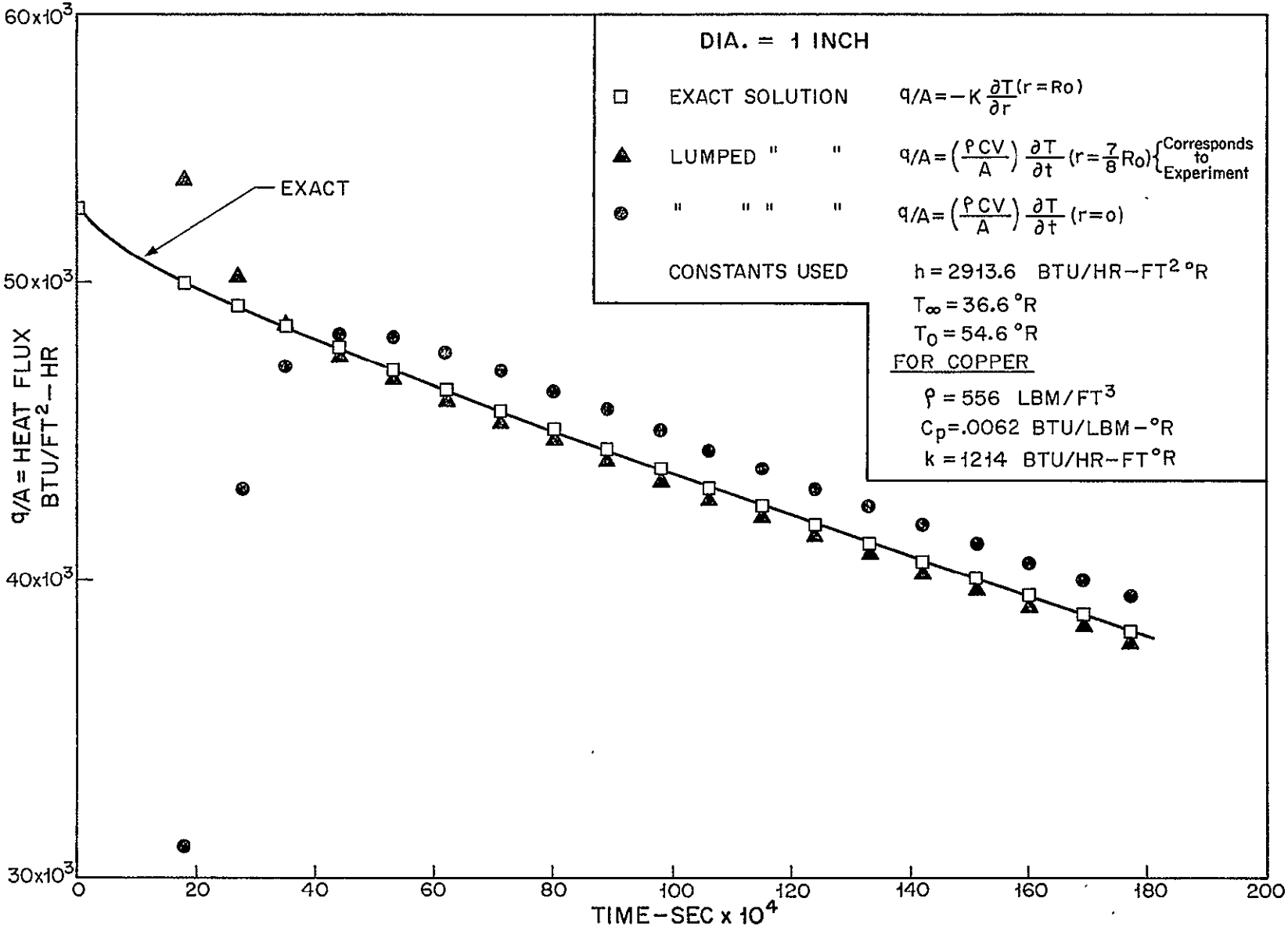

Figure 10. Computations to assess lumped character.

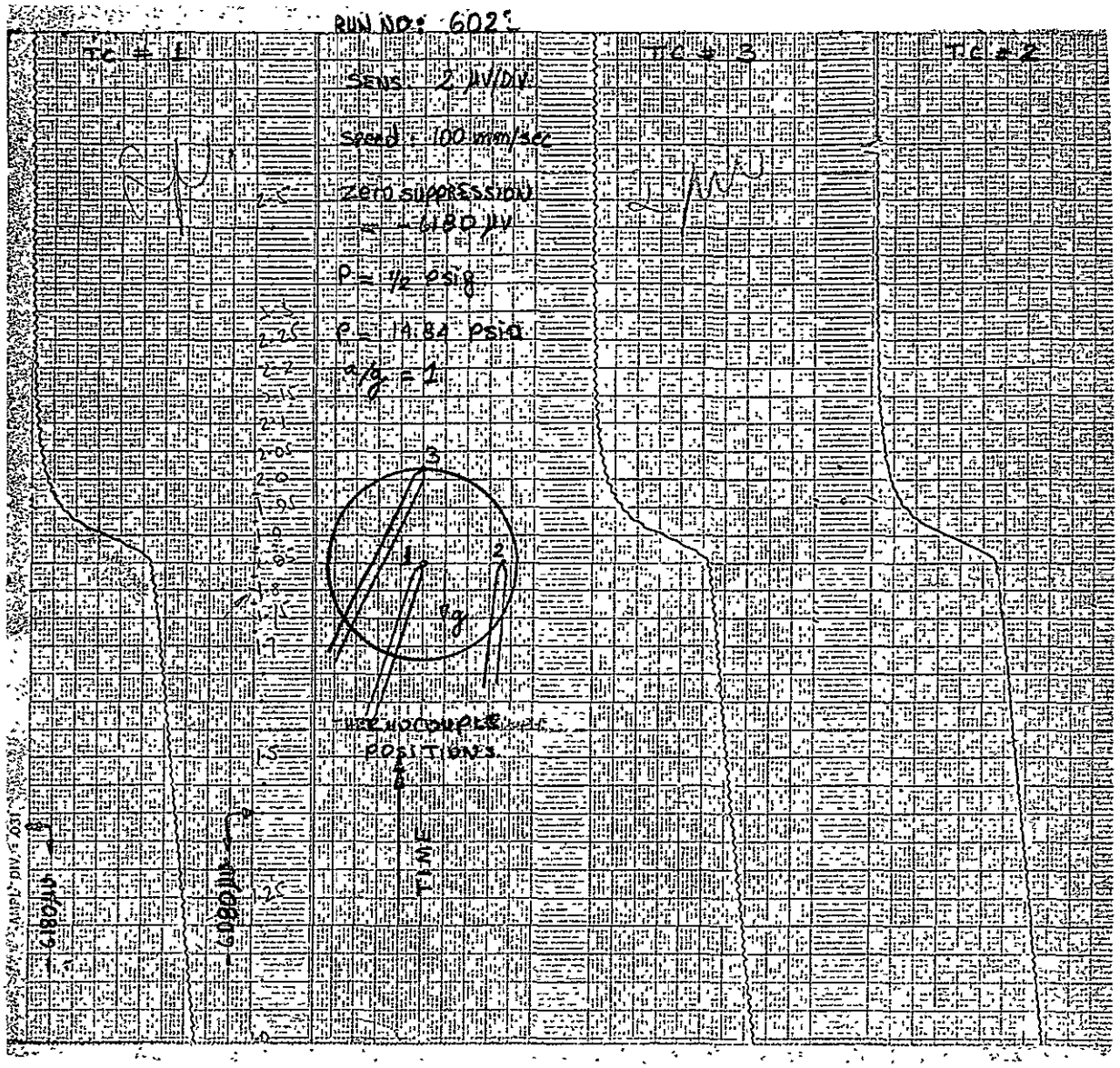

Figure 11. Representative data for 1 in. dia sphere in LH_2.

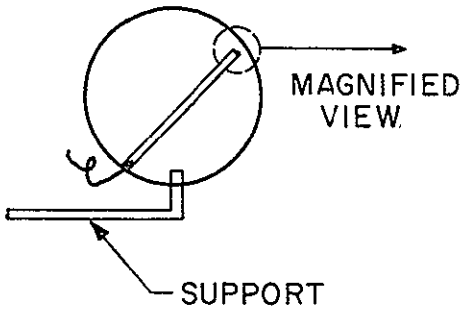

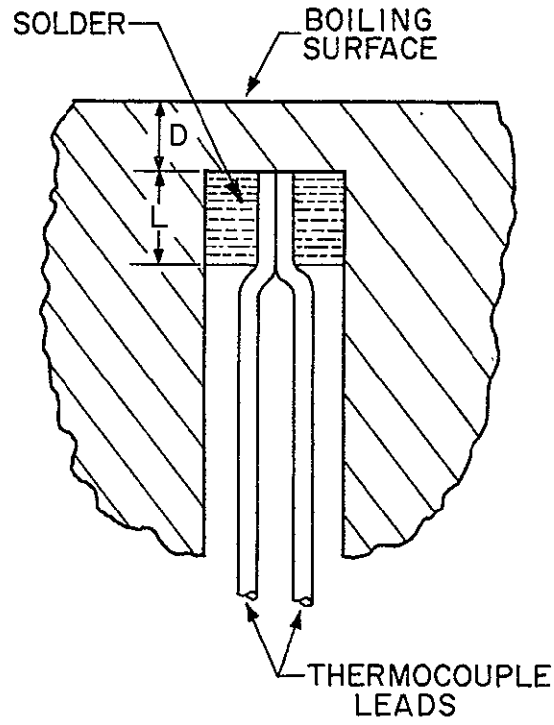

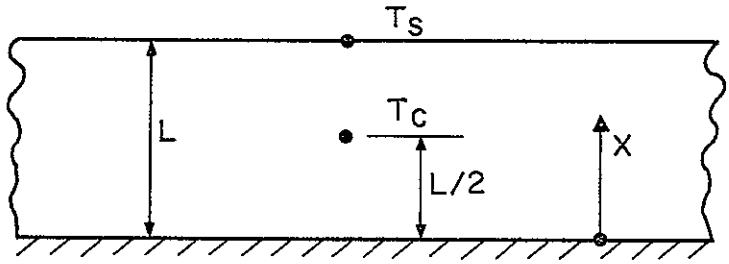

MATHEMATICAL MODEL

GOVERNING EQUATION

$$\frac{1}{a}\frac{\partial T}{\partial t} = \frac{\partial^2 T}{\partial X^2}$$

BOUNDARY CONDITIONS

$$T(X,0) = T_0 \; ; \; \frac{\partial T(o,t)}{\partial X} = 0 \; ;$$

$$T(L,t) = T_S = A_0 e^{-mt}$$

Figure 12. Model for effect of solder on error.

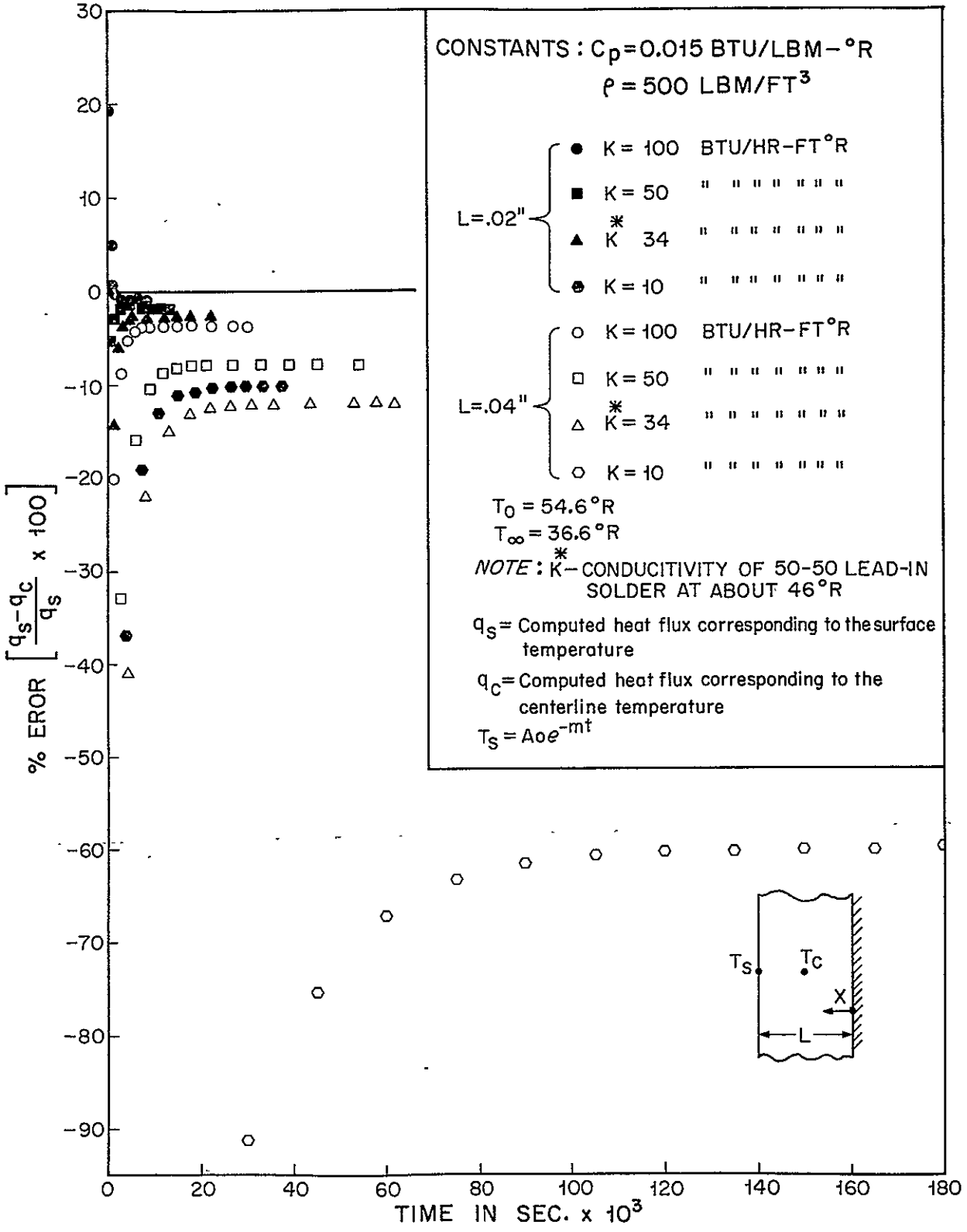

Figure 13. Effect of solder on error in heat flux.

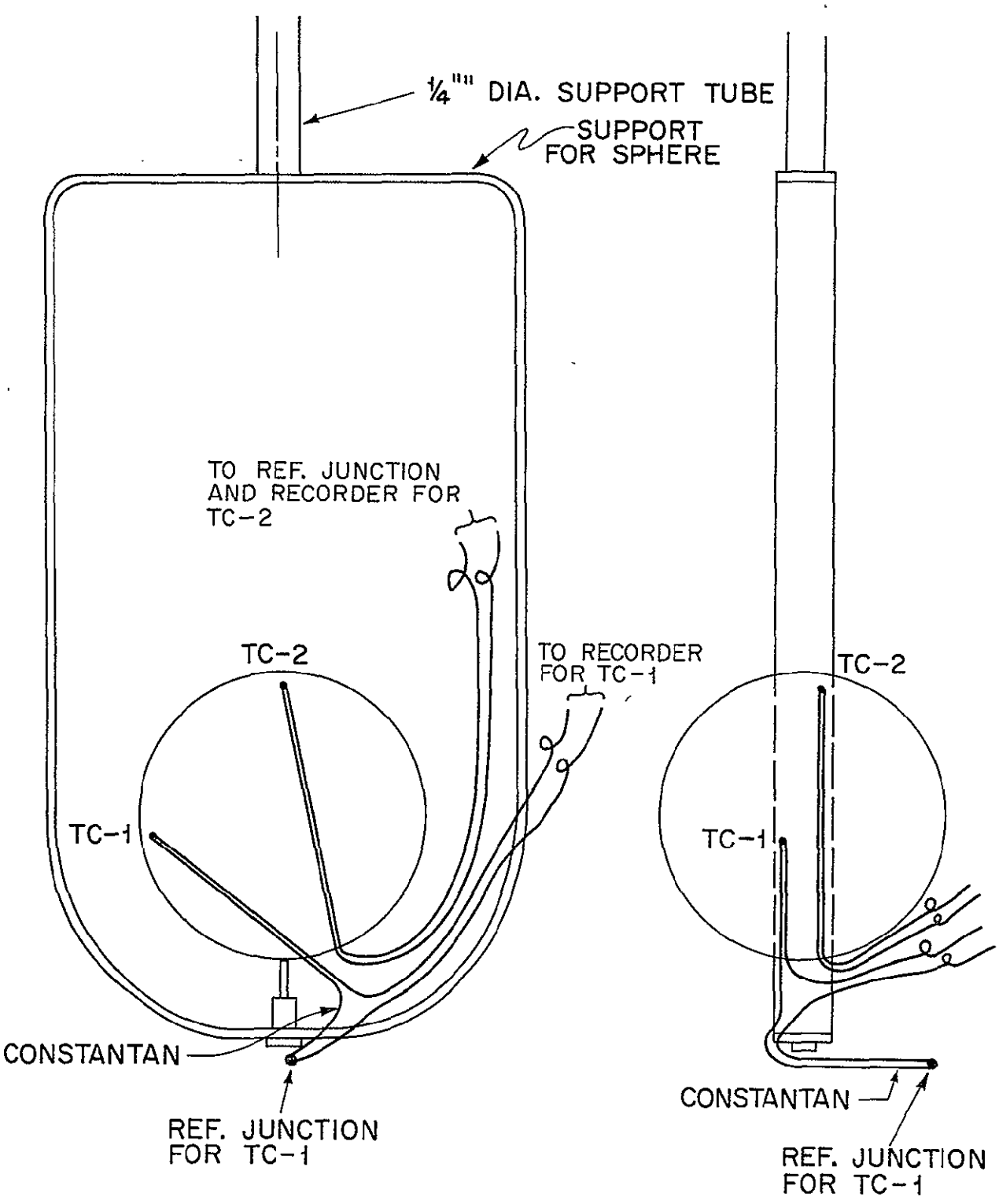

Figure 14. Location of thermocouples in sphere.

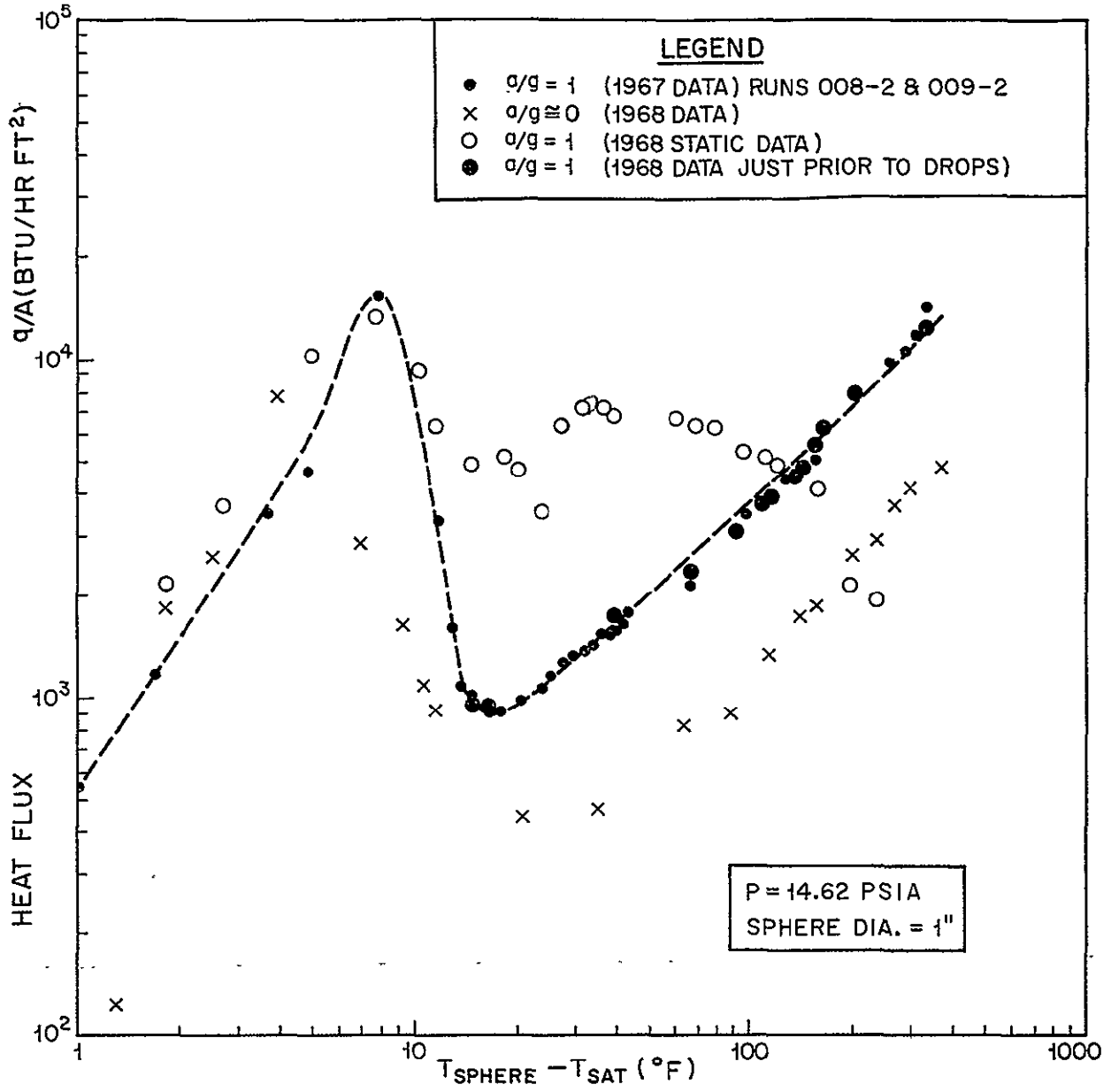

Figure 15. Preliminary boiling data, to saturated liquid hydrogen.

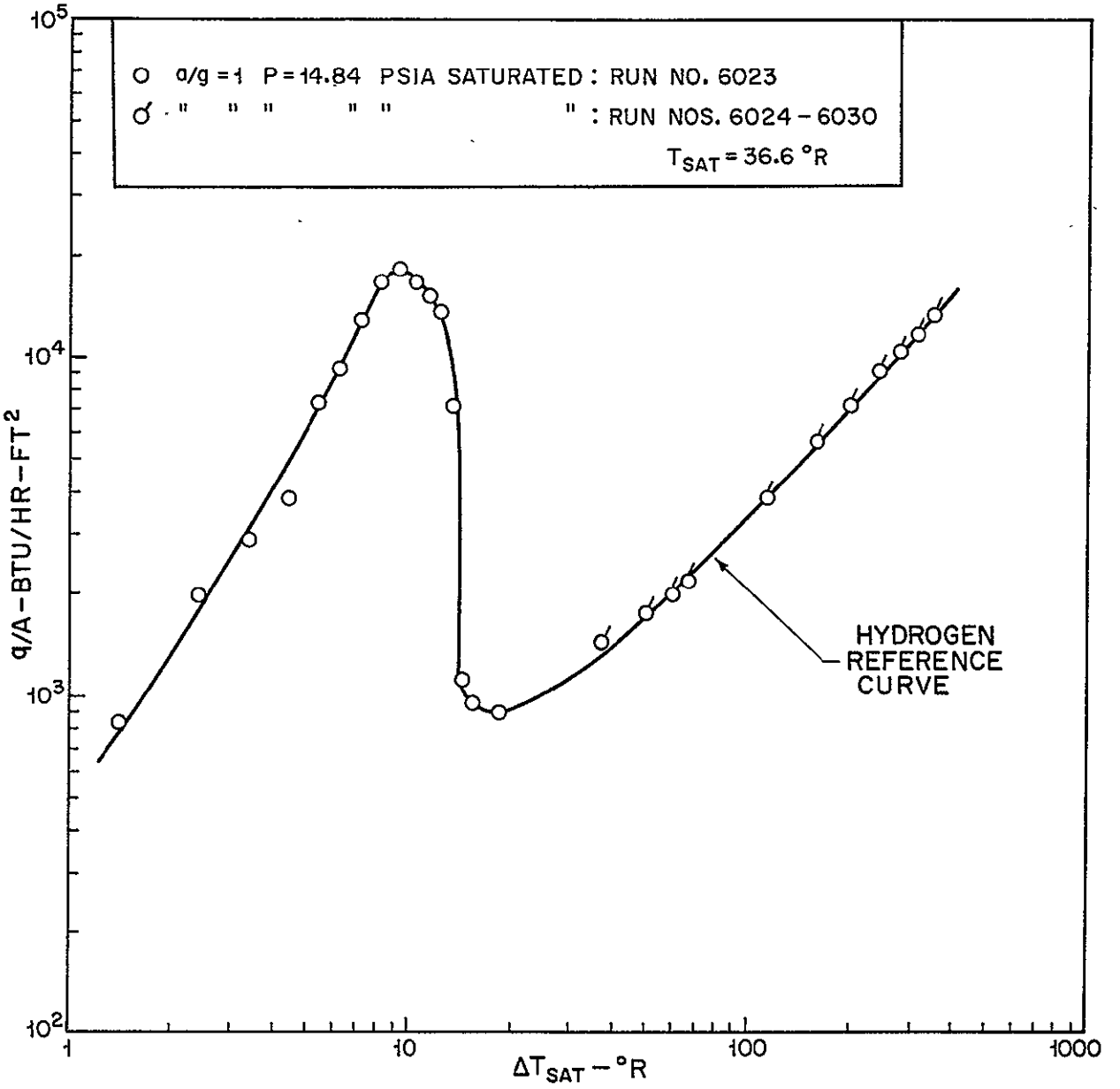

Figure 16. Basic data resulting in definition of pool boiling reference curve for saturated liquid hydrogen with 1 in. dia copper sphere.

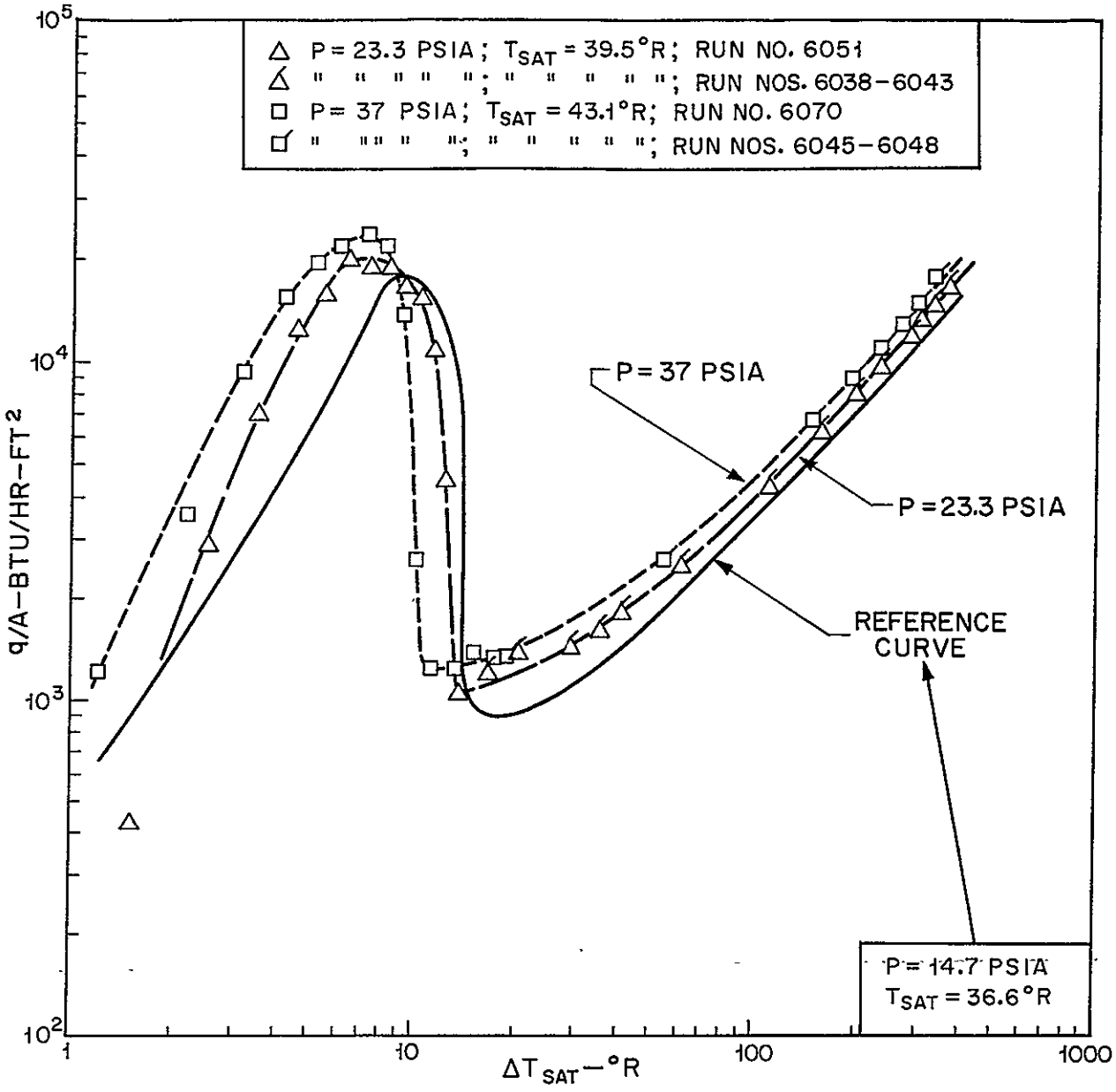

Figure 17. Effect of pressure at a/g = 1. Saturated liquid hydrogen with 1 in. dia copper sphere.

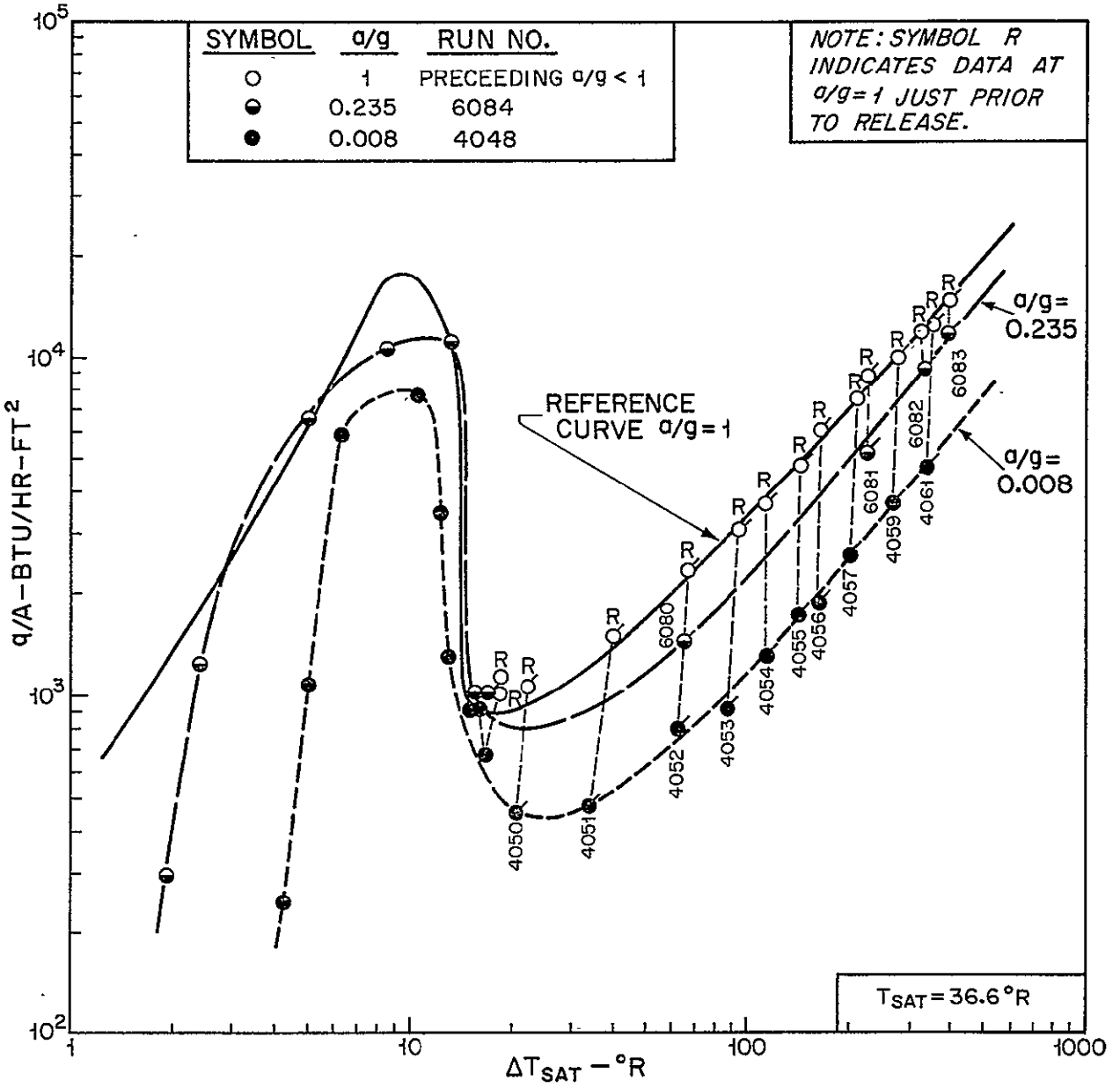

Figure 18. Effect of a/g at P = 14.7 psia. Saturated liquid hydrogen with 1 in. dia copper sphere.

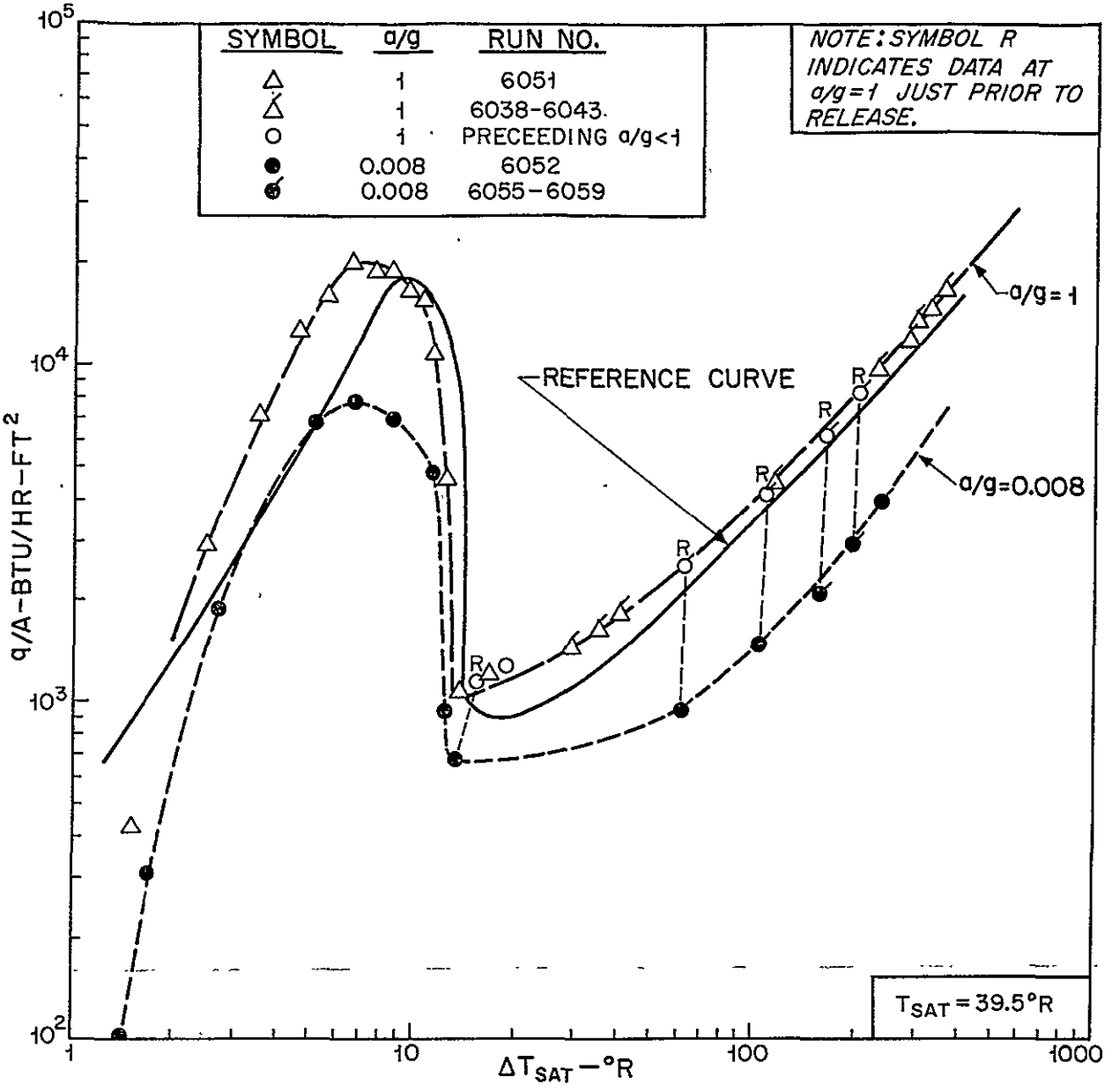

Figure 19. Effect of a/g at P = 23.3 psia. Saturated liquid hydrogen with 1 in. dia copper sphere.

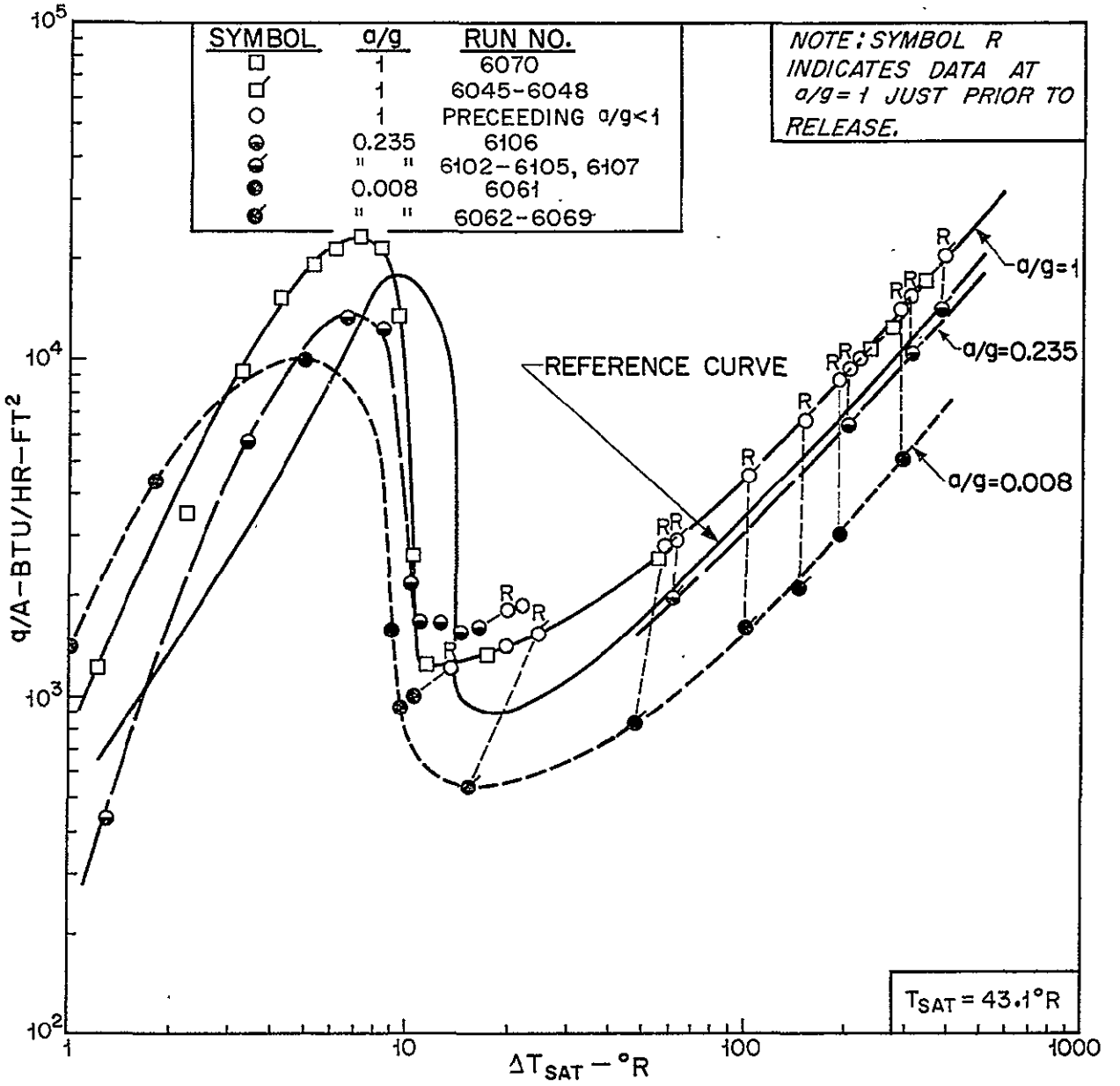

Figure 20. Effect of a/g at P = 37 psia. Saturated liquid hydrogen with 1 in. dia copper sphere.

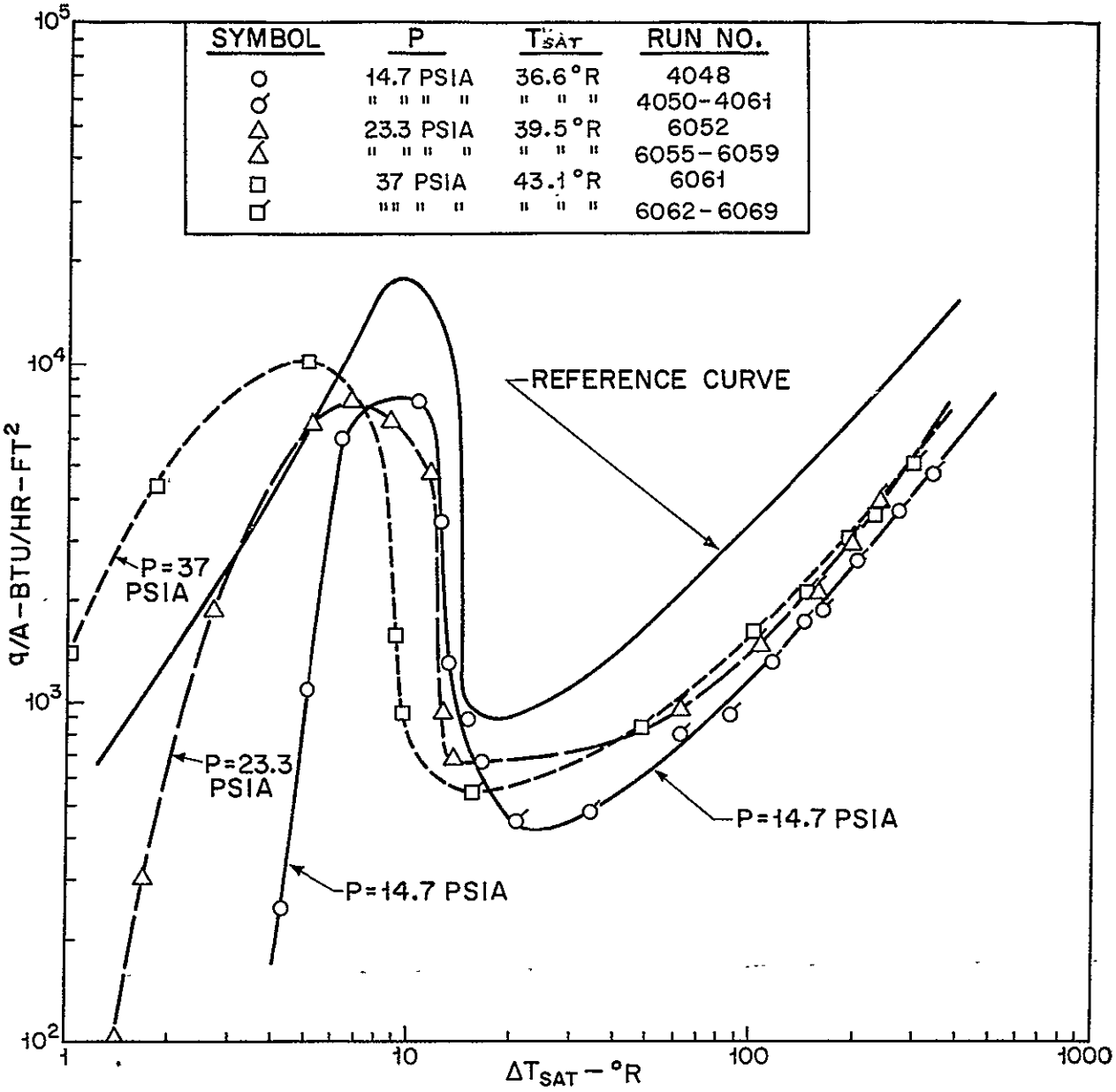

Figure 21. Effect of pressure at a/g = 0.008. Saturated liquid hydrogen with 1 in. dia copper sphere.

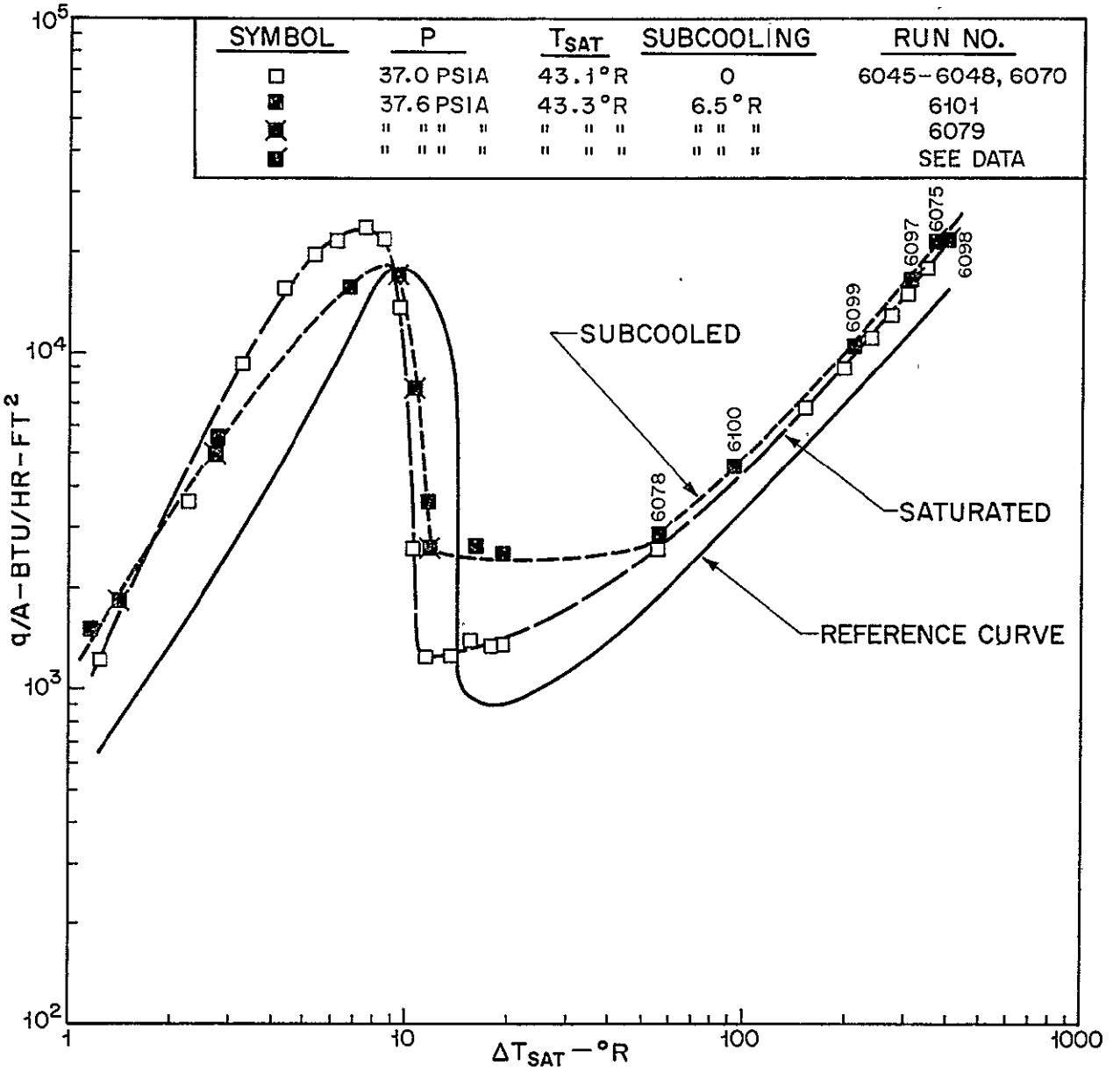

Figure 22. Effect of subcooling at a/g = 1 with P = 37 psia. Liquid hydrogen with 1 in. dia copper sphere.

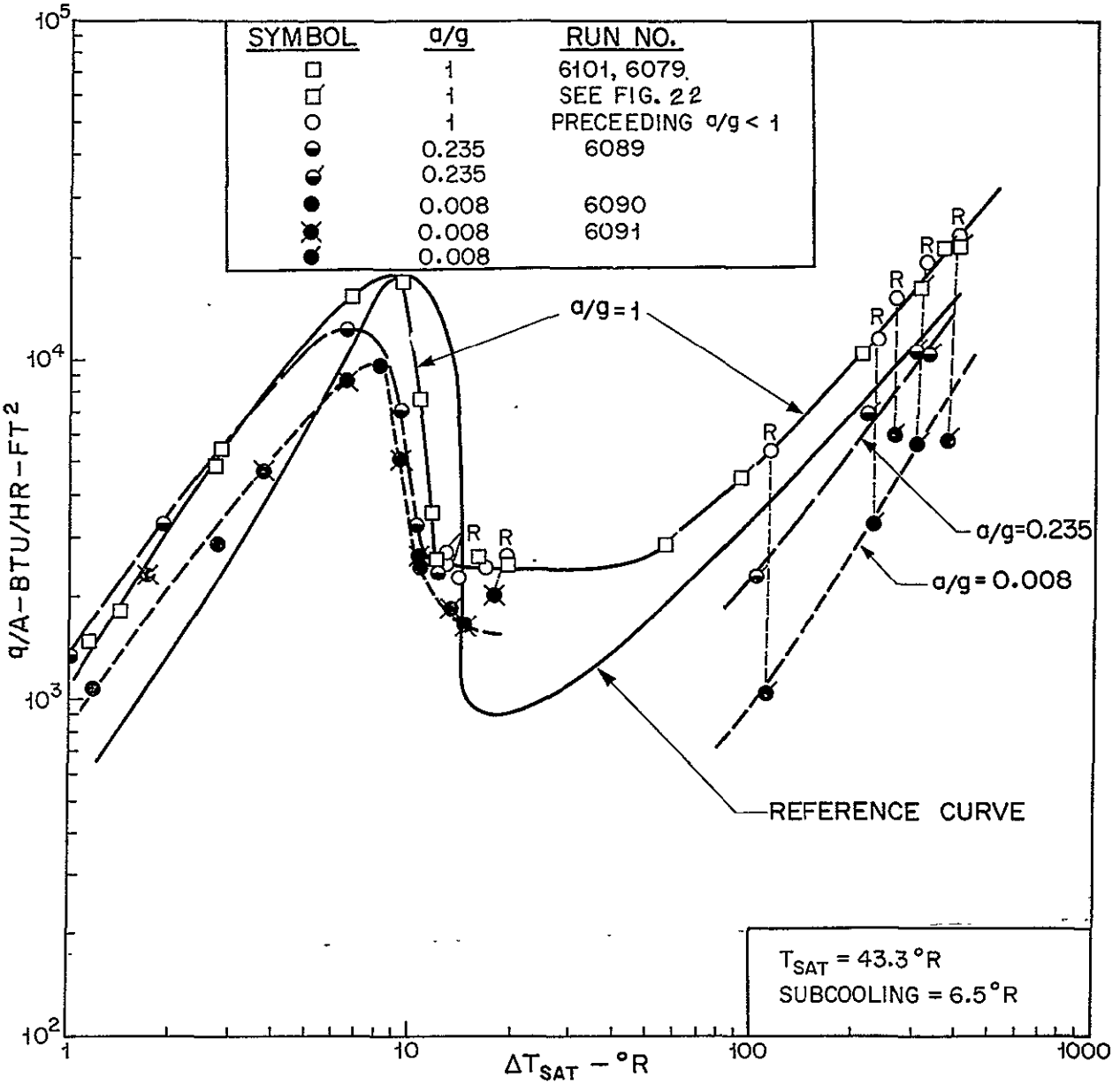

Figure 23. Effect of a/g with subcooling at P = 37 psia. Subcooled liquid hydrogen with 1 in. dia copper sphere.

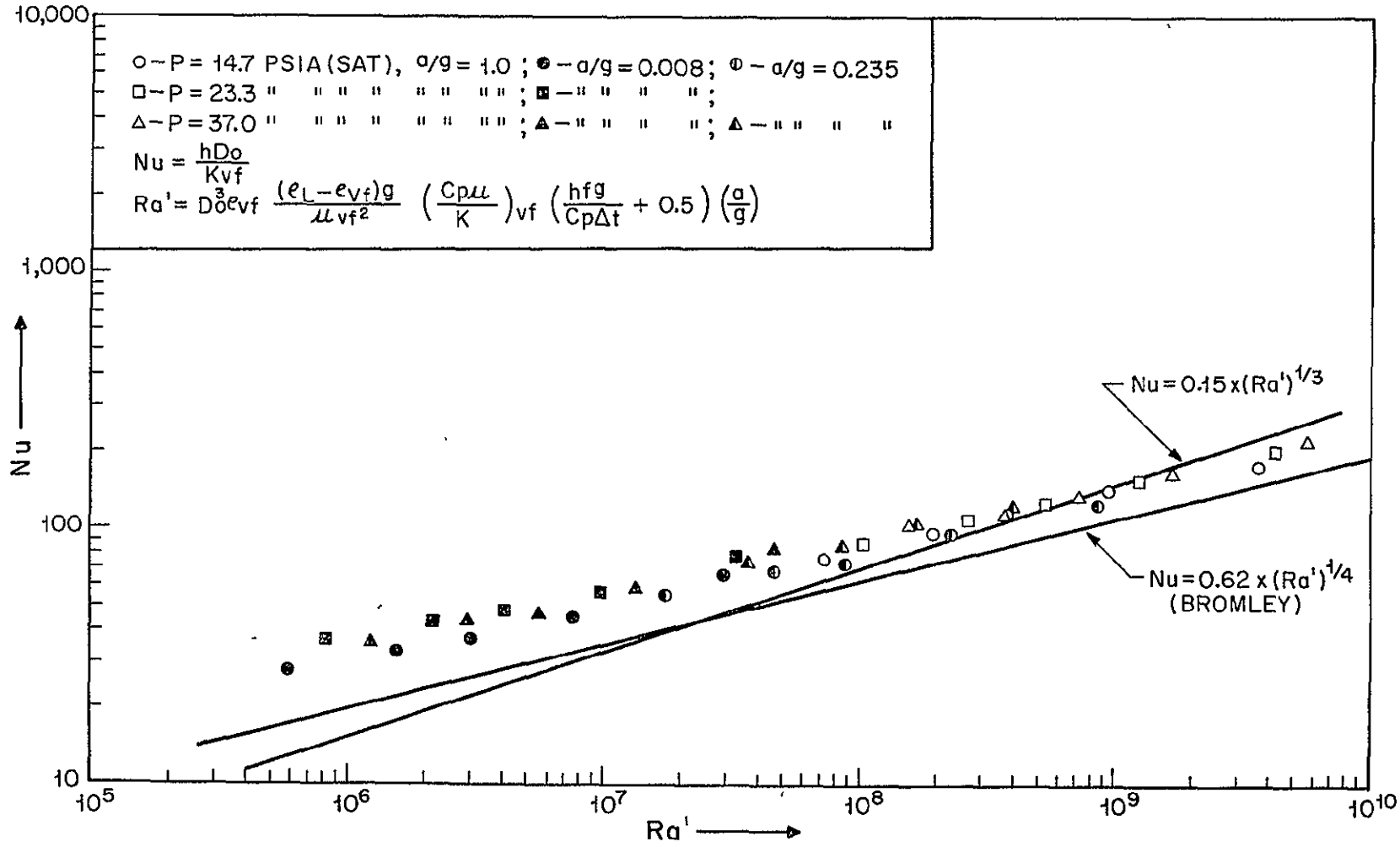

Figure 24. Correlation of film boiling from 1 in dia sphere in saturated liquid hydrogen.

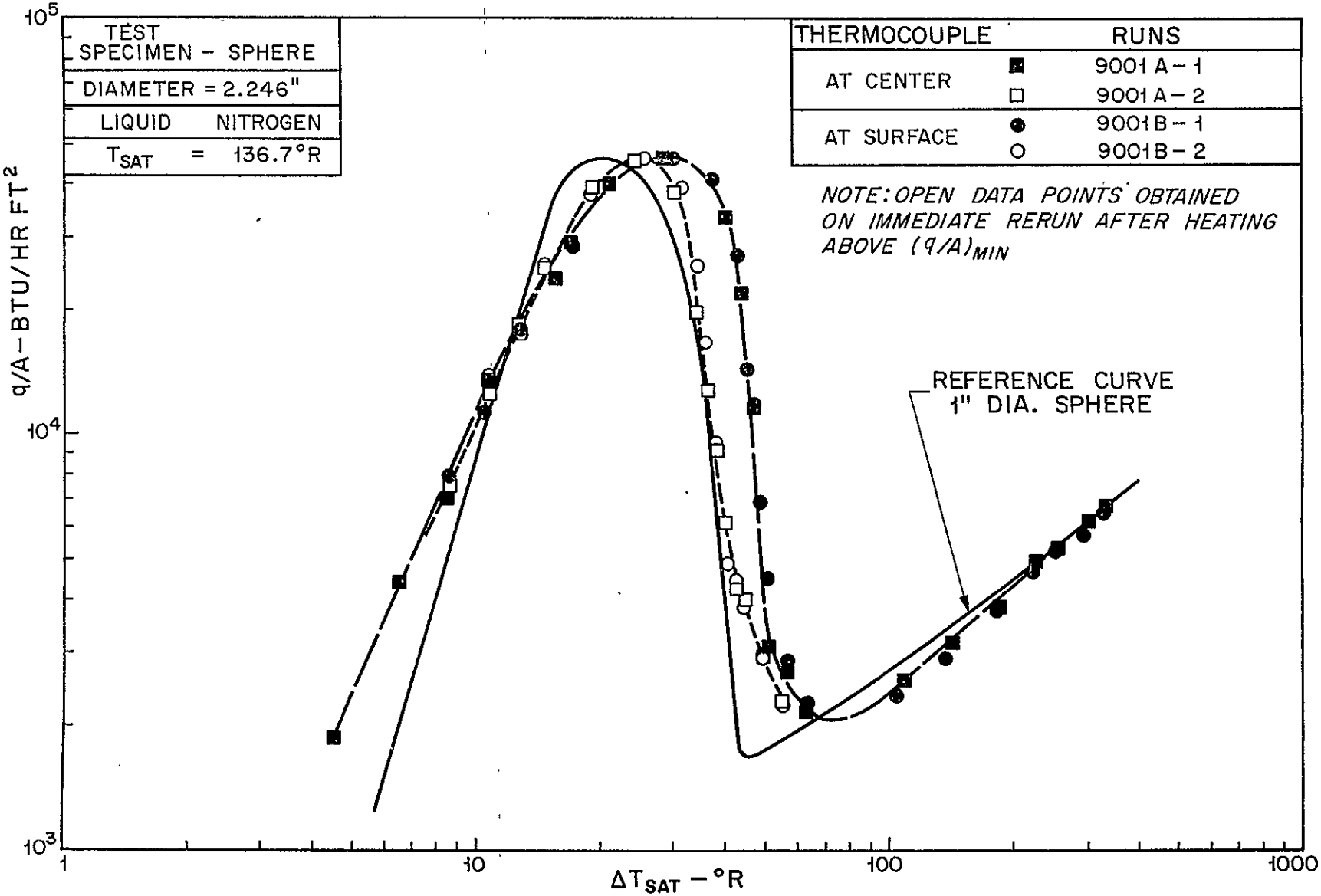

Figure 25. Boiling from 2-1/4 in. dia sphere to liquid nitrogen at atmospheric pressure, a/g = 1.

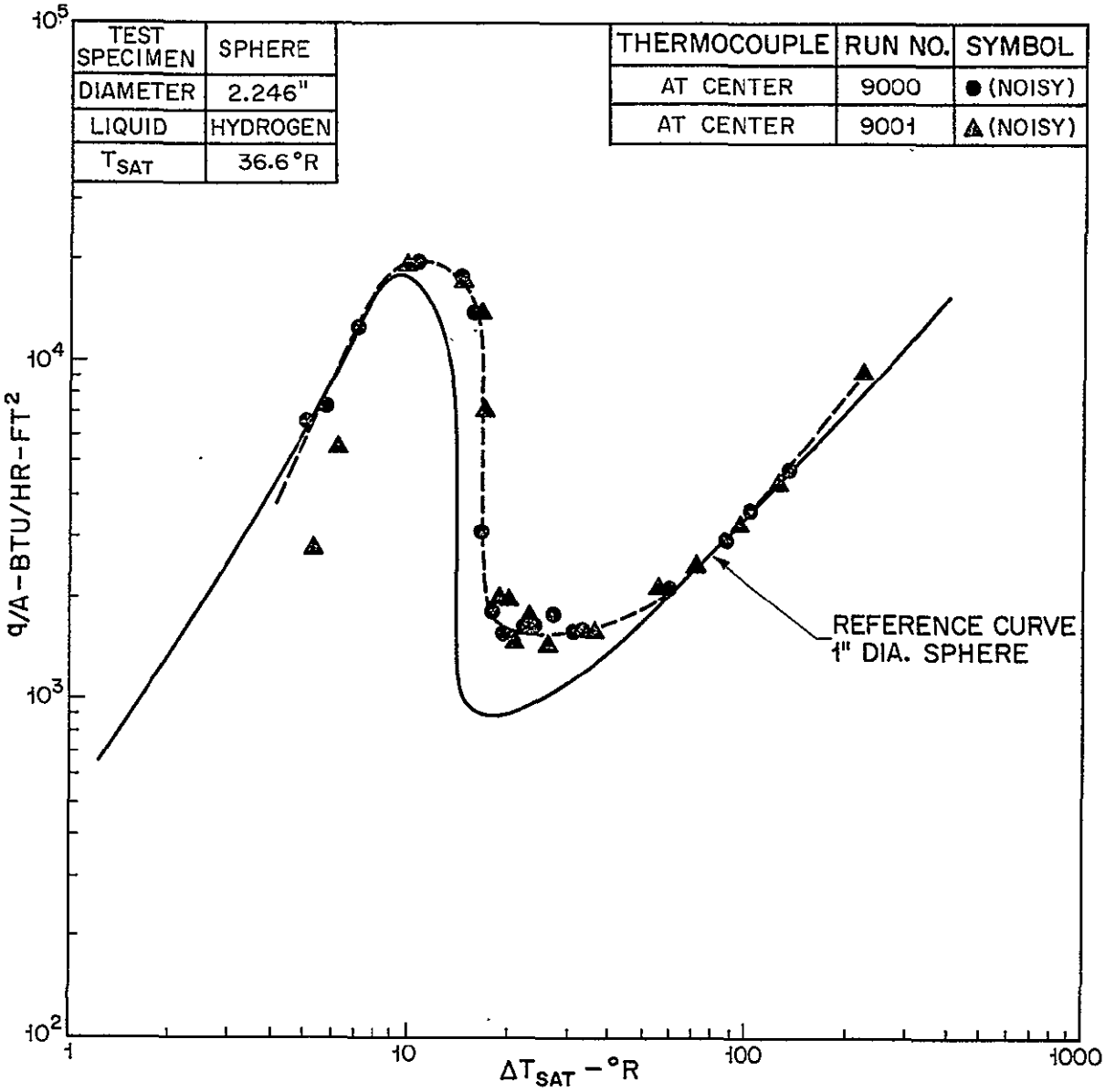

Figure 26. Boiling from 2-1/4 in. dia sphere to liquid hydrogen at atmospheric pressure, a/g = 1.

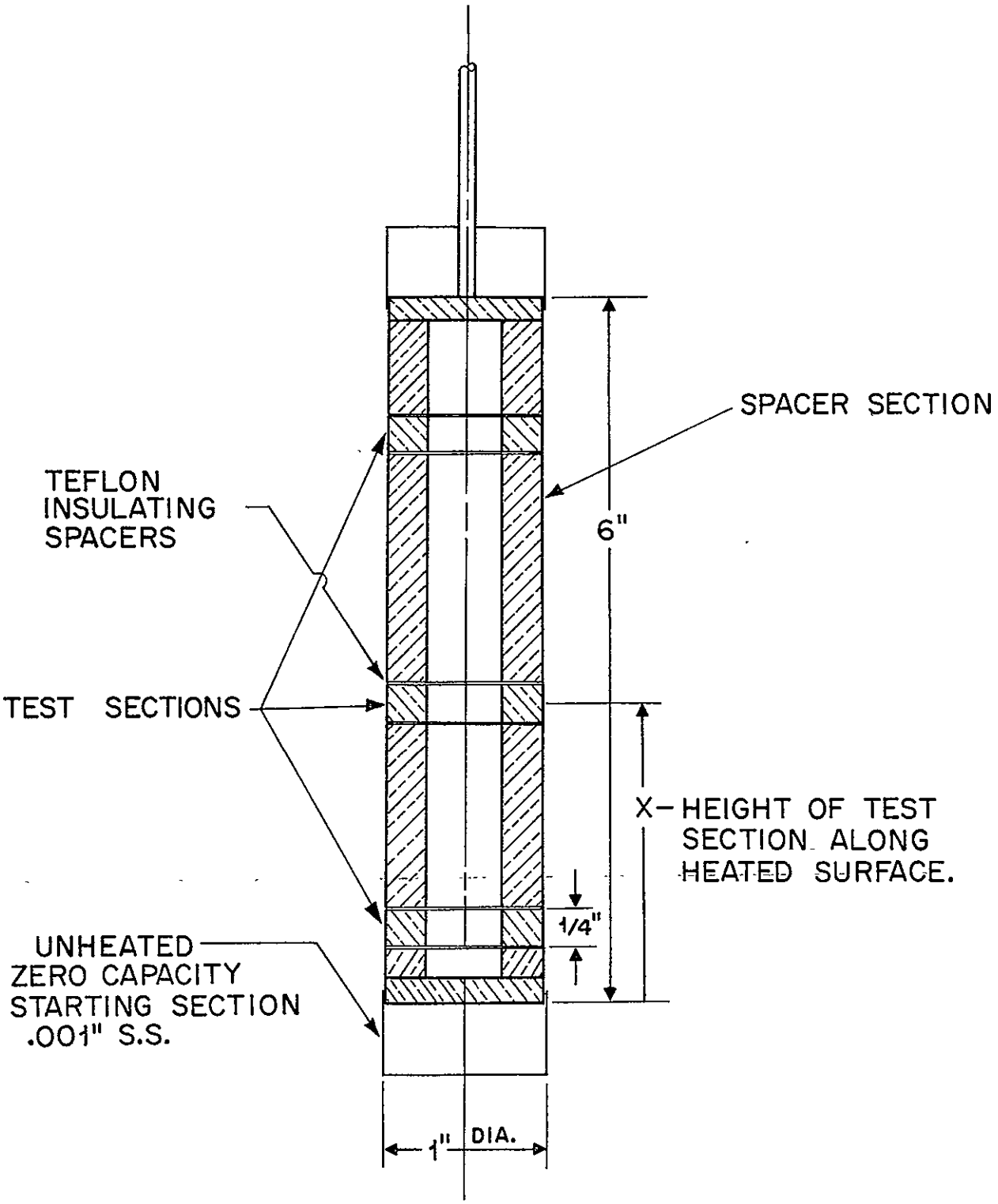

Figure 27. Vertical surface boiling calorimeter.

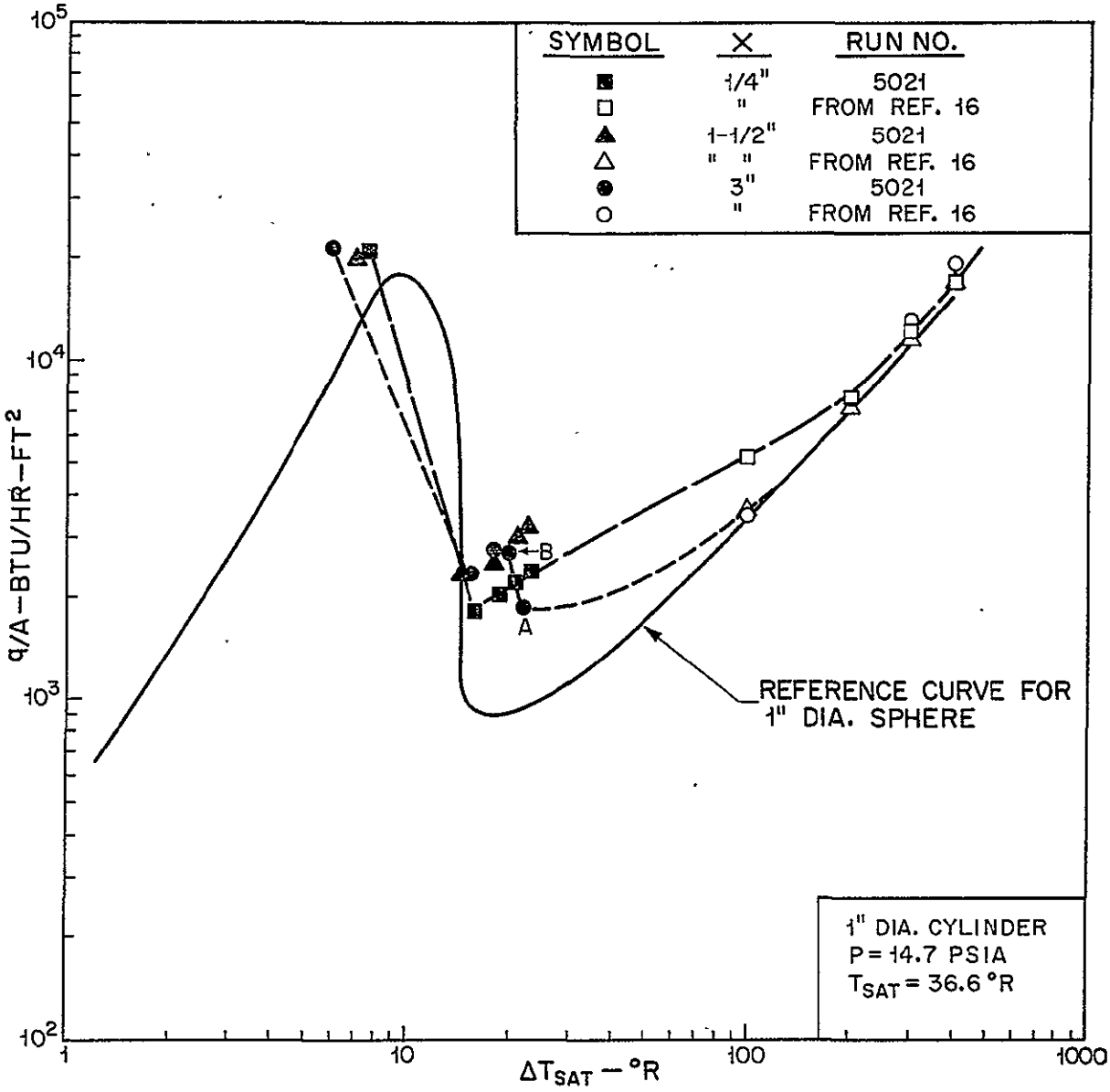

Figure 28a. Transition and film boiling of liquid hydrogen on vertical surface.

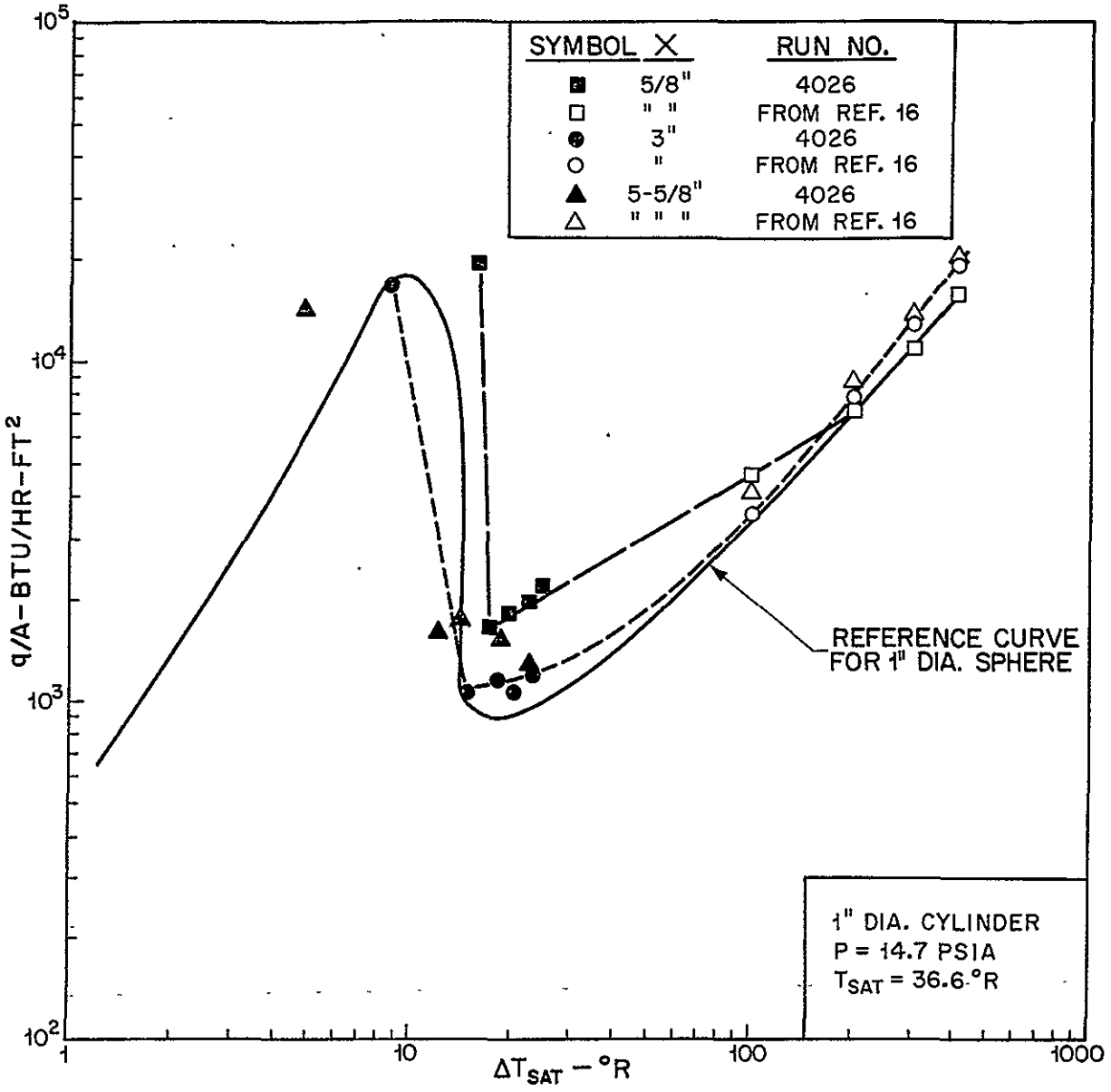

Figure 28b. Continued.

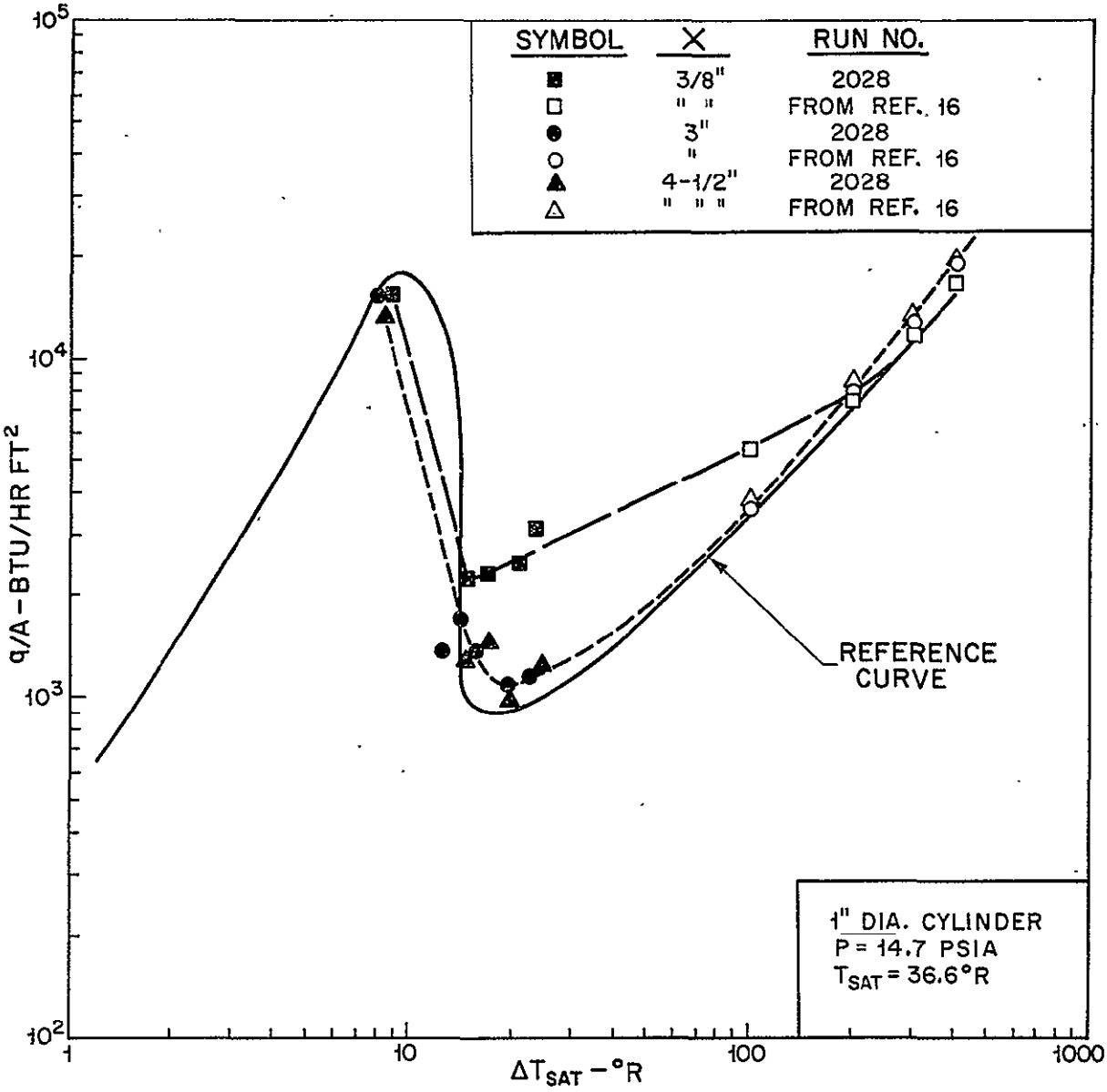

Figure 28c. Concluded.

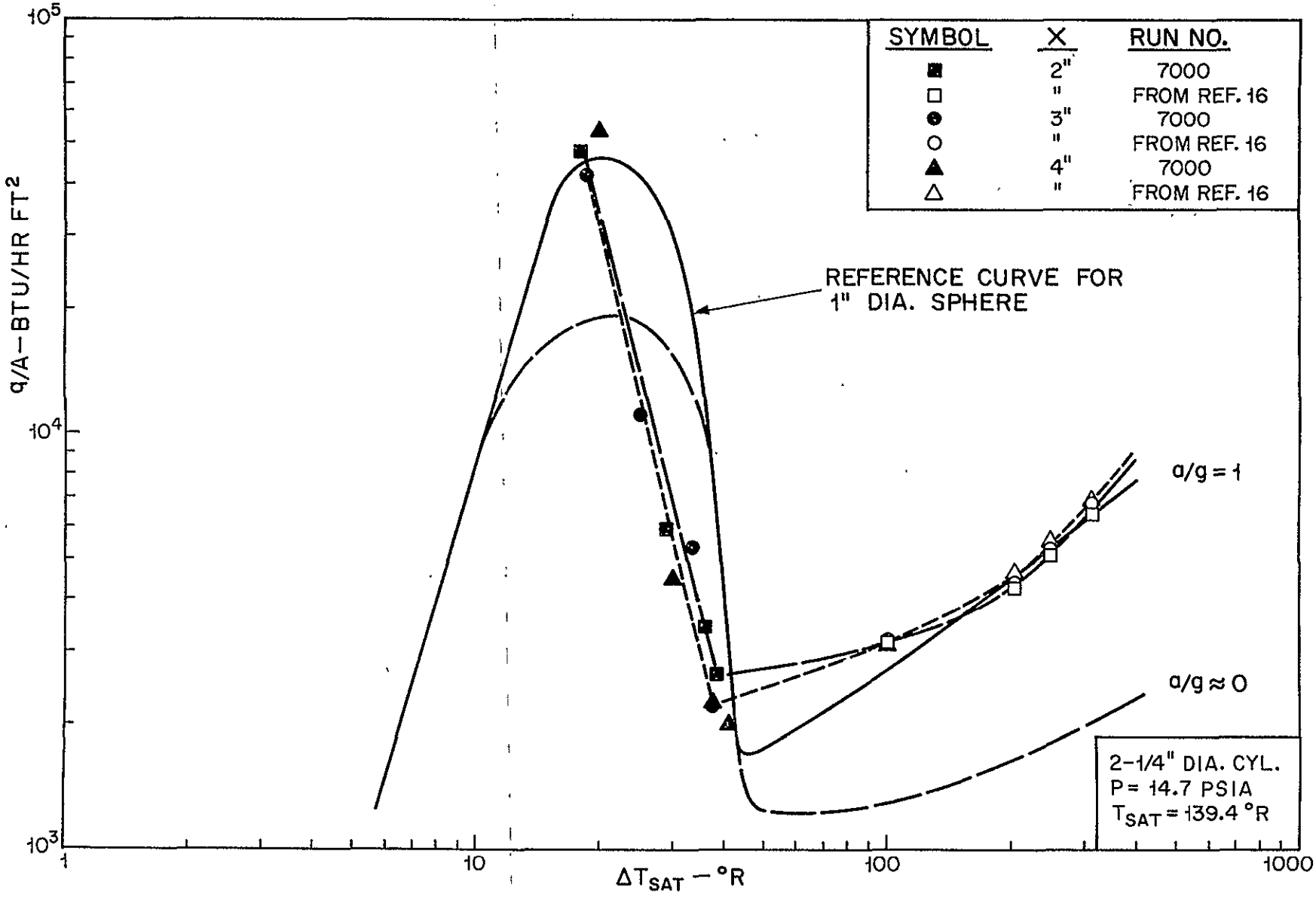

Figure 29a. Transition and film boiling of liquid nitrogen on vertical surface.

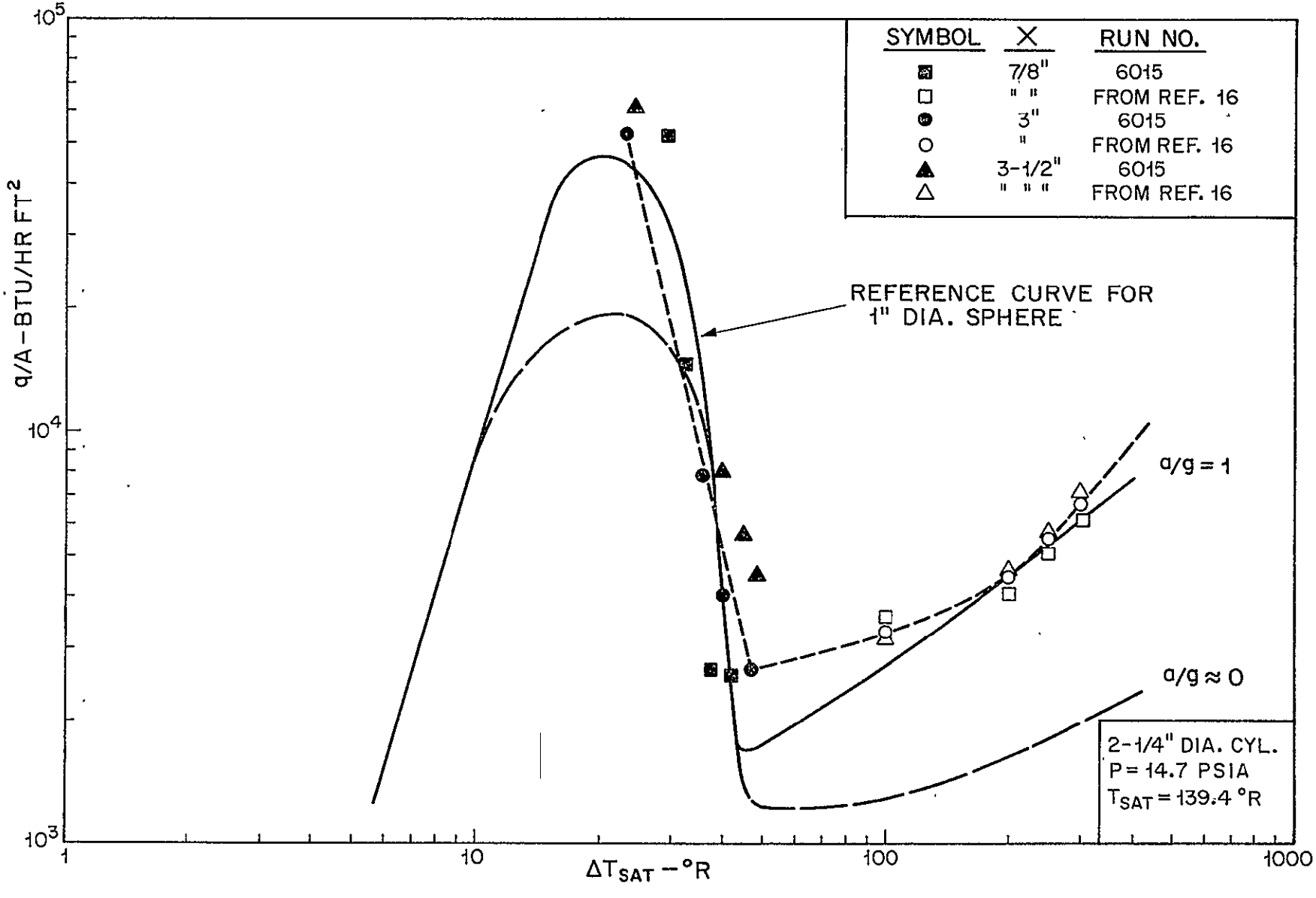

Figure 29b. Continued.

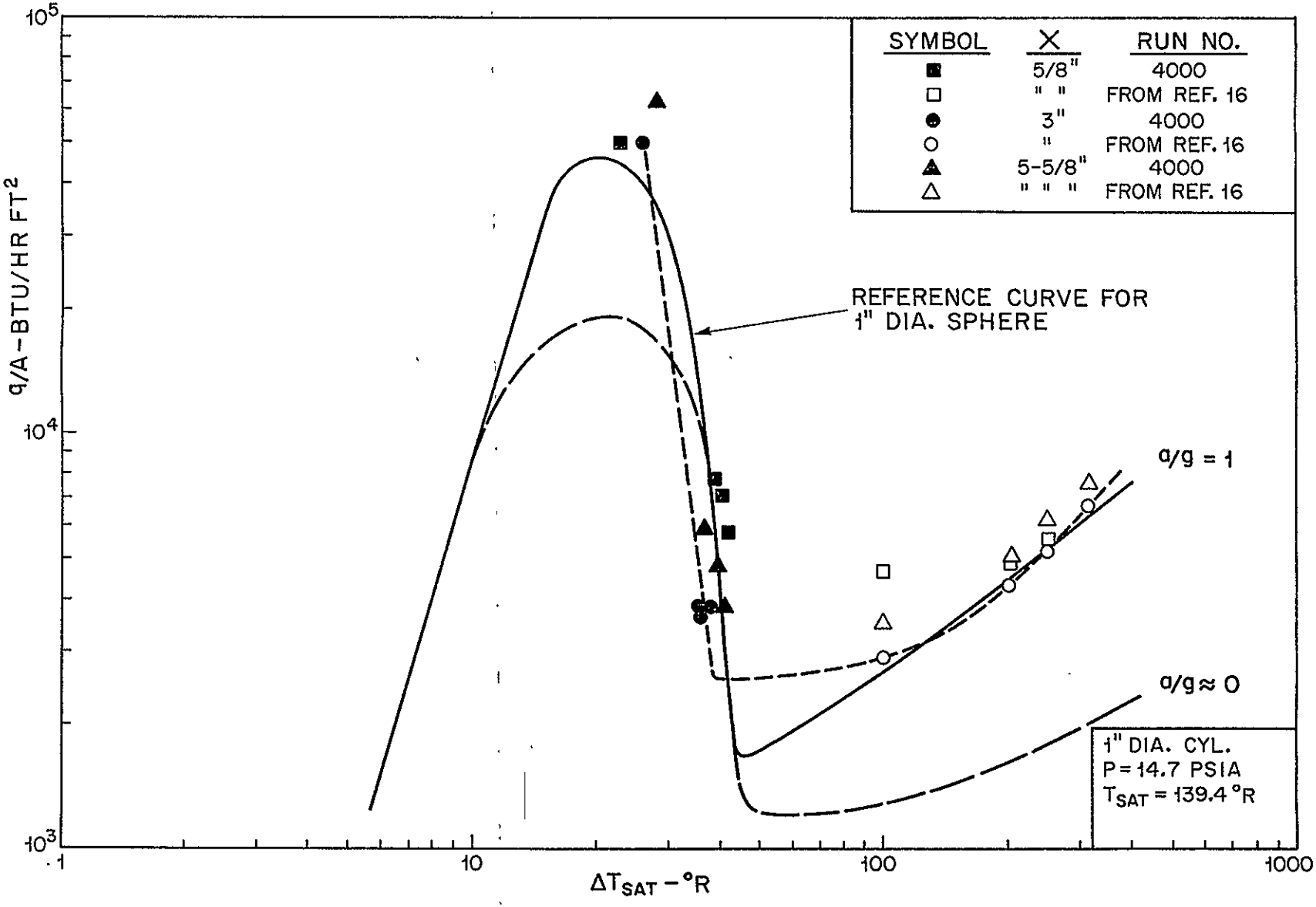

Figure 29c. Concluded.

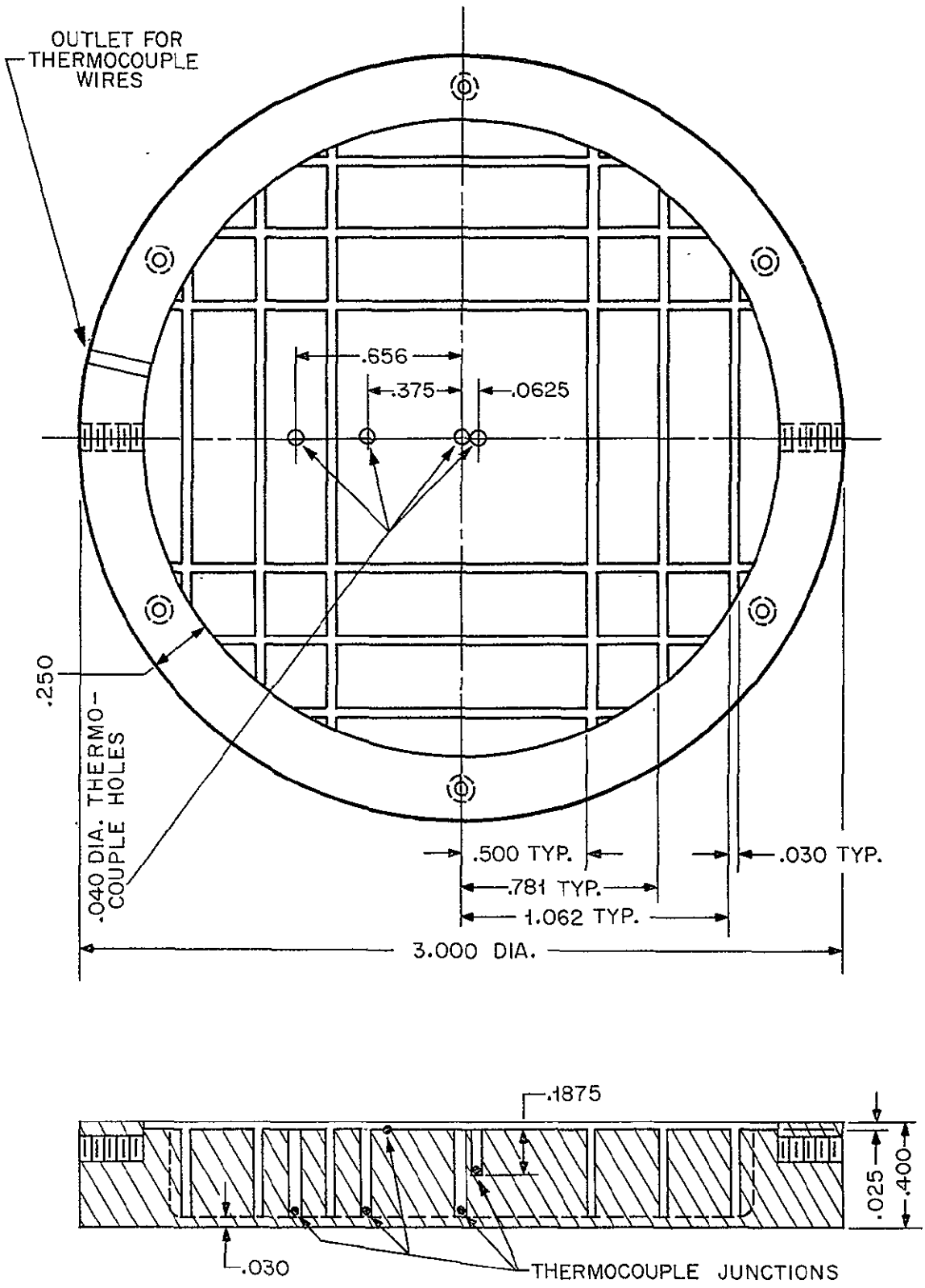

Figure 30. Disc for influence of orientation on boiling heat transfer.

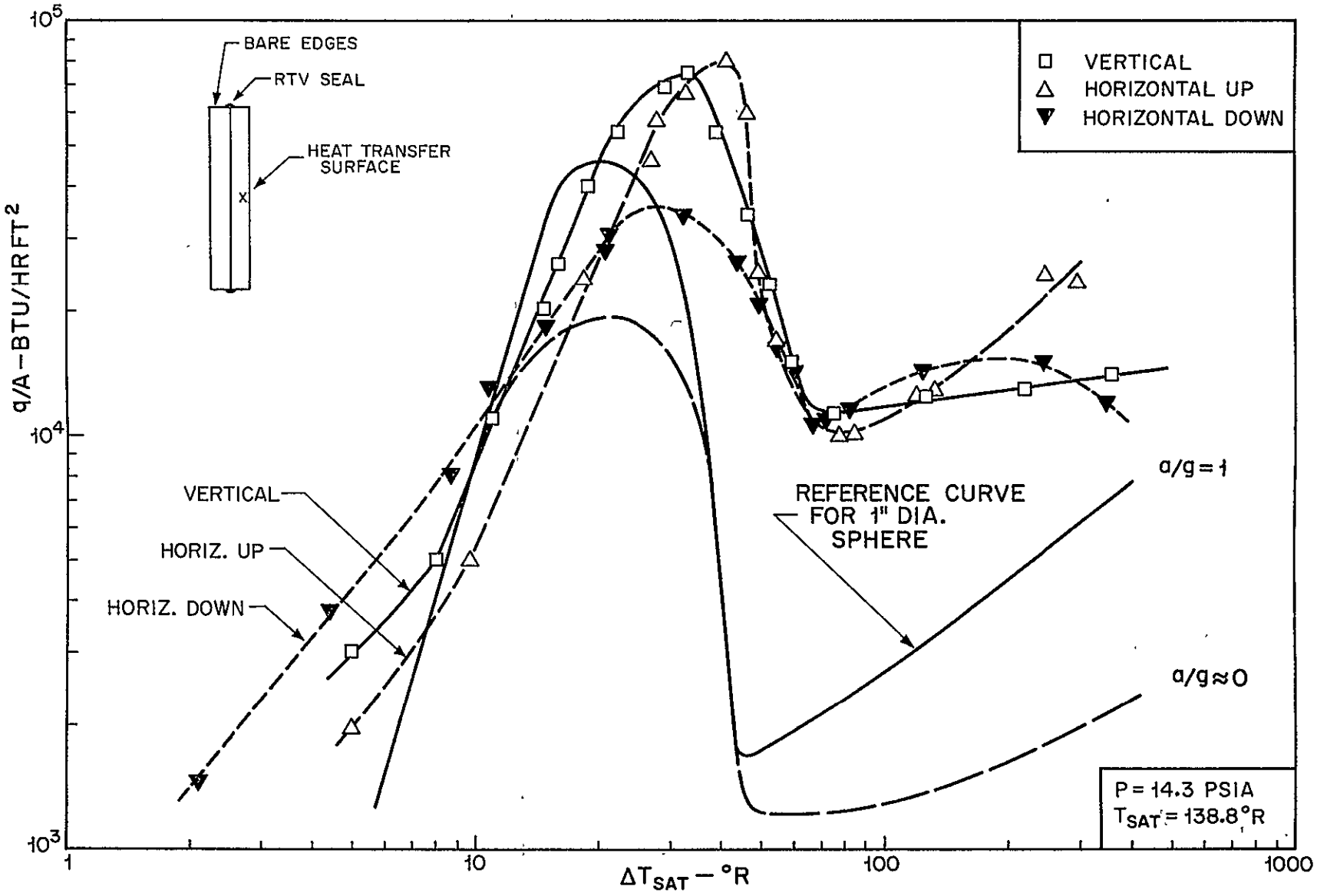

Figure 31. Preliminary tests with disc in saturated LN_2.

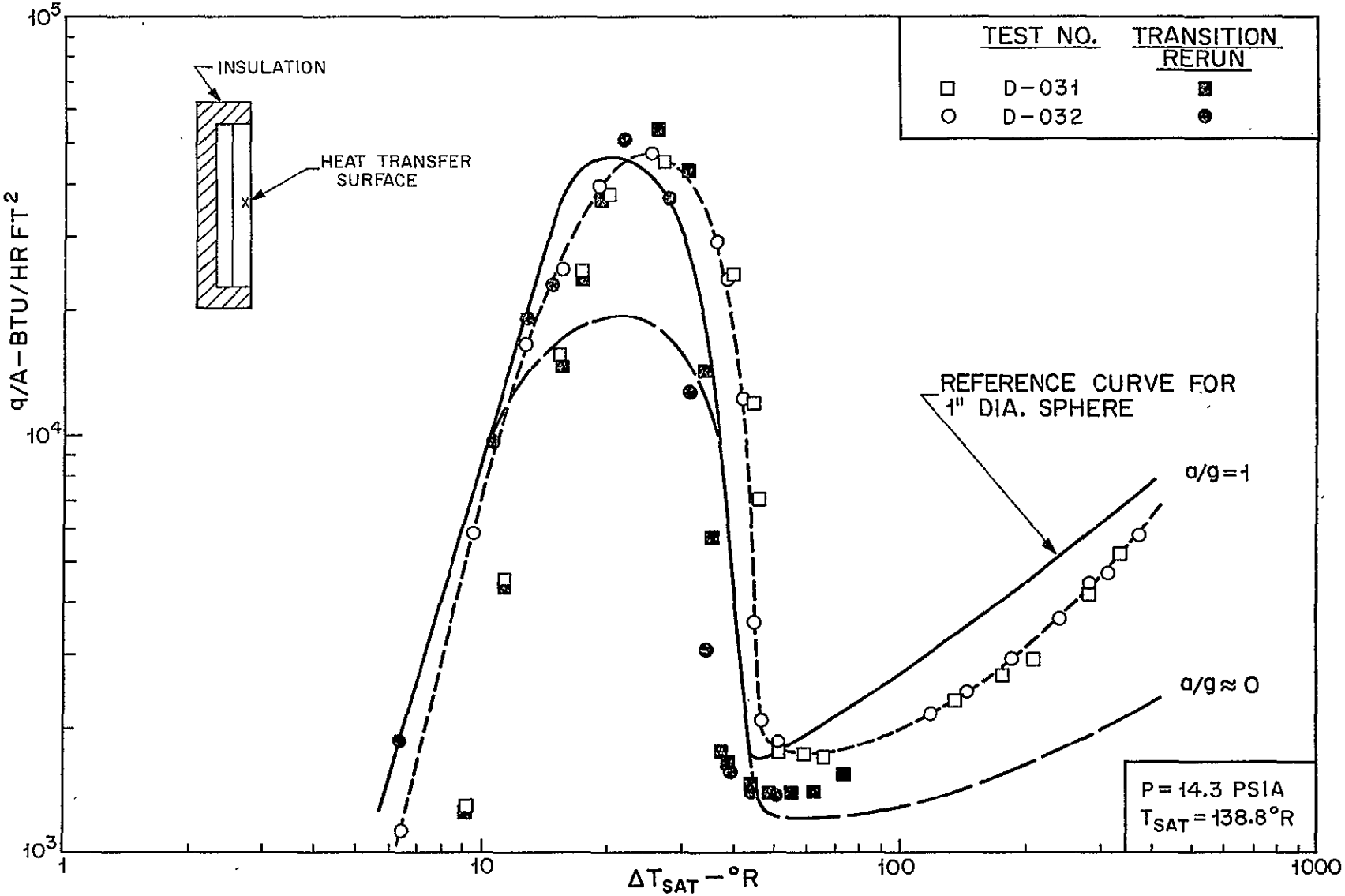

Figure 32. Preliminary tests with disc in saturated LN_2. Vertical orientation.

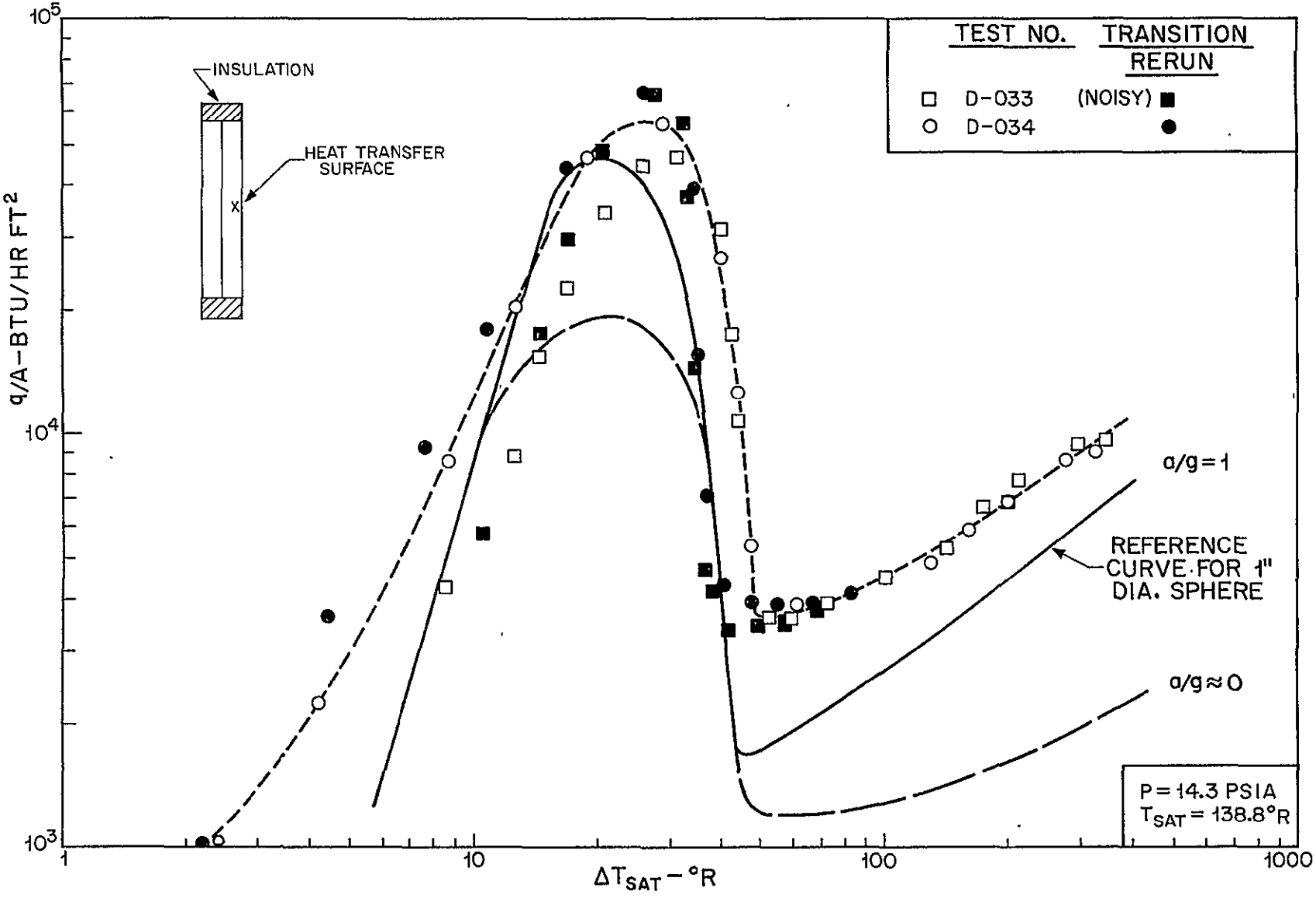

Figure 33. Disc in saturated LN_2—vertical, a/g = 1.

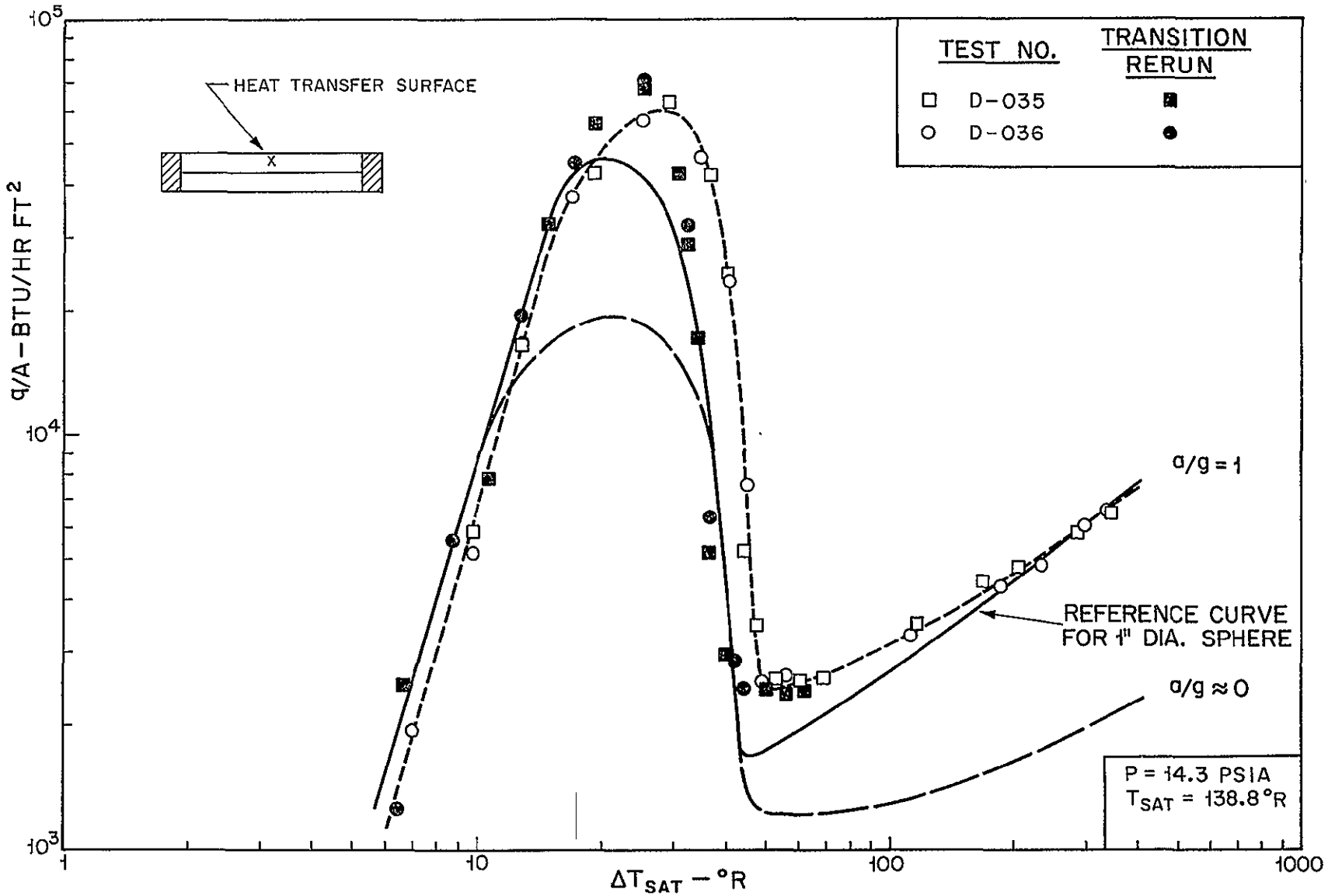

Figure 34. Disc in saturated LN_2—horizontal up, a/g = 1.

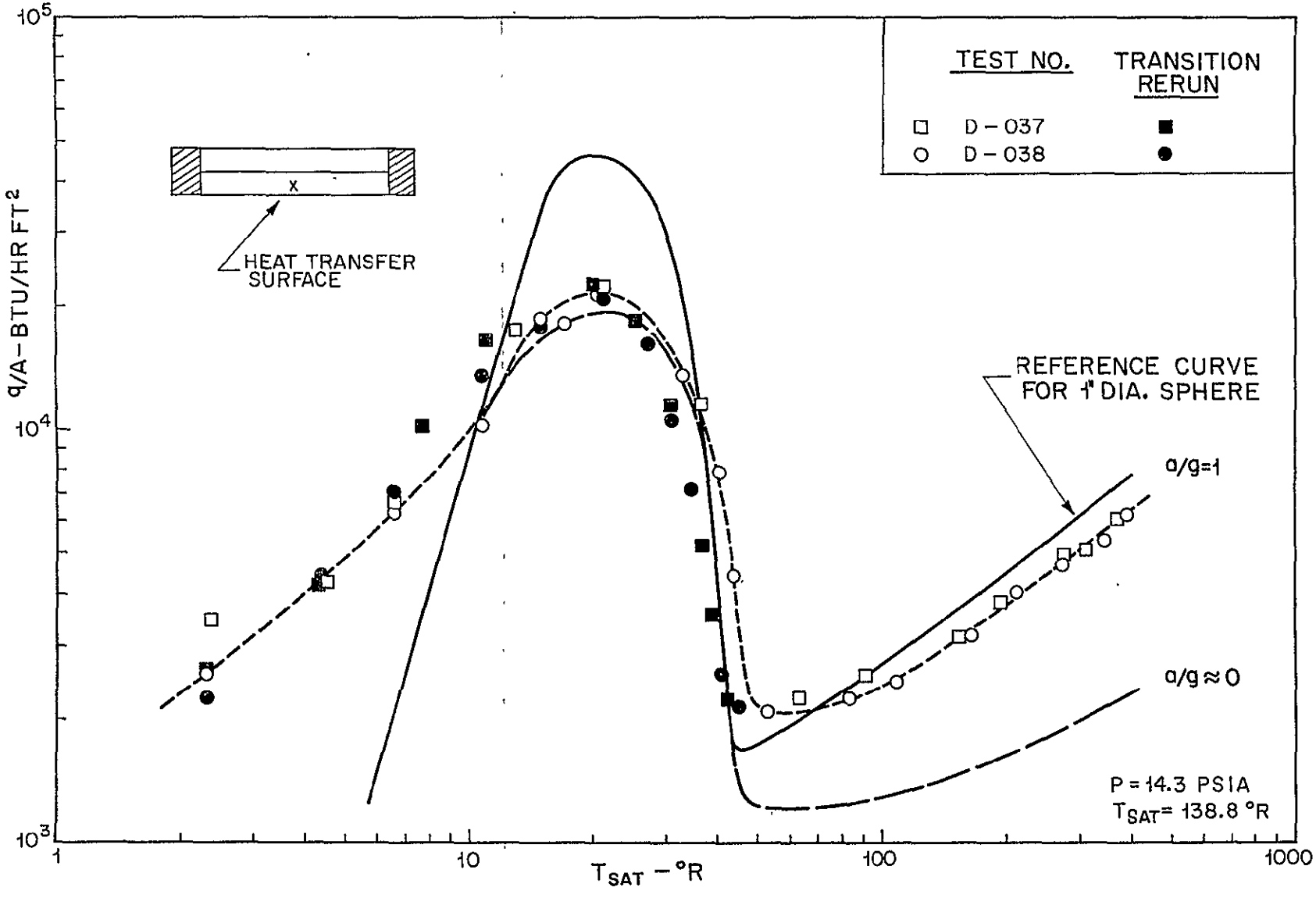

Figure 35. Disc in saturated LN_2—horizontal down, a/g = 1.

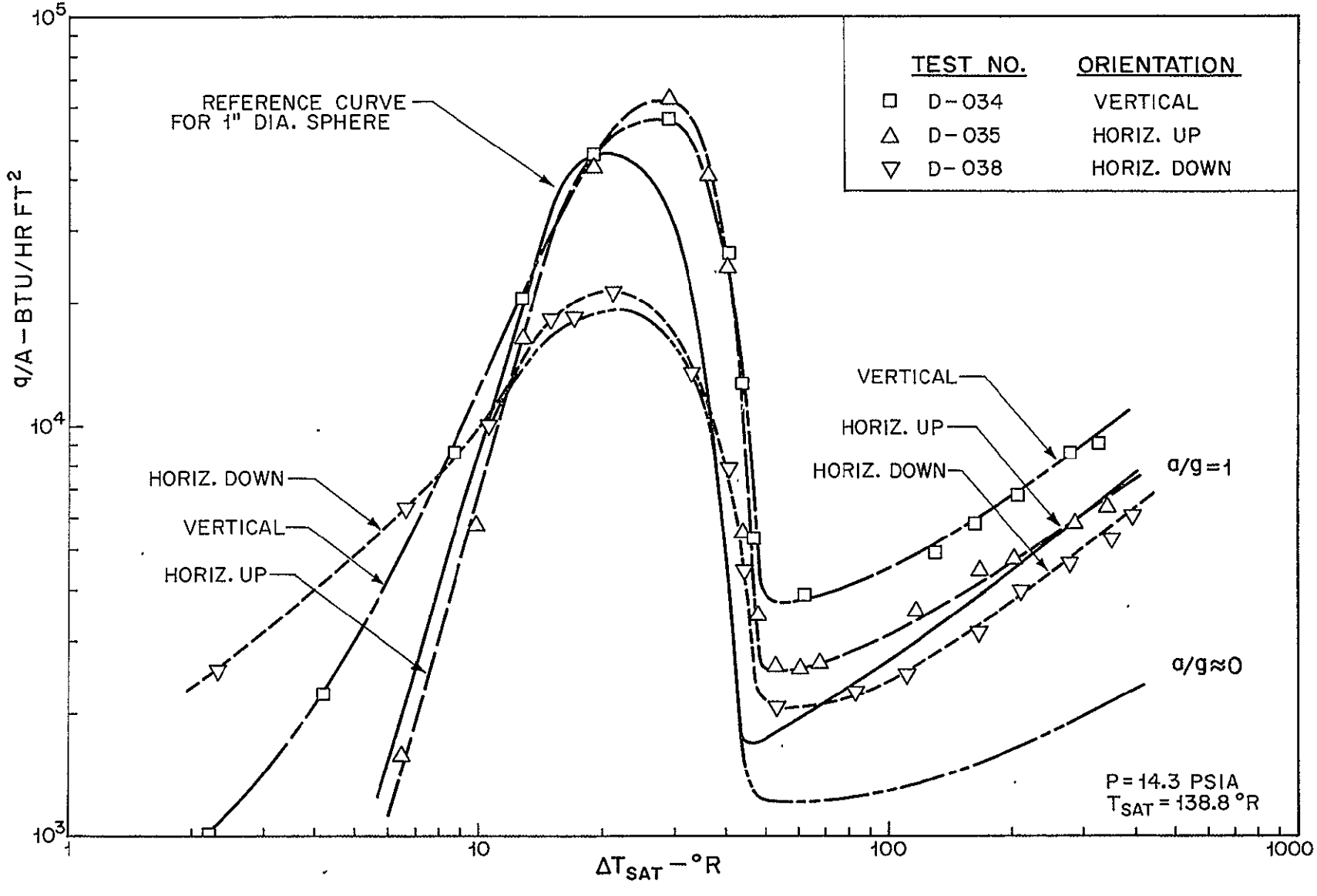

Figure 36. Disc in saturated LN_2—all orientations, a/g = 1.

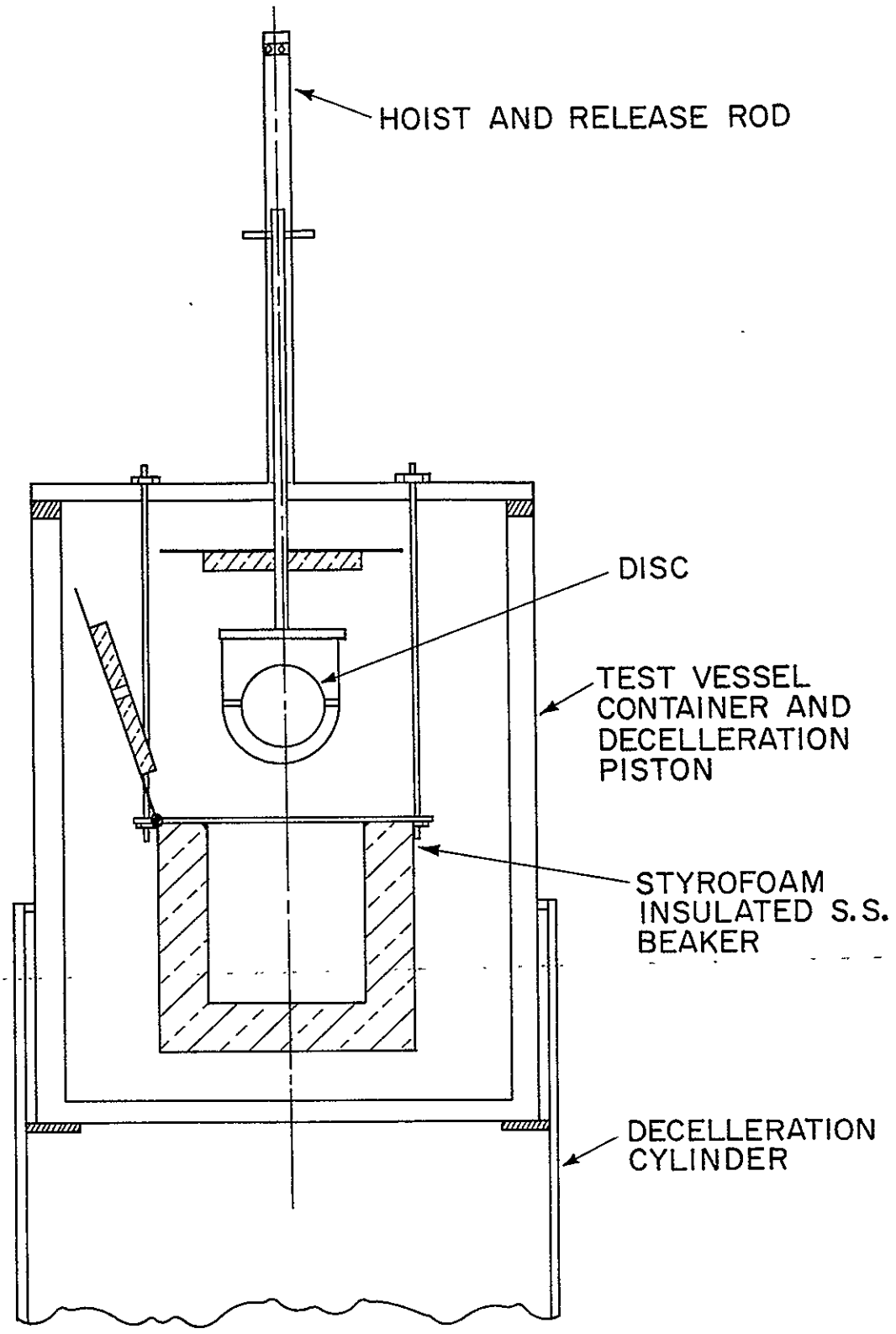

Figure 37. Disc drop package.

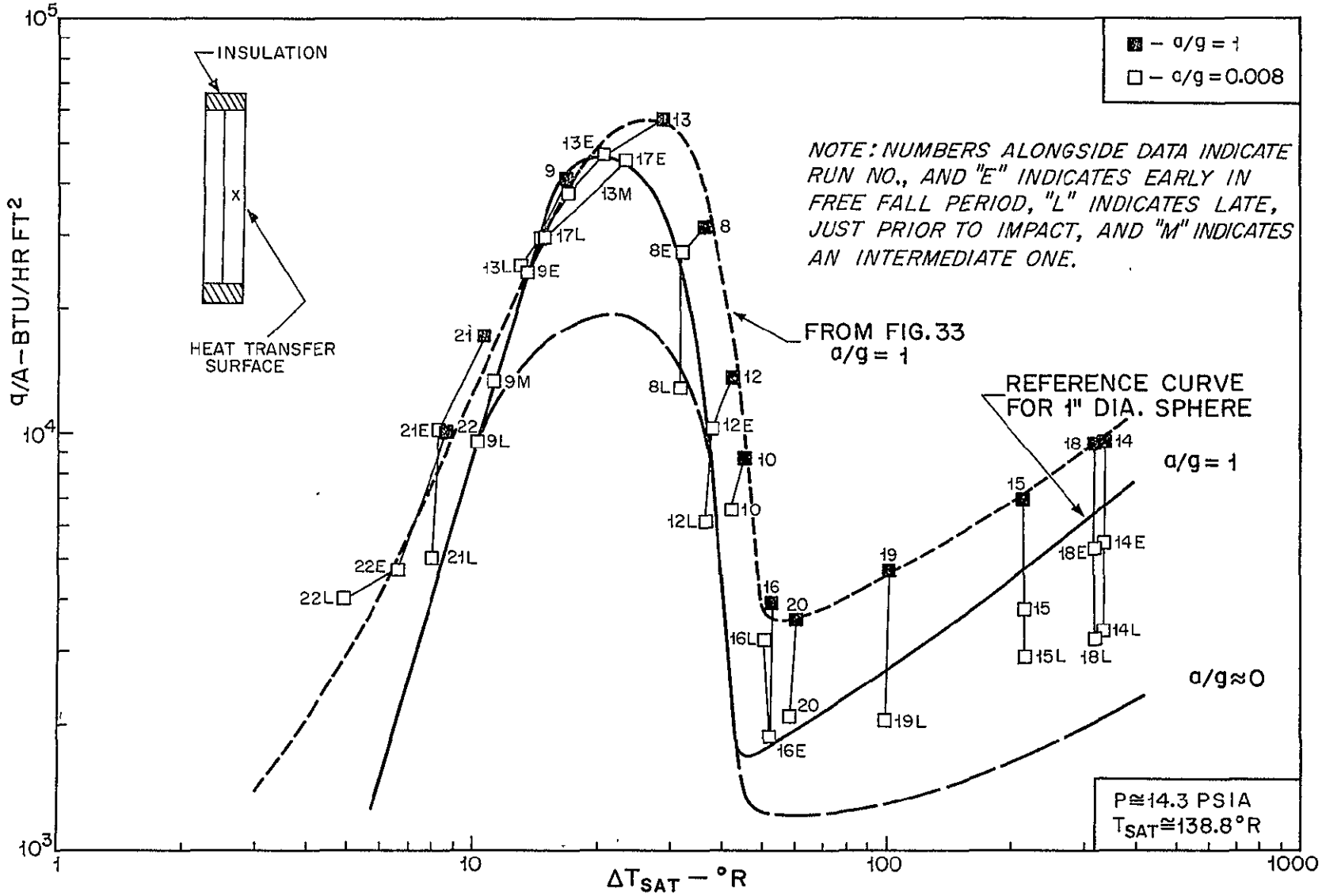

Figure 38. Disc in saturated LN_2—vertical, a/g ≅ 0.008.

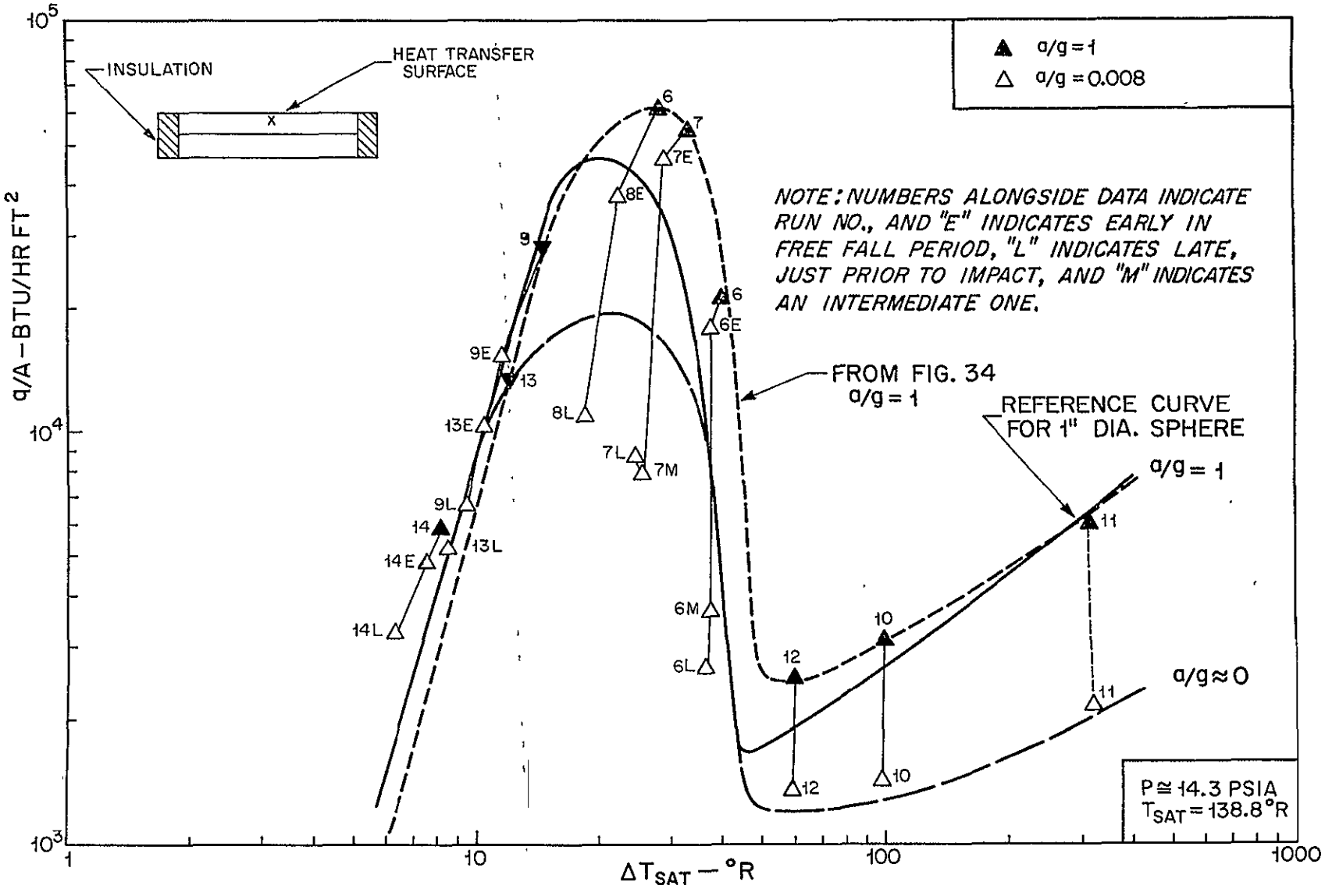

Figure 39. Disc in saturated LN_2—horizontal up, a/g ≅ 0.008.

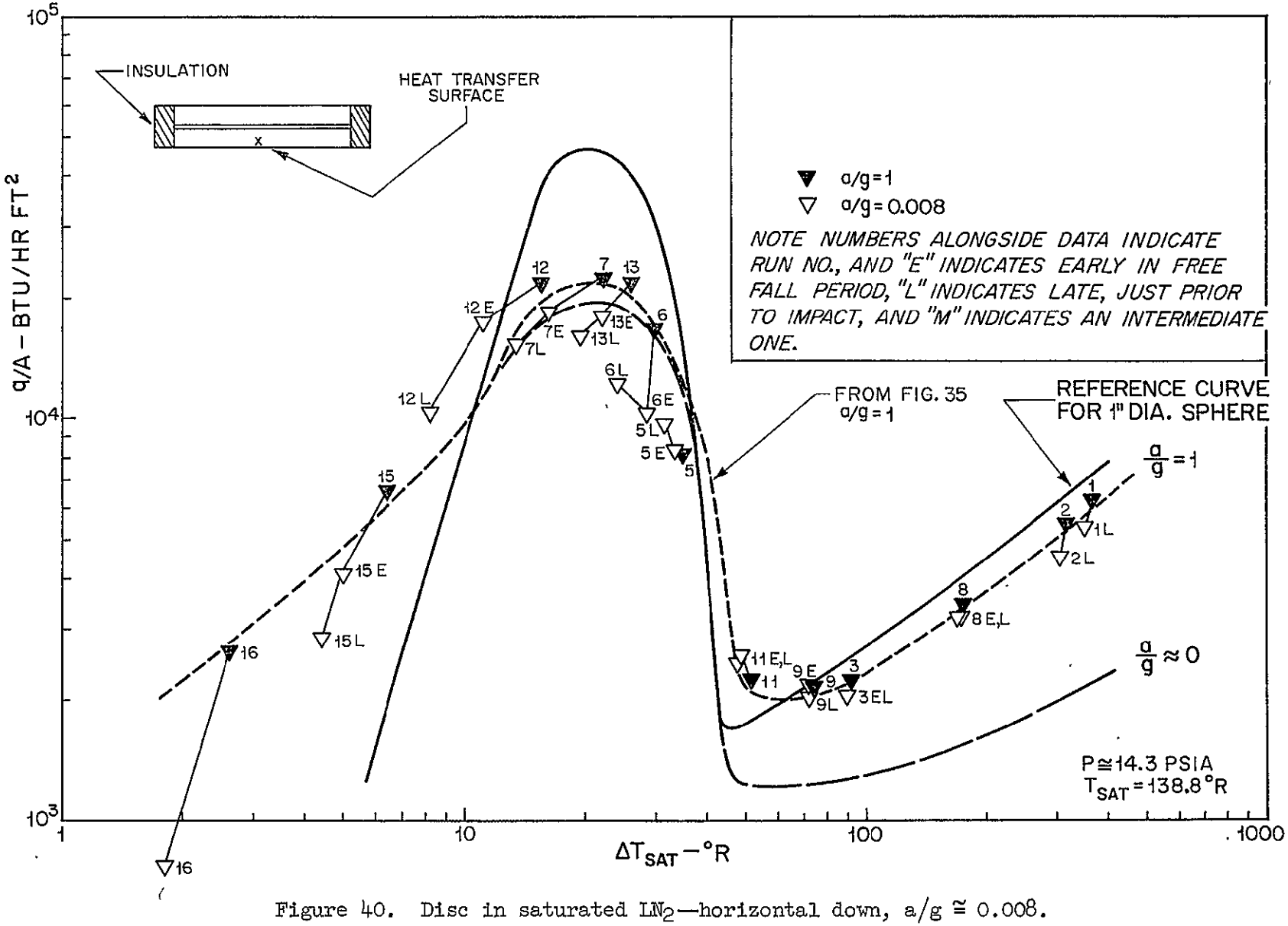

Figure 40. Disc in saturated LN_2—horizontal down, a/g ≅ 0.008.

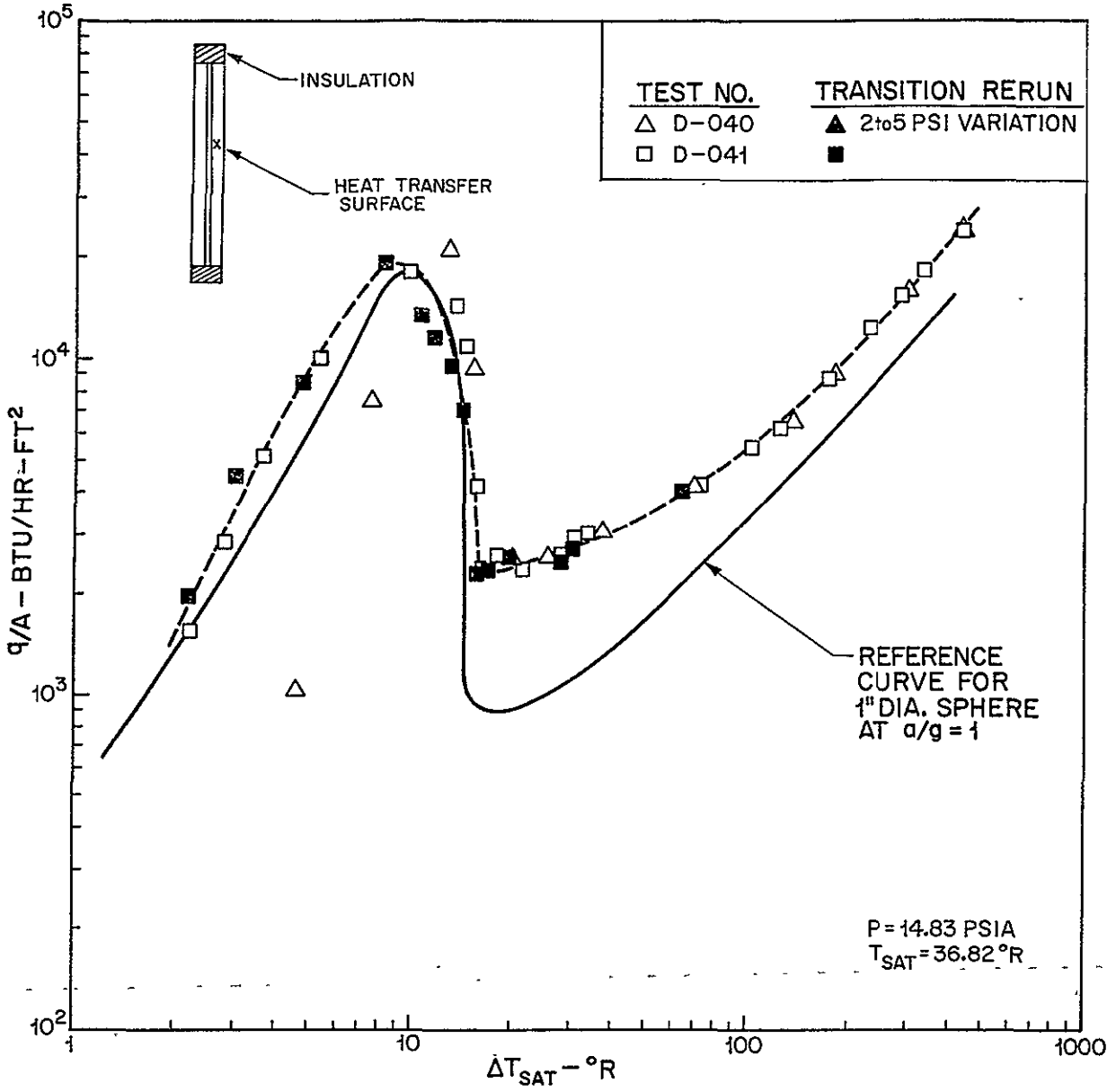

Figure 41. Disc in saturated LH_2—vertical, a/g = 1.

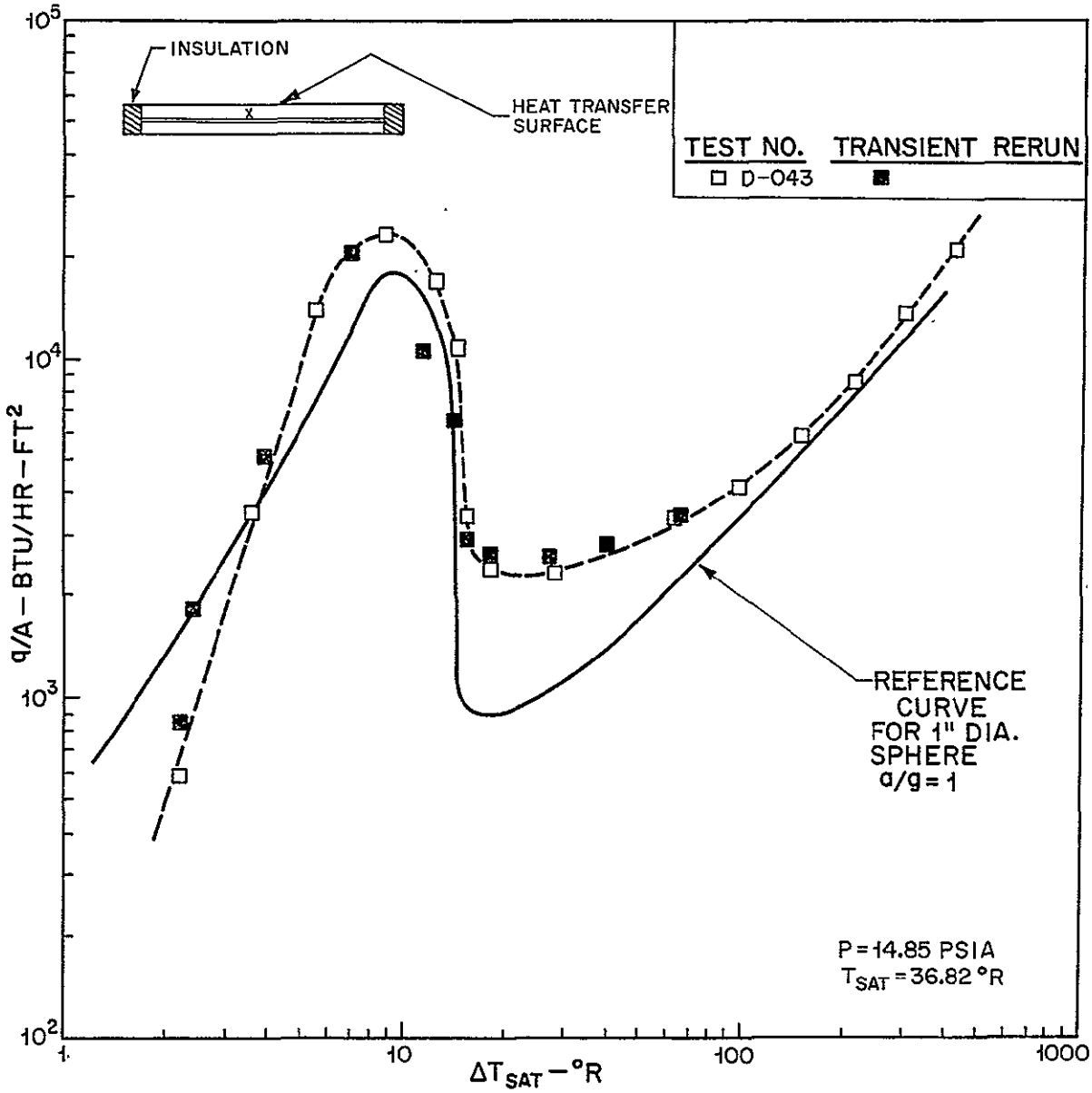

Figure 42. Disc in saturated LH_2—horizontal up, a/g = 1.

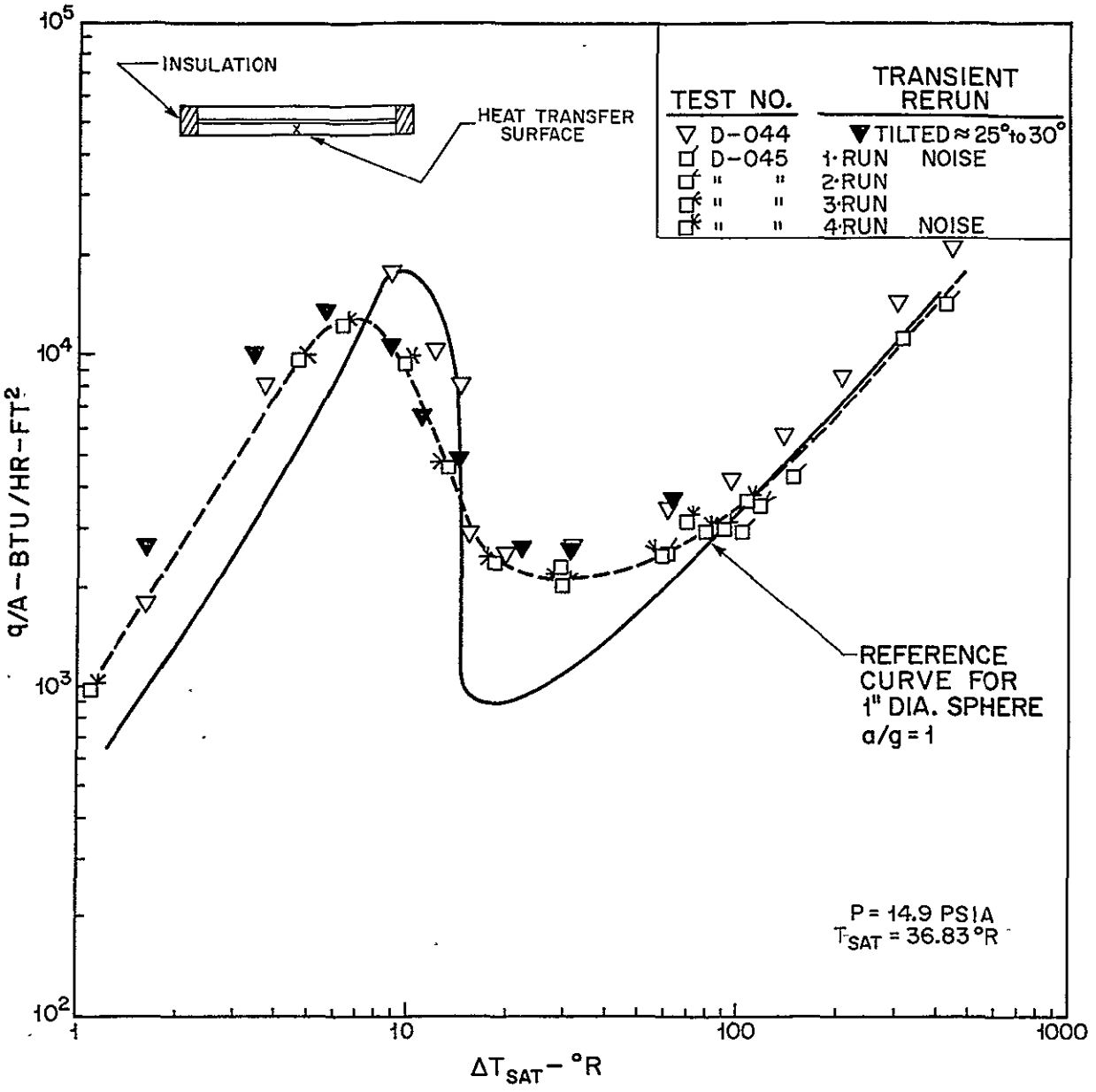

Figure 43. Disc in saturated LH_2—horizontal down, a/g = 1.

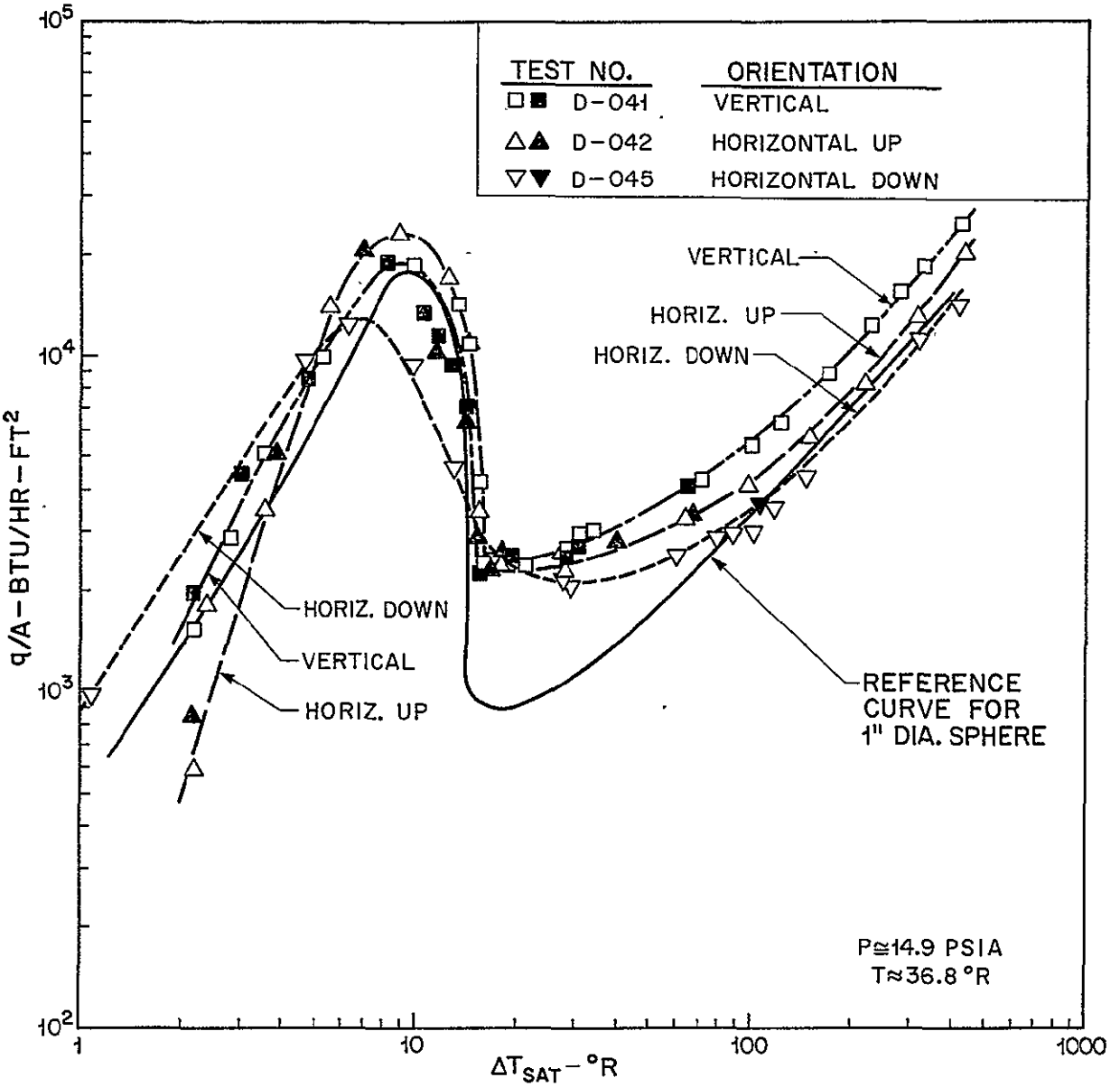

Figure 44. Disc in saturated LH_2—all orientations, a/g = 1.

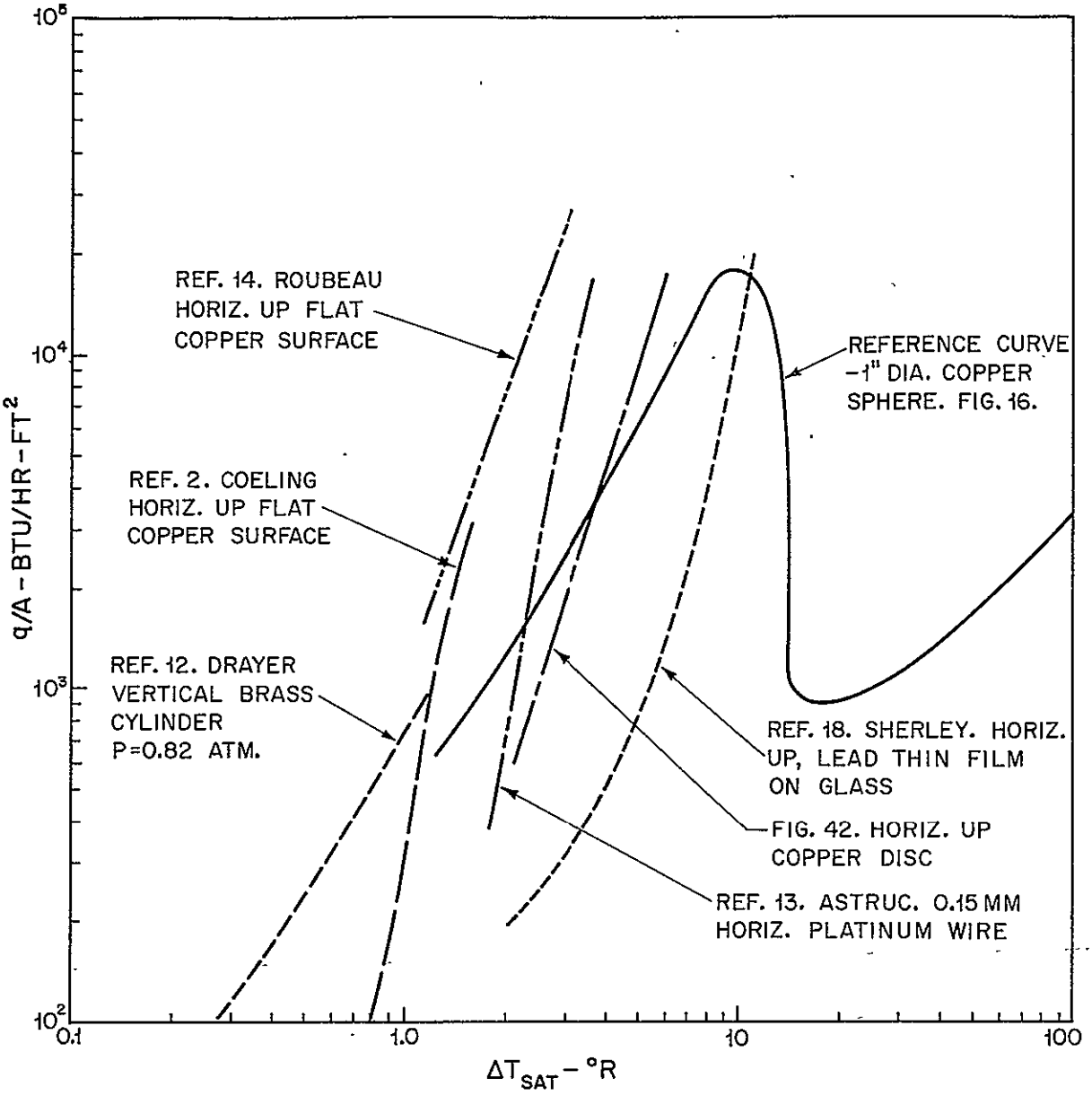

Figure 45. Comparisons of nucleate pool boiling of LH_2 at atmospheric pressure, a/g = 1.

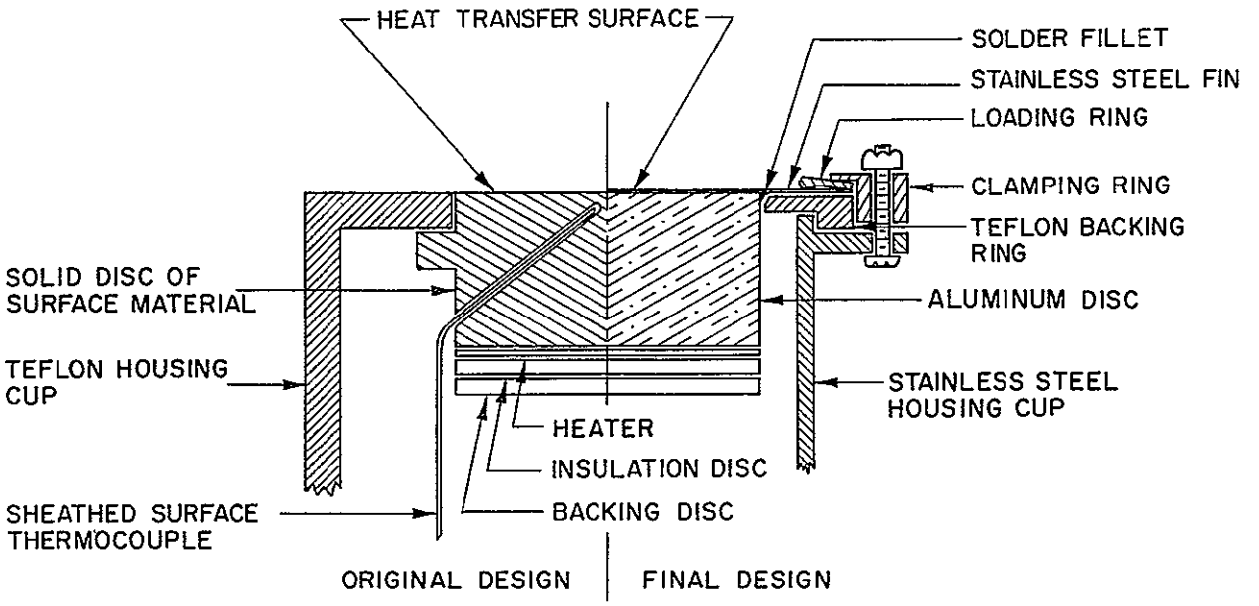

Figure 46. Schematic of test surface mounting technique.

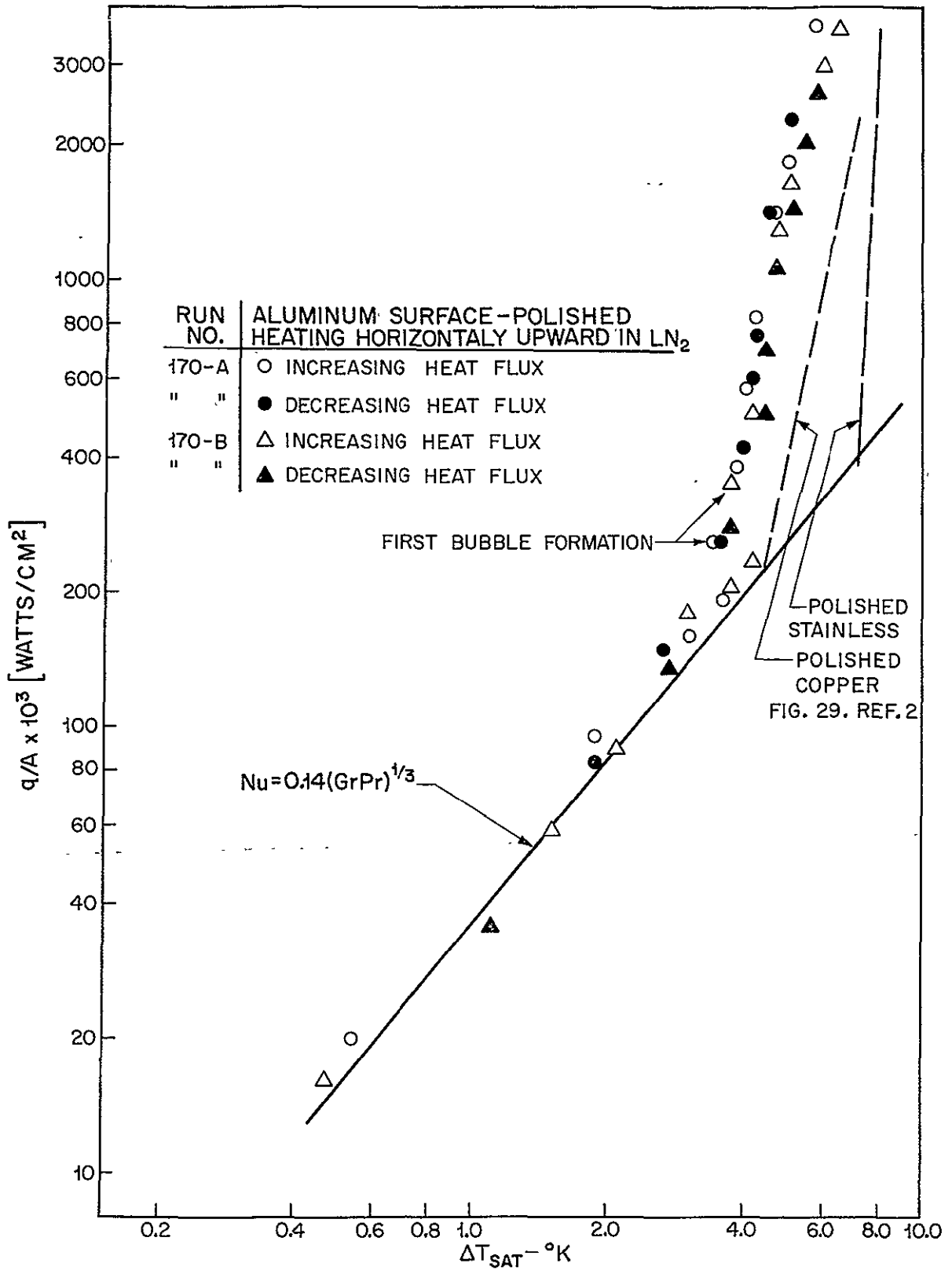

Figure 47. Incipient and nucleate boiling of LN_2 on polished aluminum. P = 1 atm.

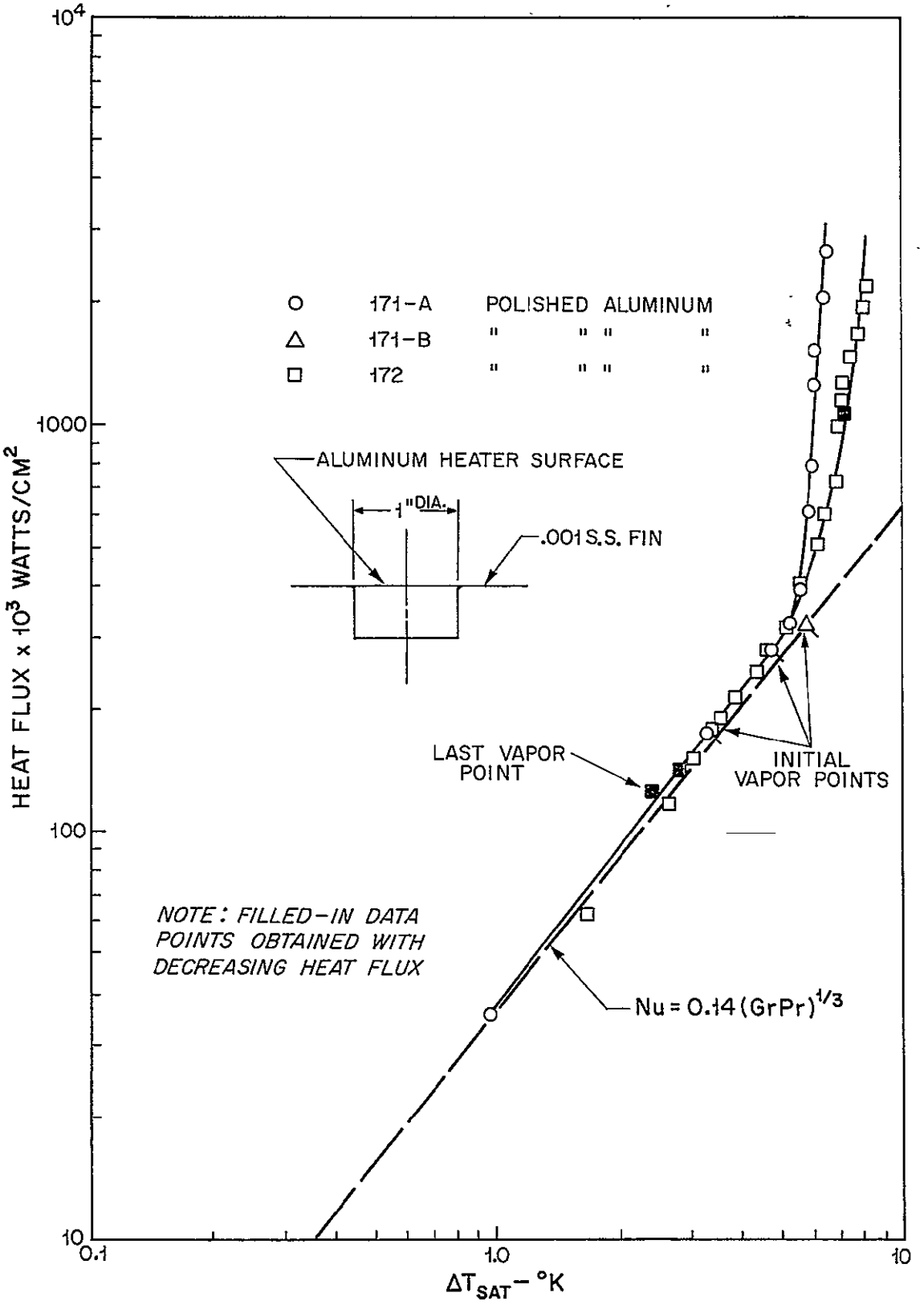

Figure 48. Incipient and nucleate boiling of LN_2 on polished aluminum. P = 1 atm.

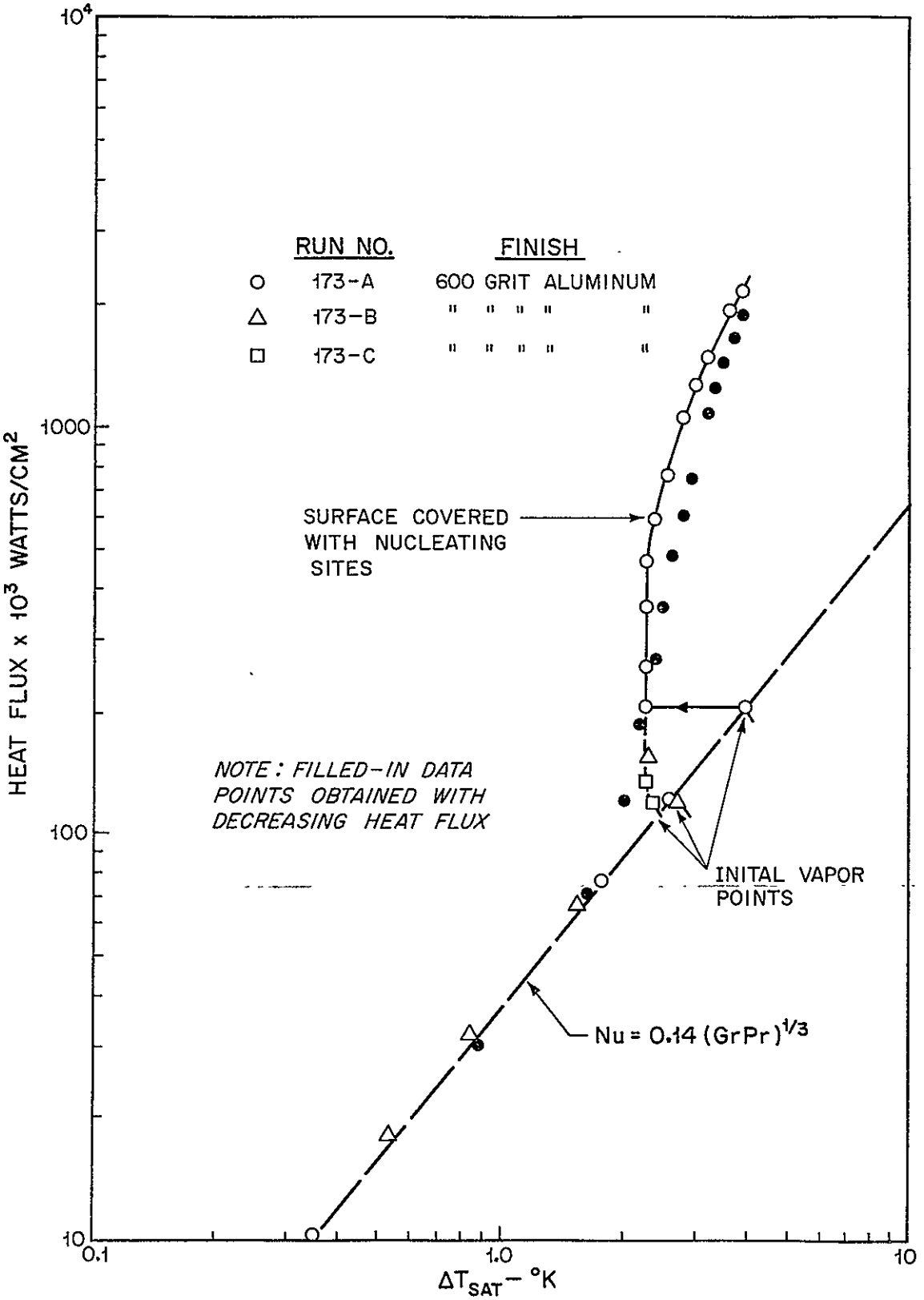

Figure 49. Incipient and nucleate boiling of LN_2 on roughened aluminum. P = 1 atm.

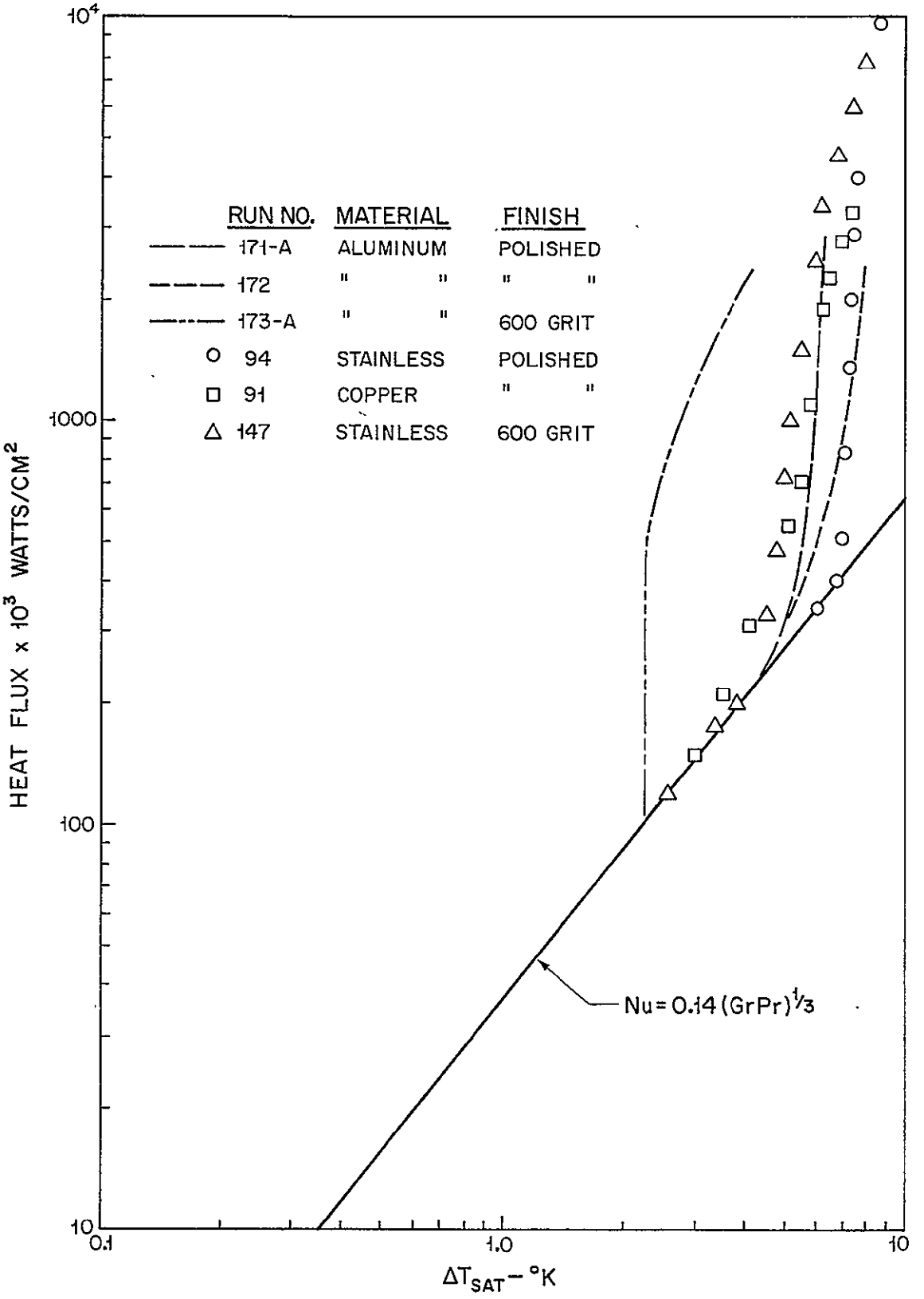

Figure 50. Effect of material and roughness on nucleate boiling of LN_2.

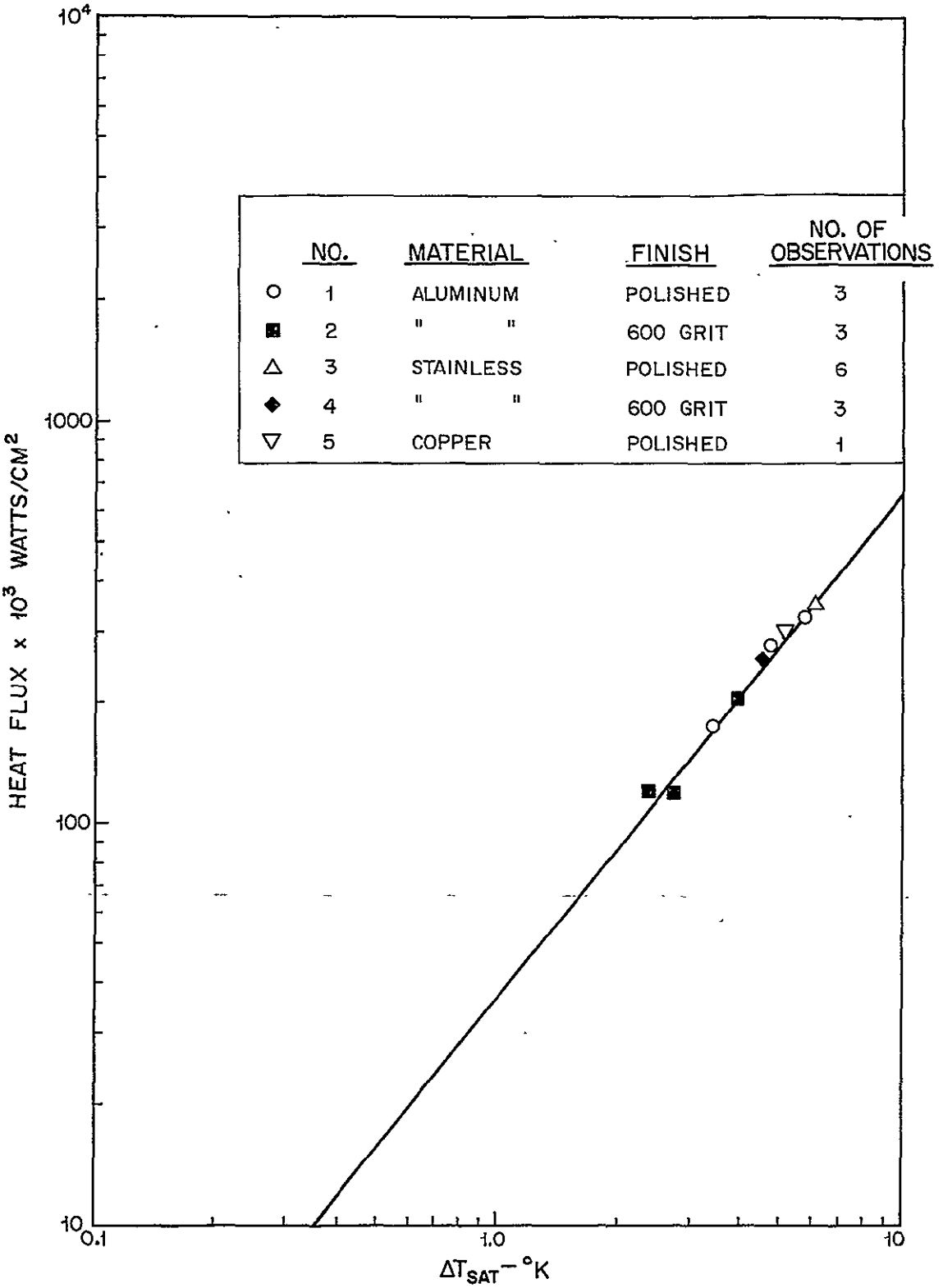

Figure 51. Initial vapor formation. Liquid nitrogen with horizontal surface.

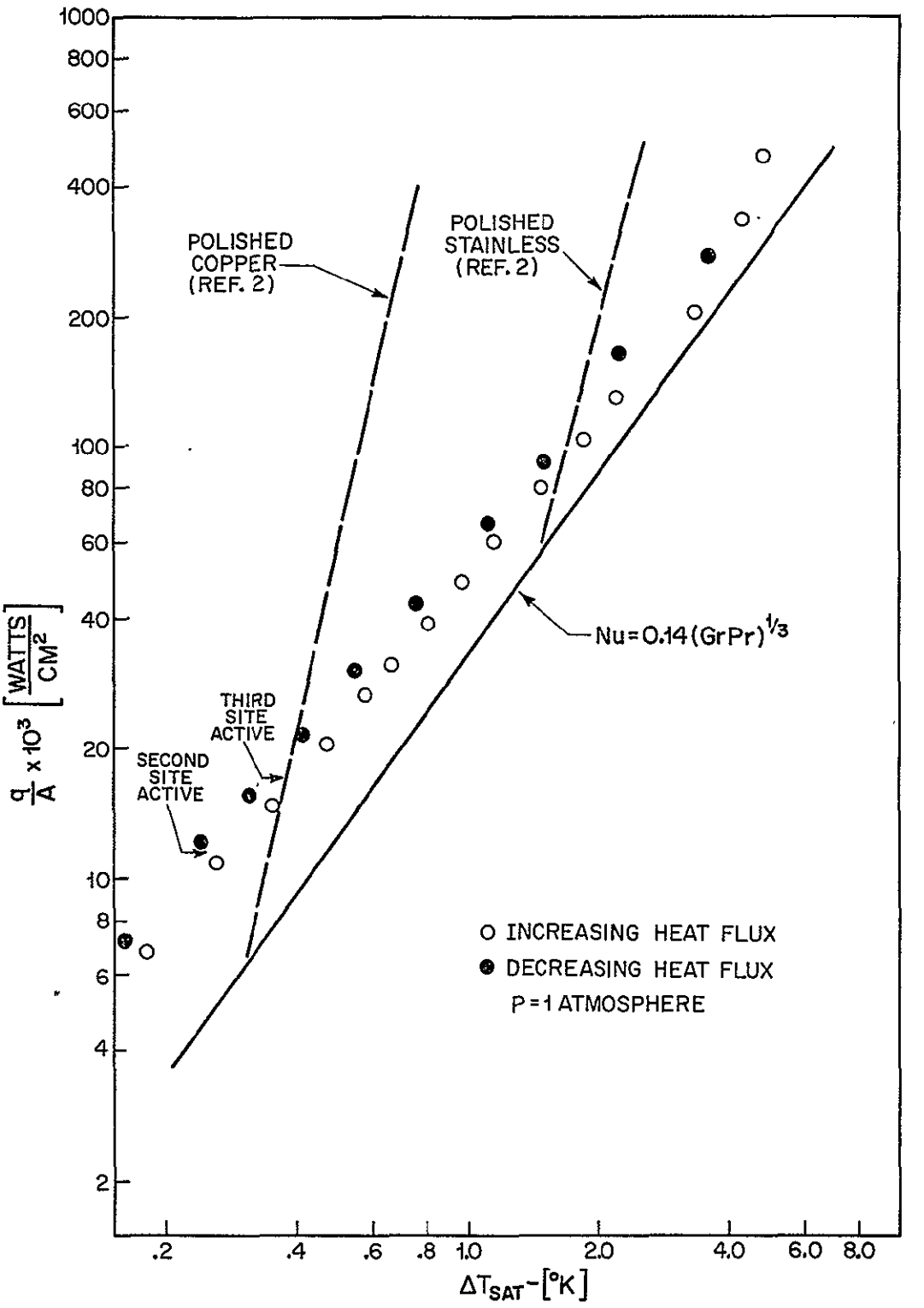

Figure 52. Incipient boiling of LH from a fiber glass surface—horizontal up.

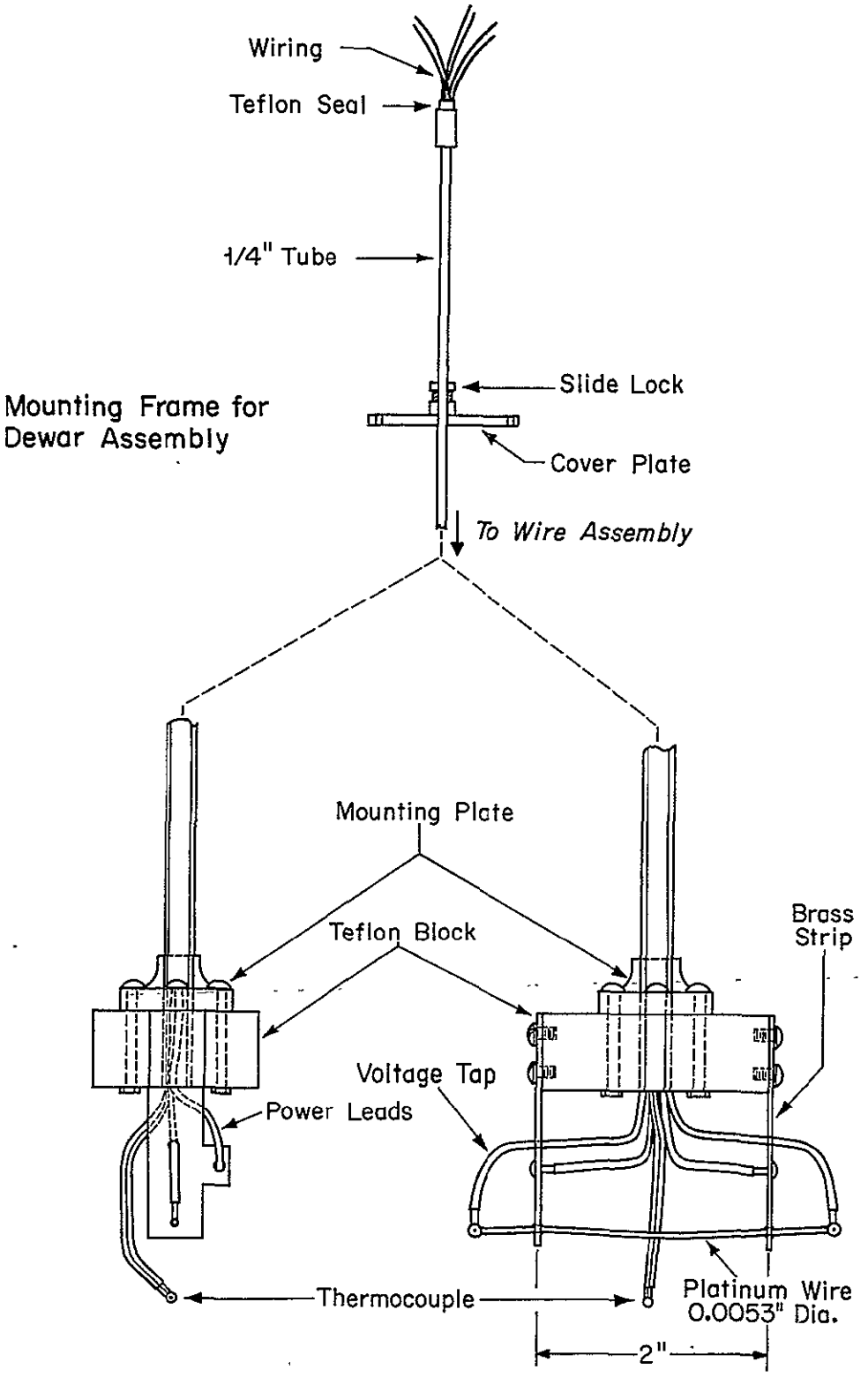

Figure 53. Schematic diagram of platinum wire assembly.

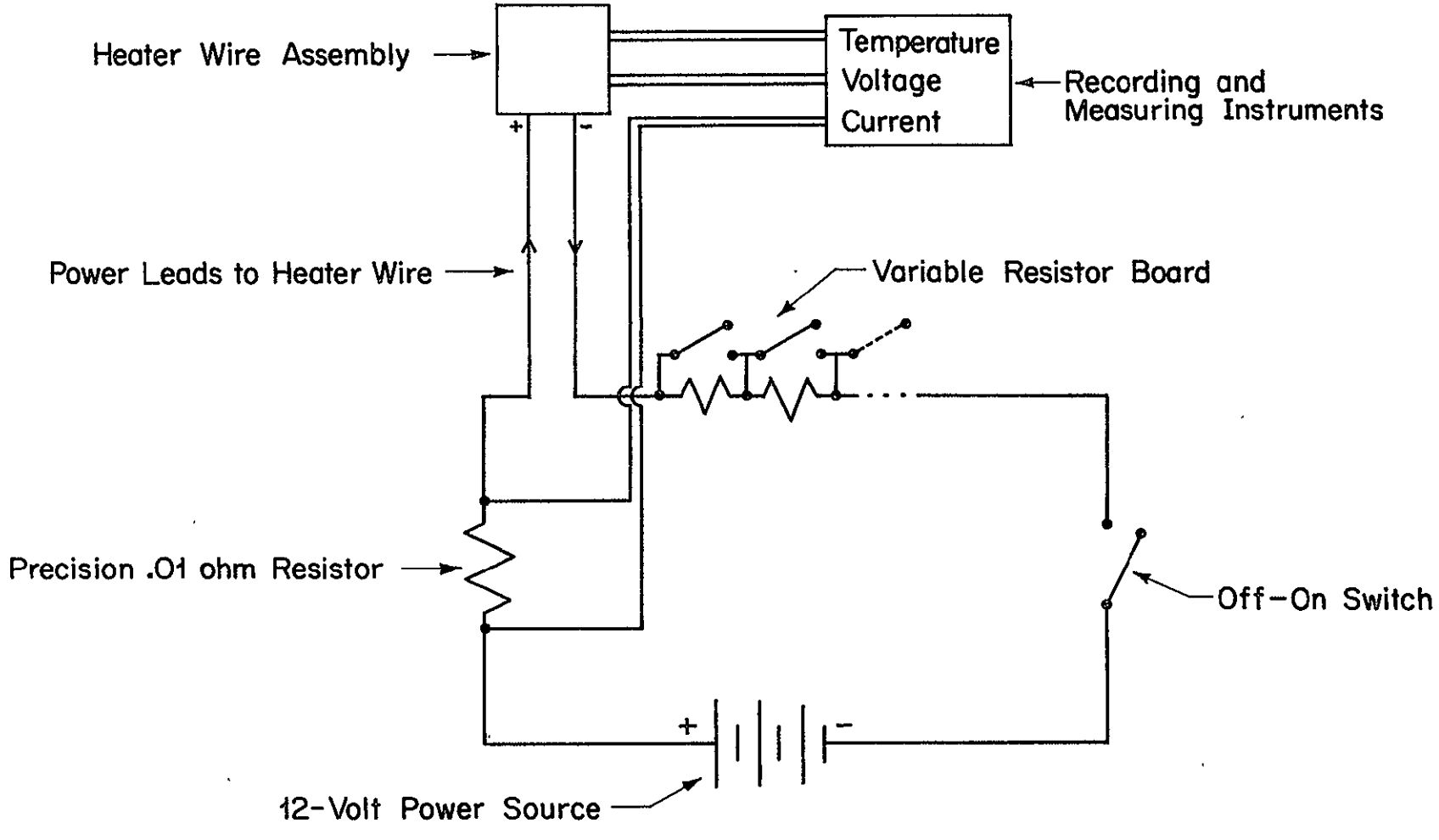

Figure 54. Schematic diagram of D.C. power supply.

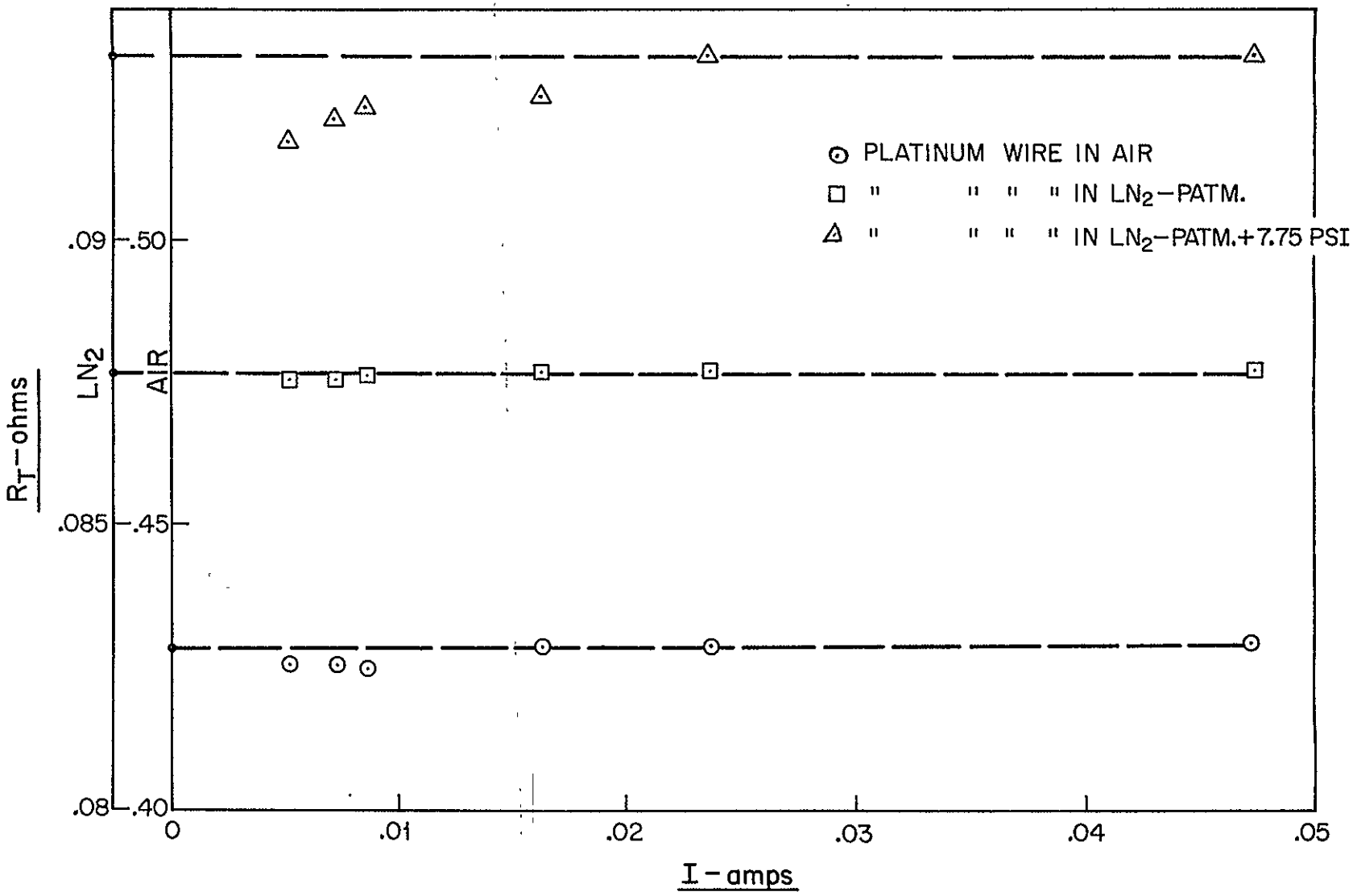

Figure 55. Platinum wire calibration current.

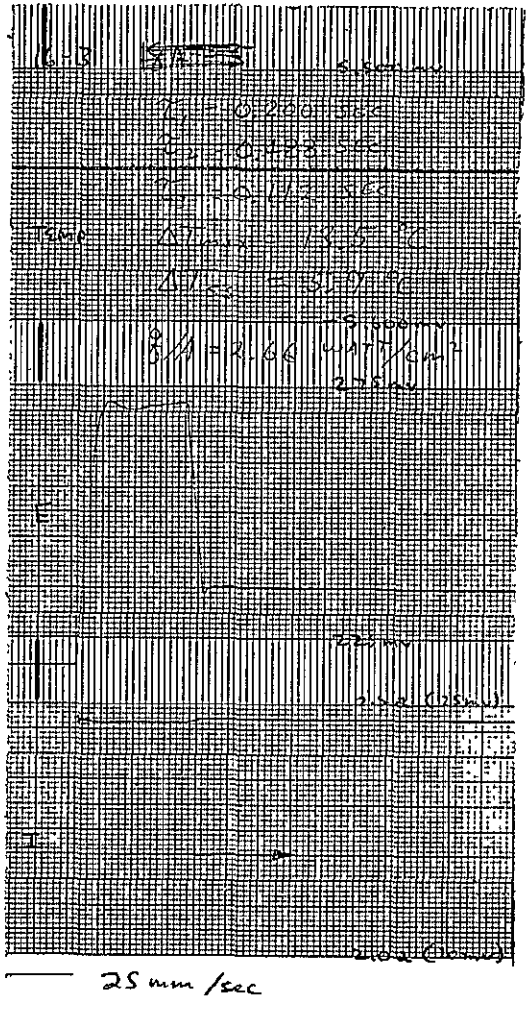

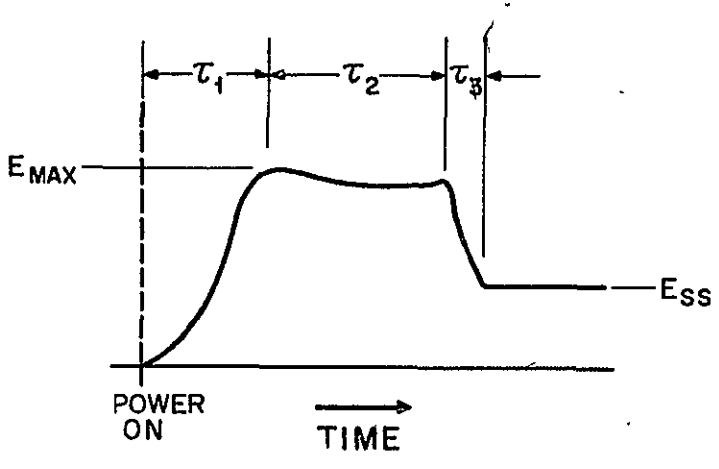

b. Schematic.

Figure 56. Definitions of delay times.

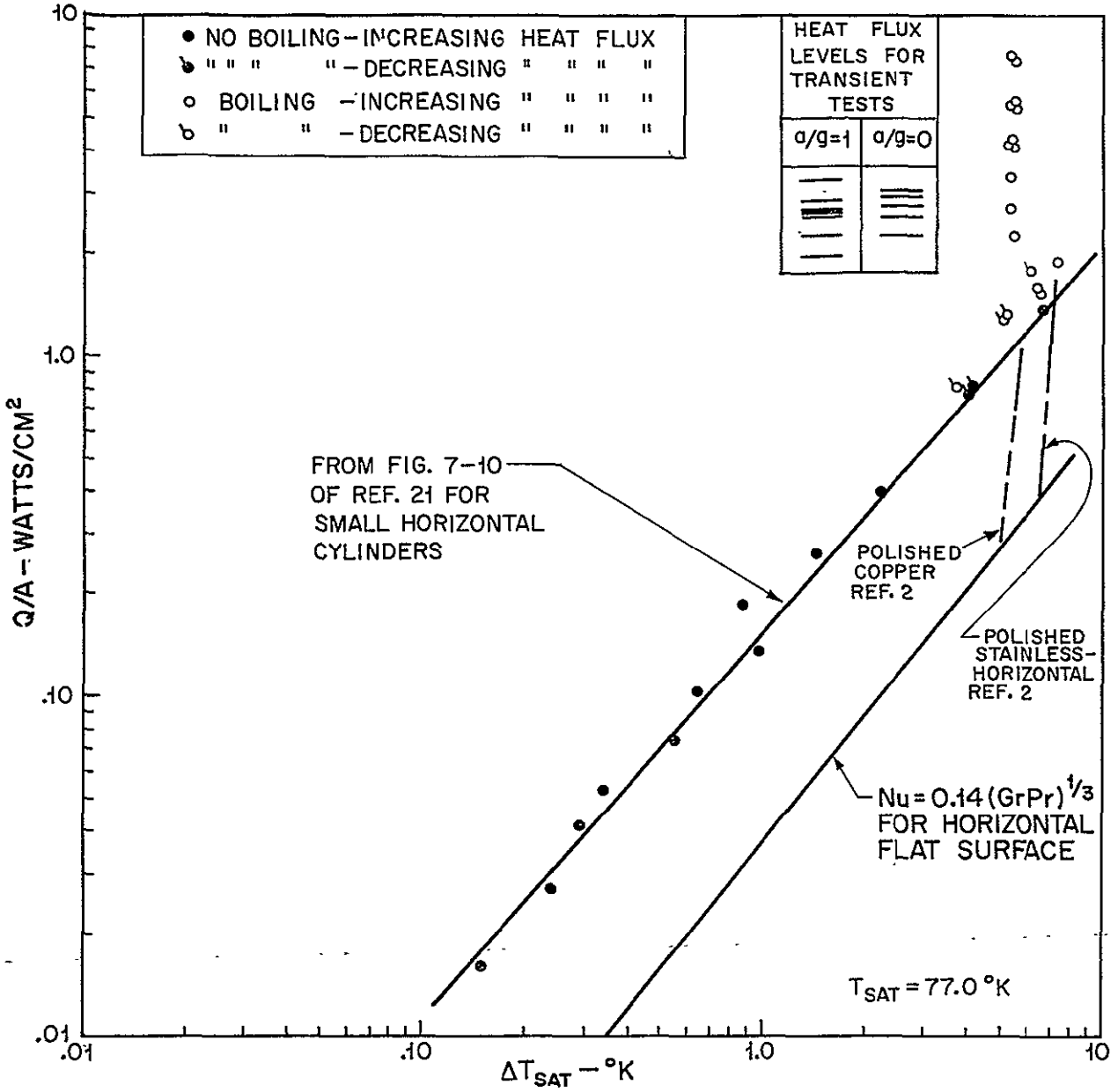

Figure 57. Nucleate boiling for platinum wire in liquid nitrogen.

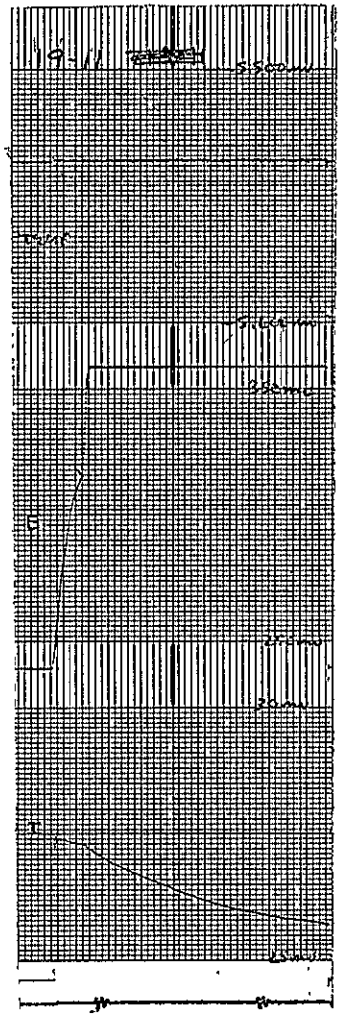

τ_1 = 0.200
τ_2 = 0
ΔT_{max} = 16.2 °C
q/A = 3.26 watt/cm^2

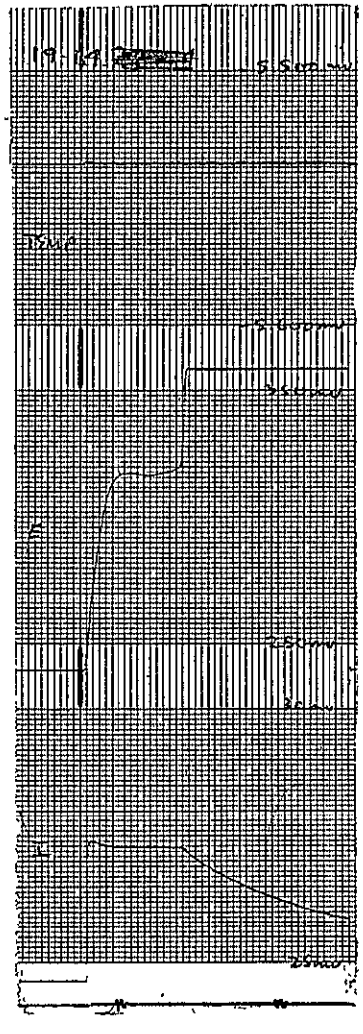

τ_1 = 0.216
τ_2 = 0.333 sec
ΔT_{max} = 16.4 °C
q/A = 3.26 watt/cm^2

a. Directly to film boiling

b. Delay time to film boiling

Figure 58. Typical transient in LN_2 at a/g = 1. Film boiling.

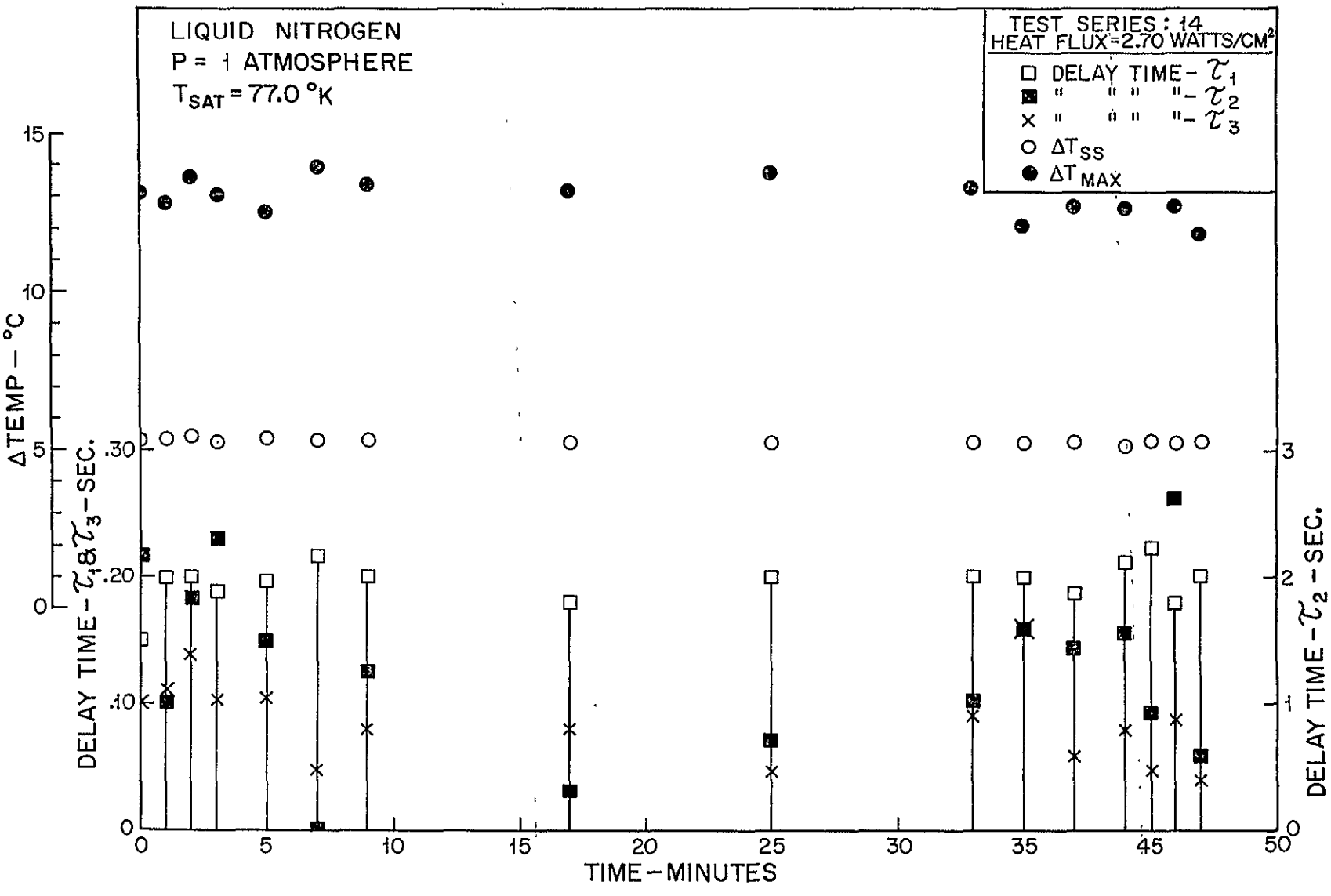

Figure 59. Reproducibility of repeated transient tests.

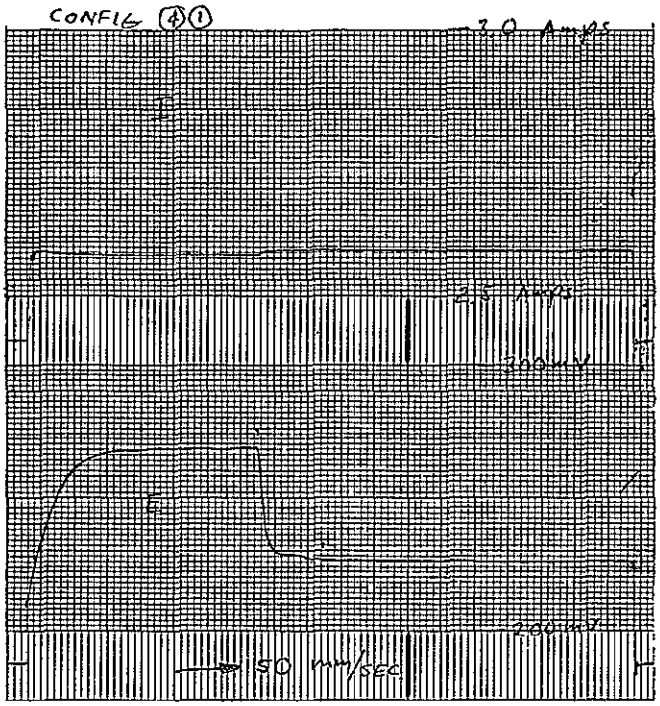

$\leftarrow$ q/A = 2.74 watts/cm^2

a/g = 1: τ_1 = .244 sec
τ_2 = .450 sec
τ_3 = .190 sec
ΔT_{max} = 14.2 °C
ΔT_{ss} = 5.3 °C

a/g $\simeq$ 0: τ_1 = .196 sec
τ_2 = .122 sec
$\downarrow$ τ_3 = .342 sec
ΔT_{max} = 14.2 °C
ΔT_{ss} = 4.9 °C

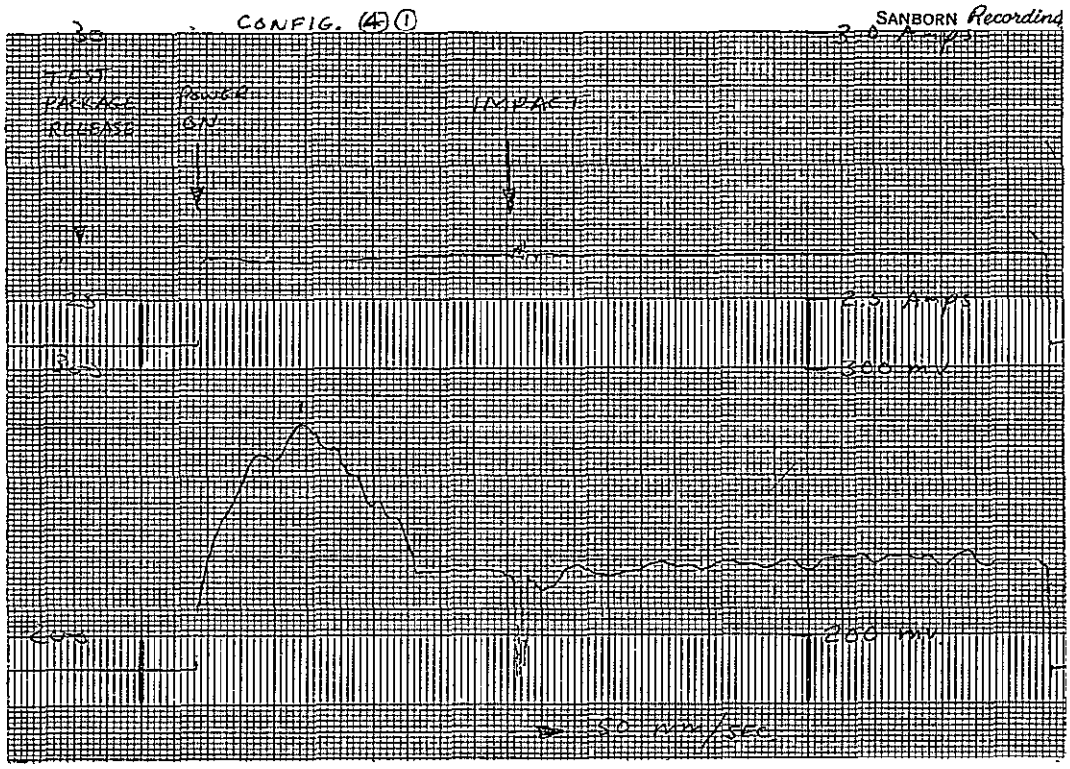

Figure 60. Incipient nucleate boiling in LN_2, p = 1 atm, at a/g and a/g $\approx$ 0.

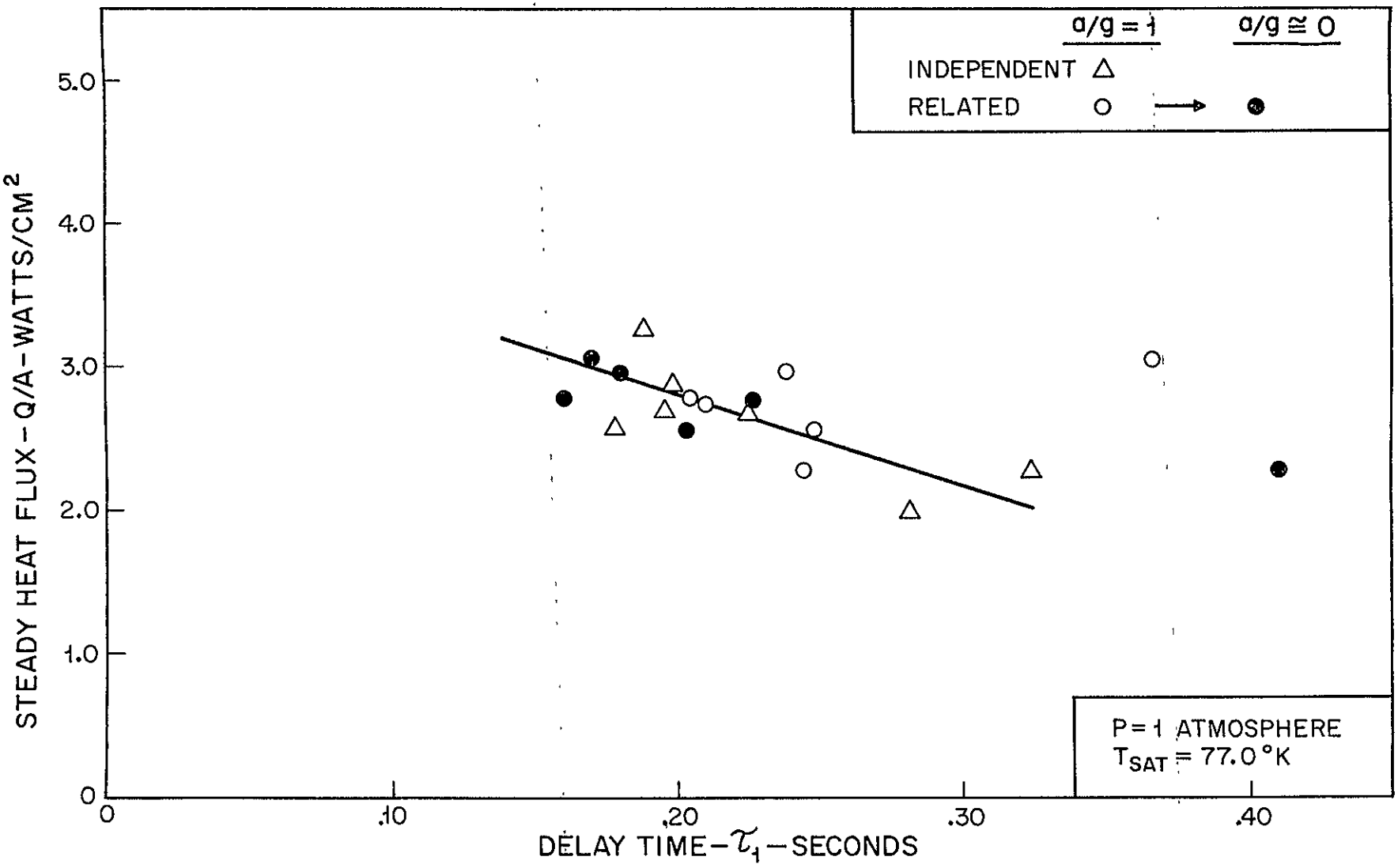

Figure 61. Transient delay time τ_1. Platinum wire in LN_2.

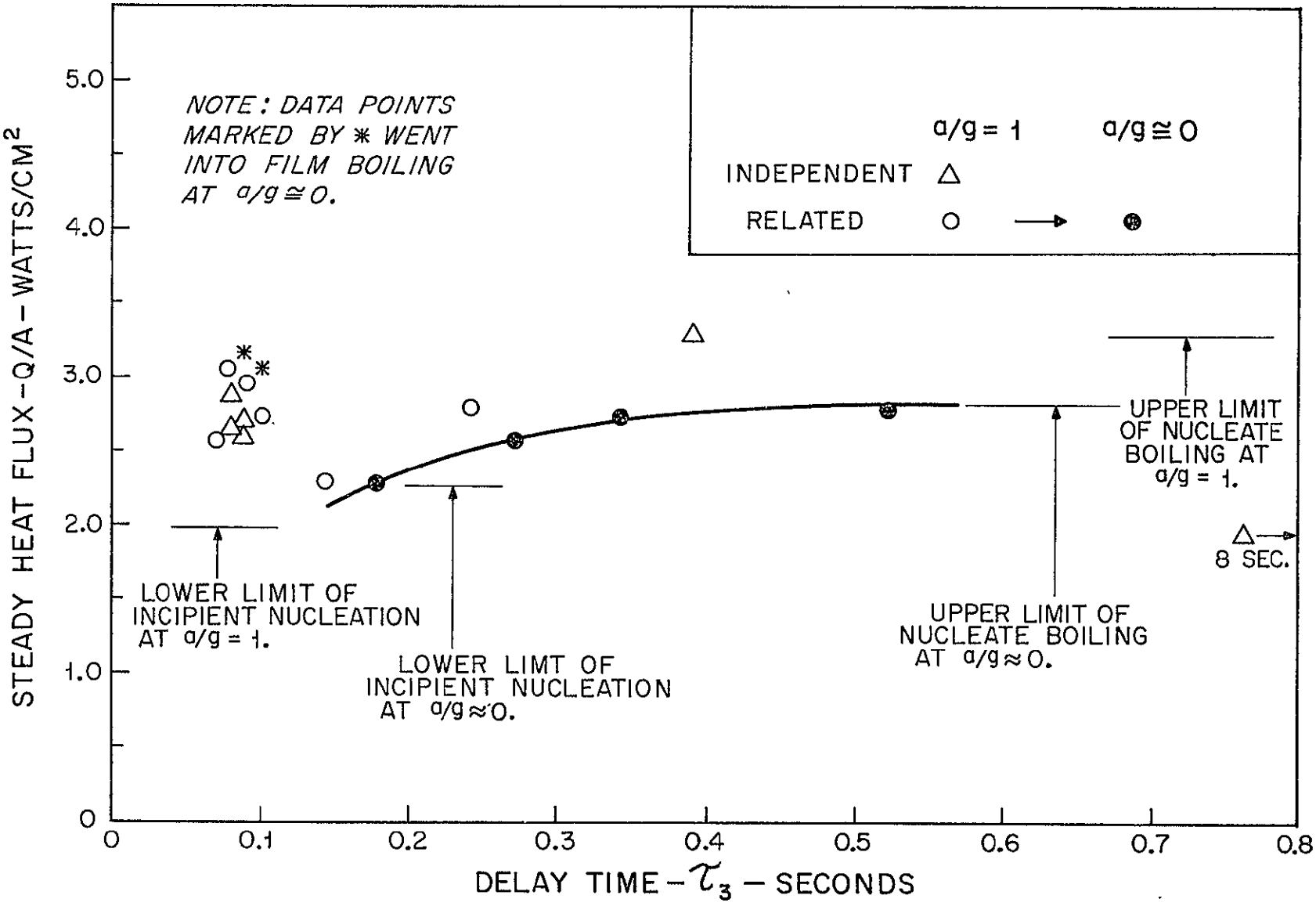

Figure 62. Transient delay time τ_3. Platinum wire in LN_2.

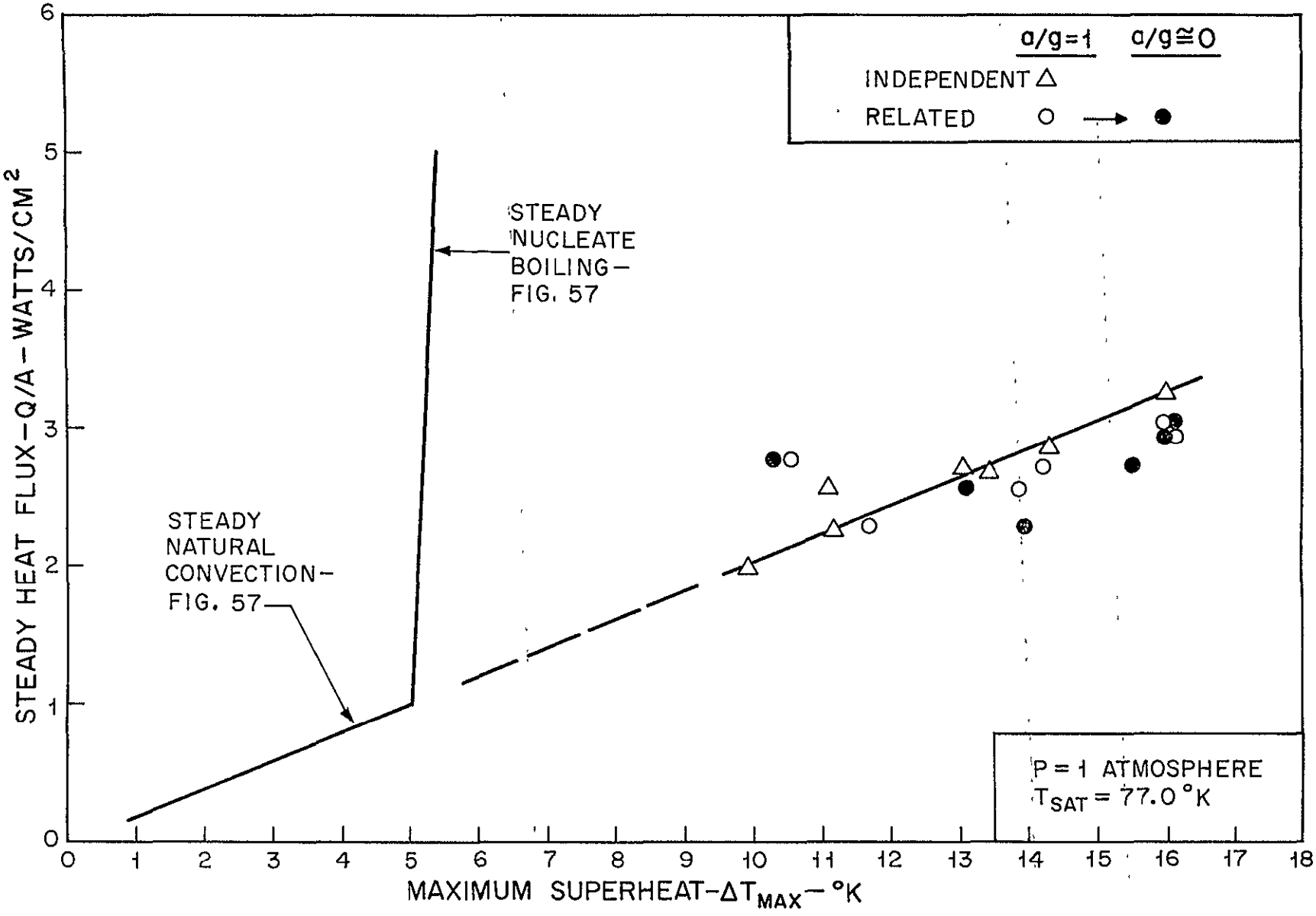

Figure 63. Maximum transient superheat—LN_2.

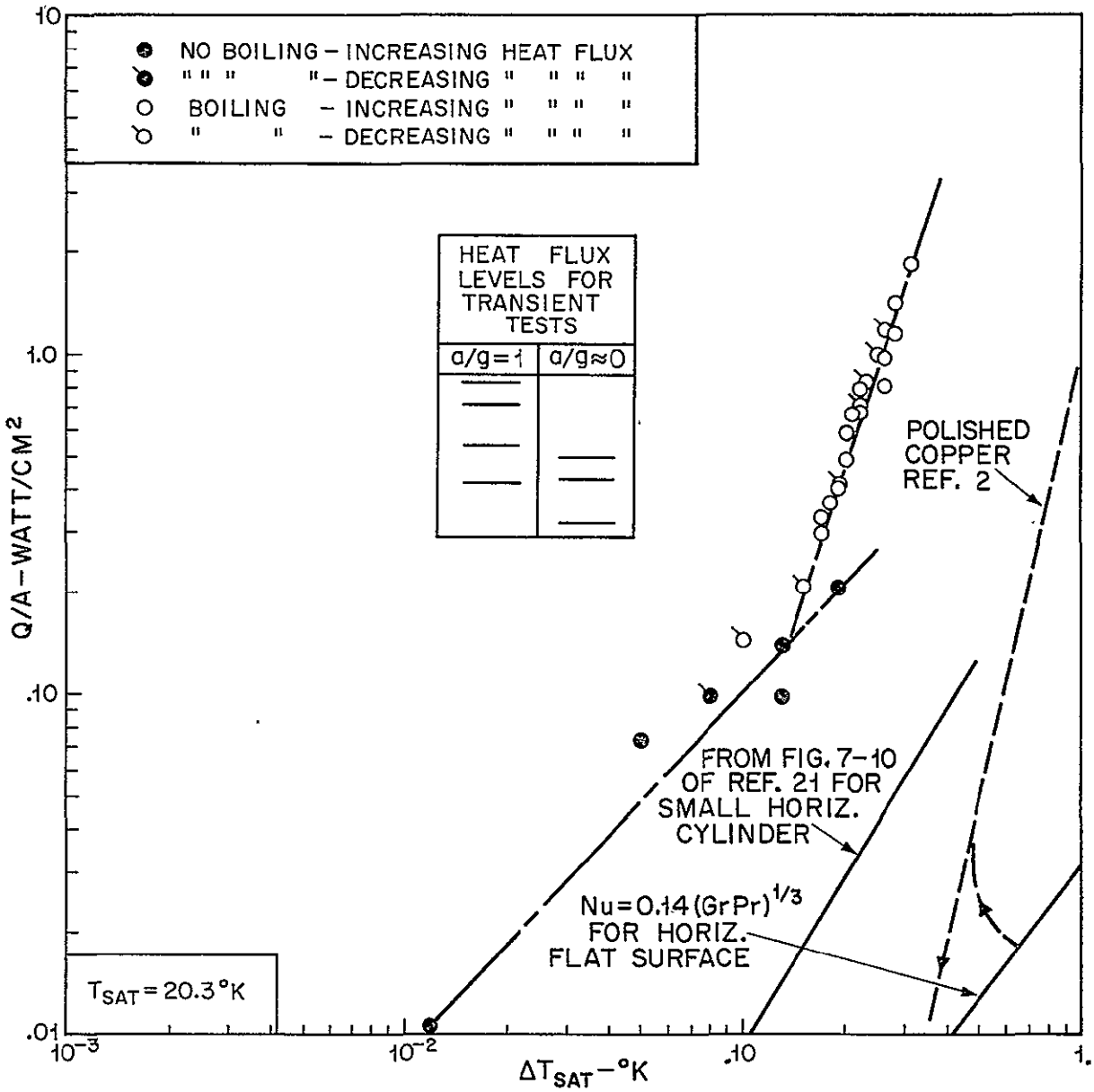

Figure 64. Nucleate boiling for platinum wire in liquid hydrogen. P = 1 atm.

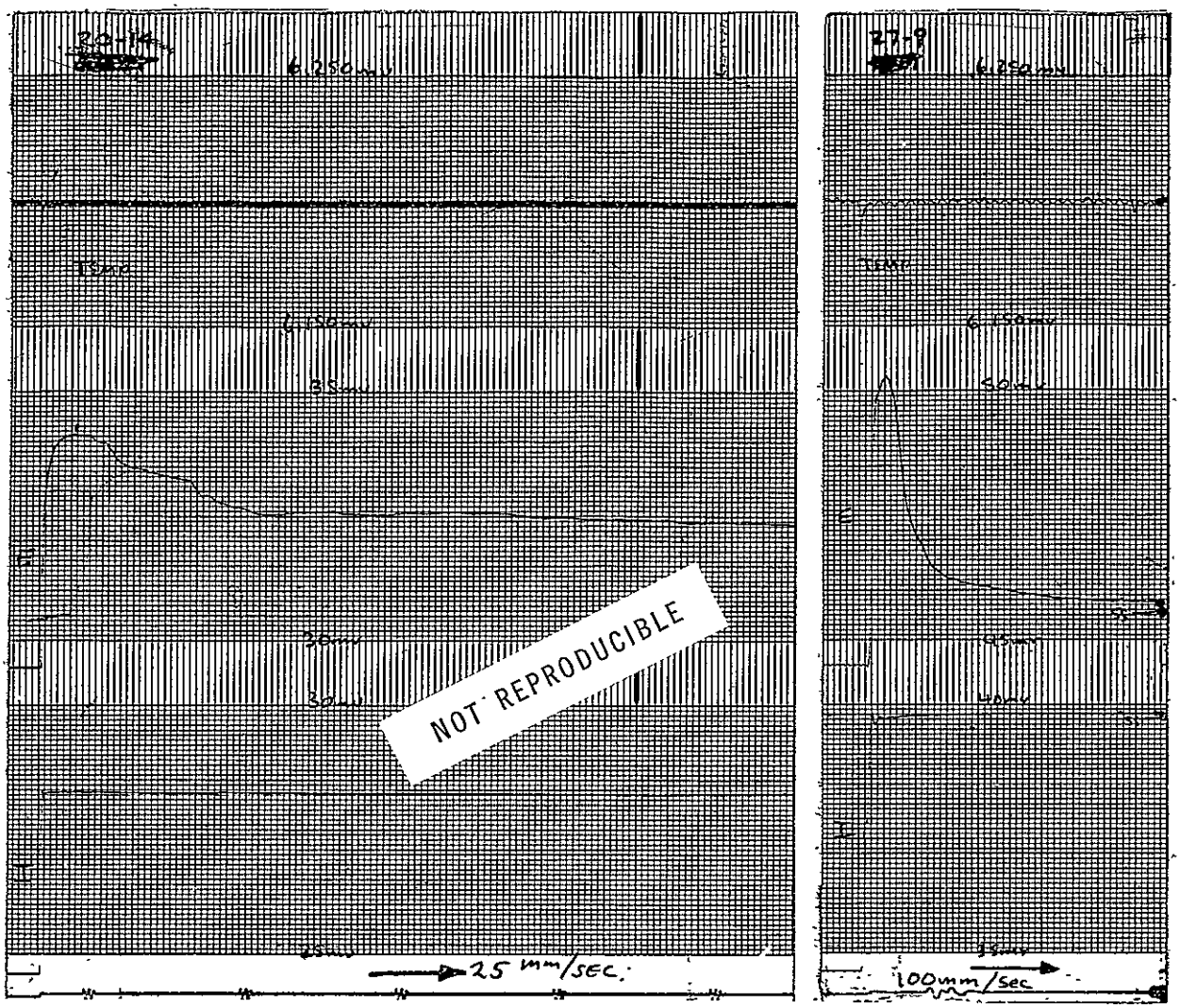

q/A	=	0.42 watts/cm^2	q/A	=	0.83 watts/cm^2
τ_1	=	0.22 sec	τ_1	=	0.022 sec
τ_2	=	0.08 sec	τ_2	=	0
τ_3	=	3.0 sec	τ_3	=	0.5 sec
ΔT_{max}	=	1.00 °C	ΔT_{max}	=	1.34 °C
ΔT_{ss}	=	0.66 °C	ΔT_{ss}	=	0.71 °C

Figure 65. Incipient nucleate boiling in LH_2. P = 1 atm. Typical transients at a/g = 1.

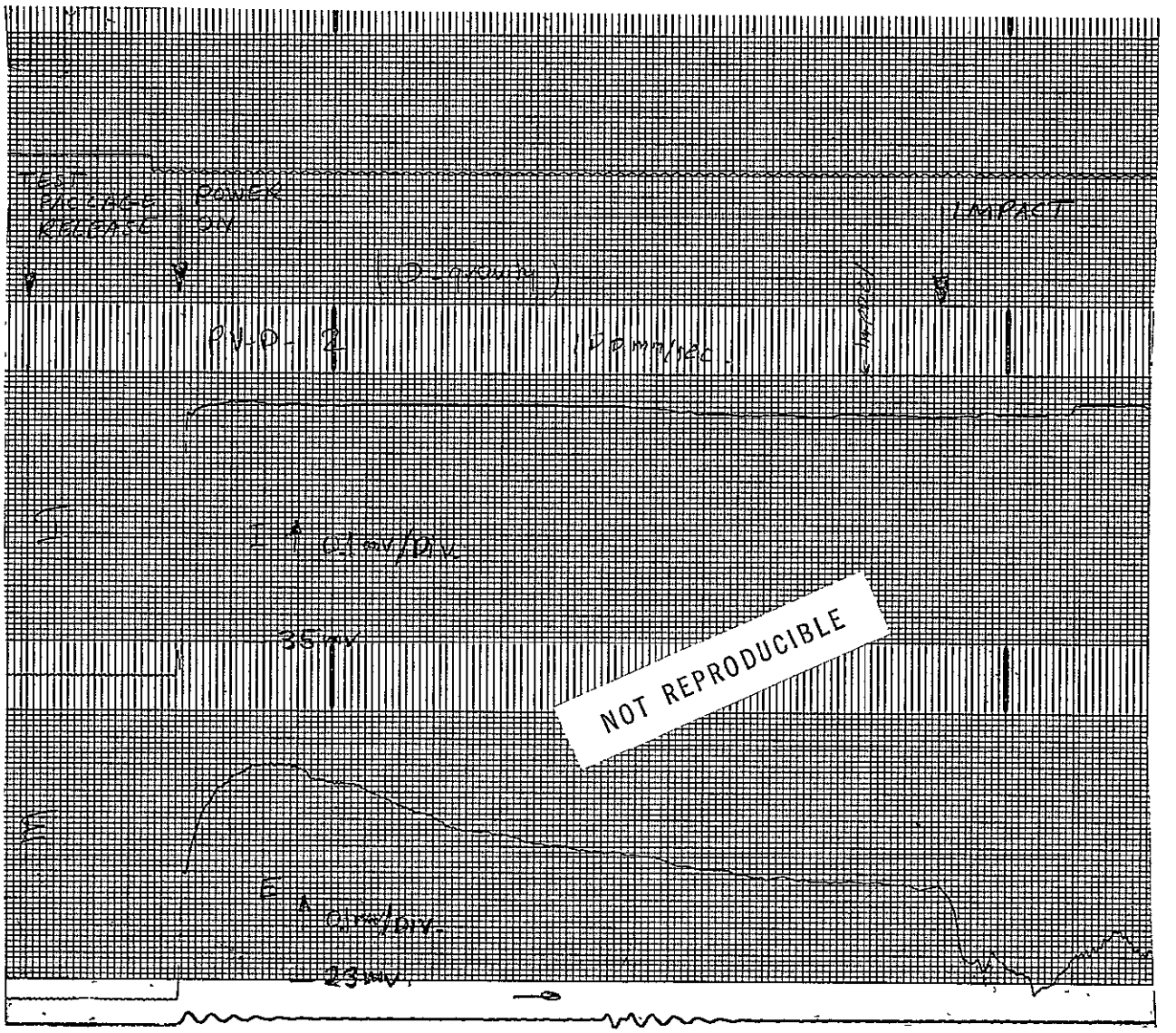

$q/A = 0.50$ watts/cm^2
$\tau_1 = 0.125$ sec
$\tau_2 = 0.07$ sec
$\tau_3 = 0.85$ sec
$\Delta T_{max} = 1.12$ °C
$\Delta T_{ss} = 0.59$ °C

Figure 66. Incipient nucleate boiling in LH_2. P = 1 atm, at $a/g \approx 0$.

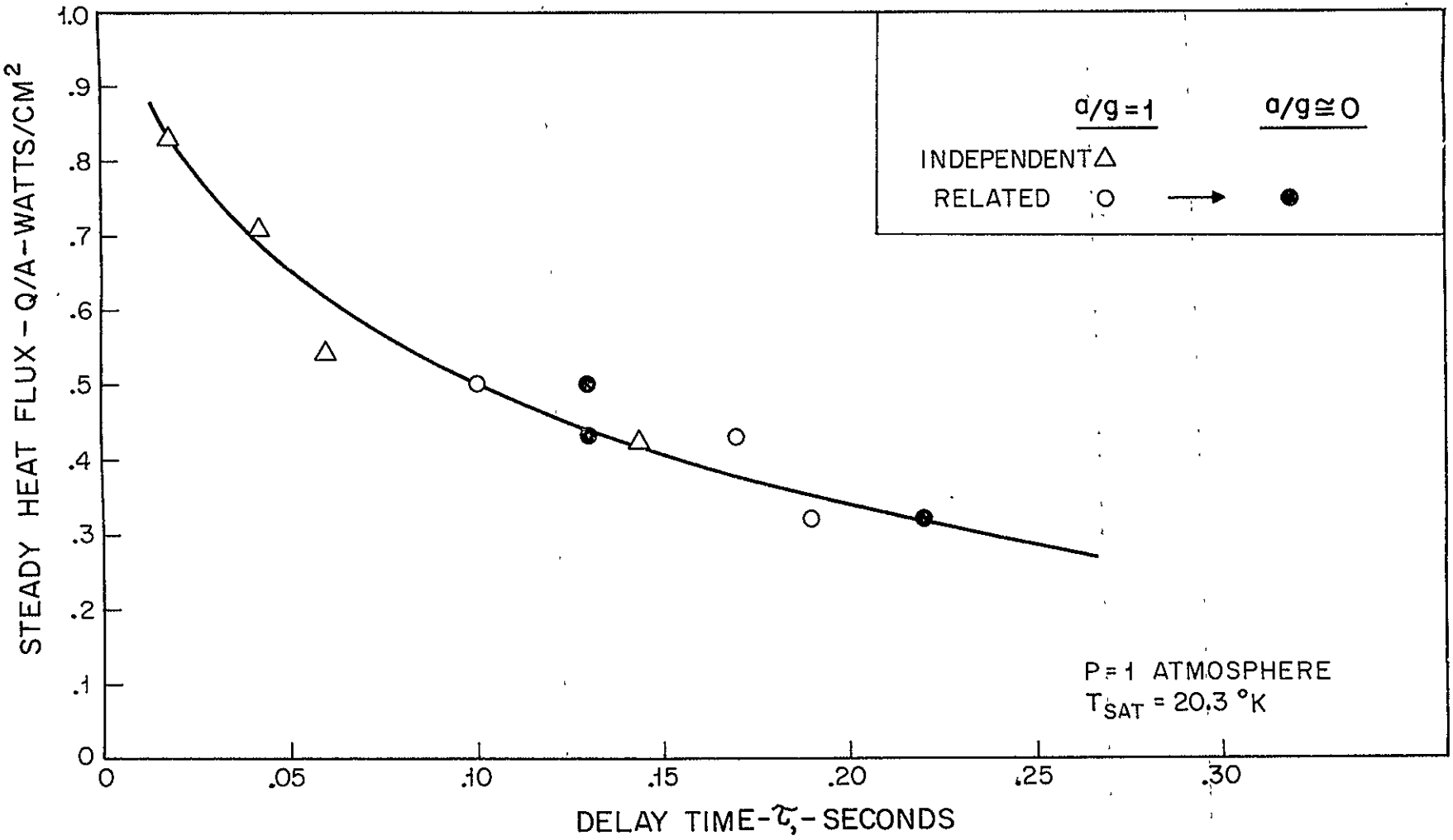

Figure 67. Transient delay time τ_1. Platinum wire in LH_2.

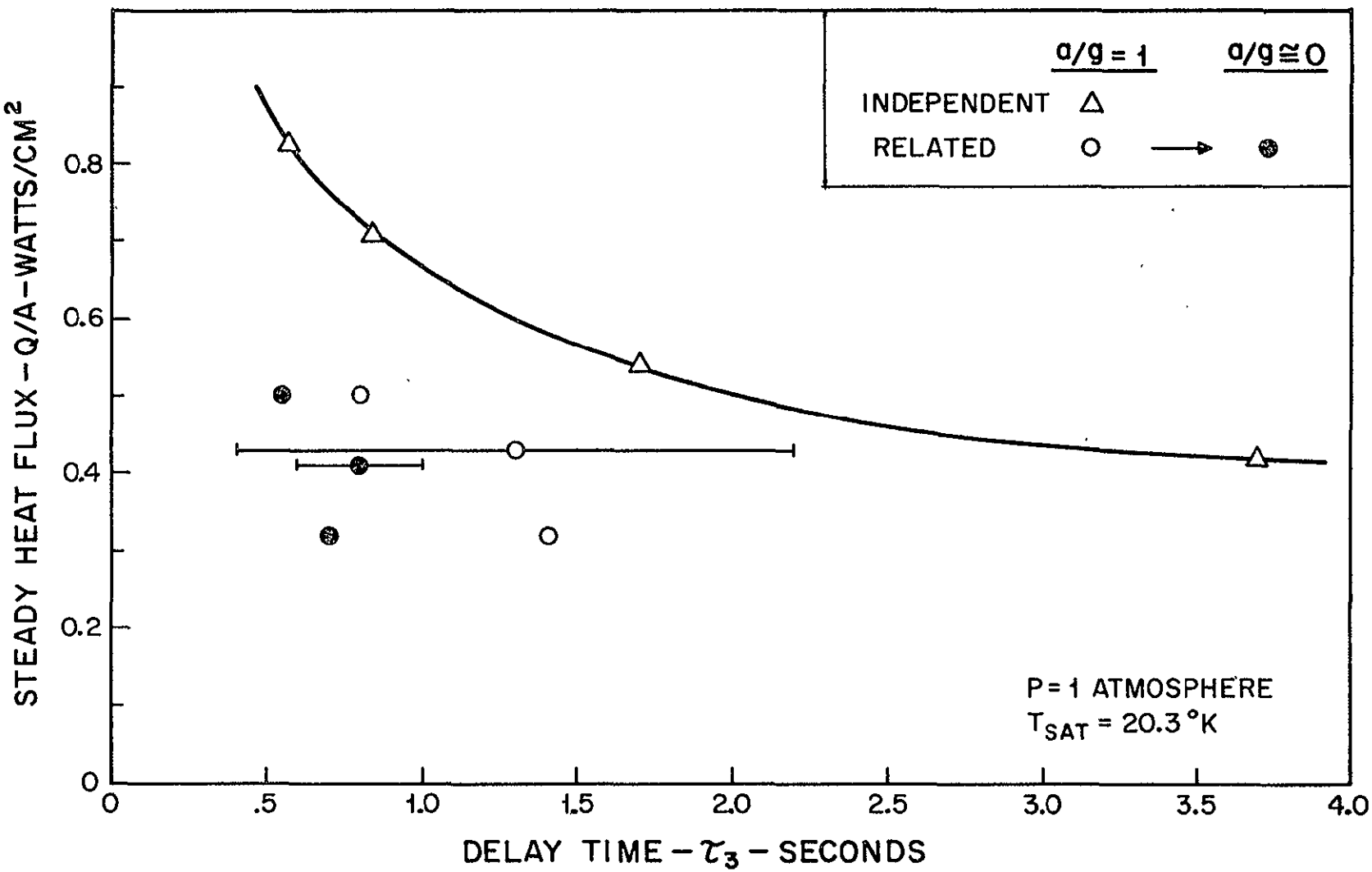

Figure 68. Transient delay time τ_3. Platinum wire in LH_2.

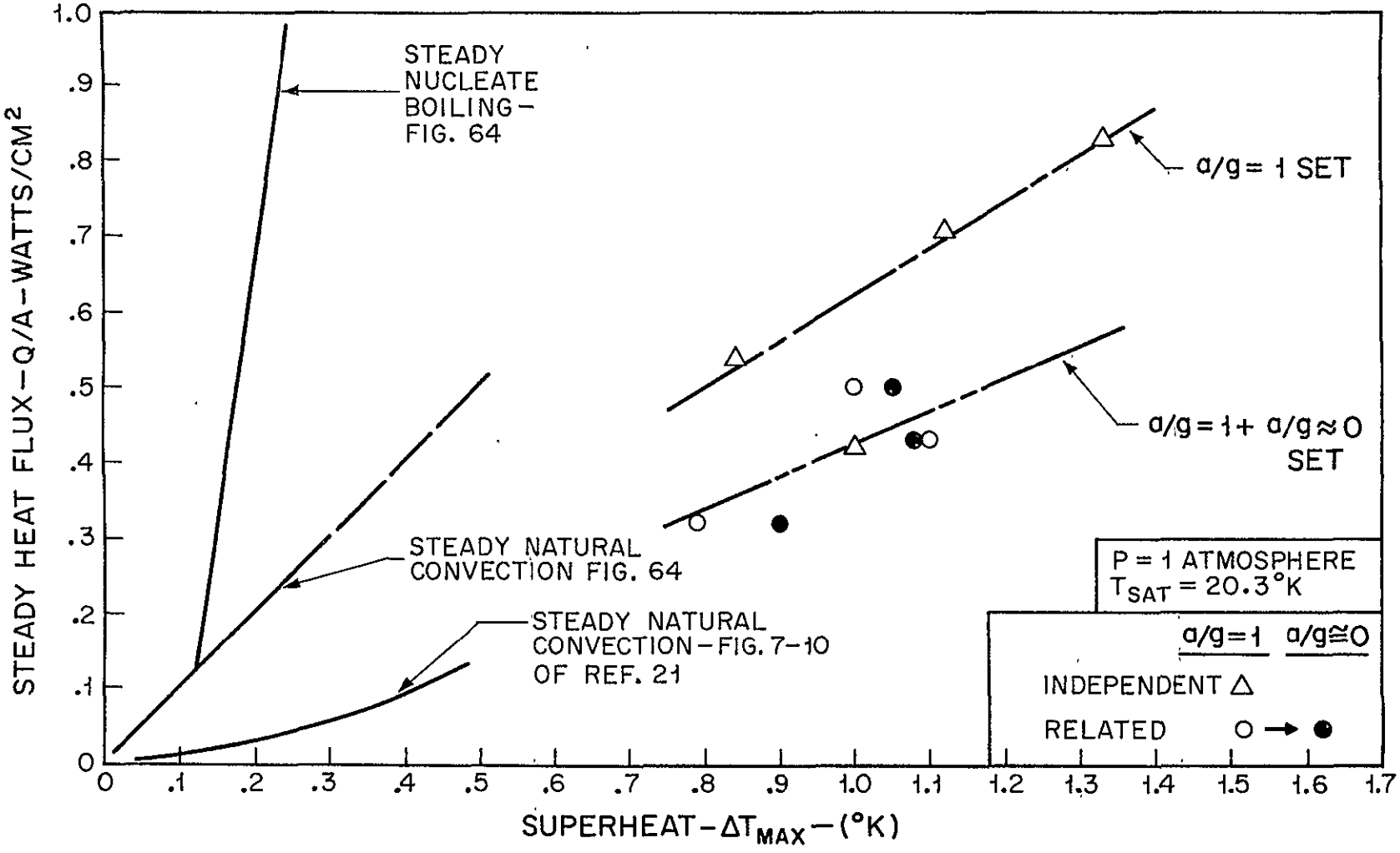

Figure 69. Maximum transient superheat—LH_2.

APPENDIX

ABSTRACTS OF PRIOR TECHNICAL REPORTS

Technical Report No. 1

THE DYNAMICS OF MOVING BUBBLES IN SINGLE- AND BINARY-COMPONENT SYSTEMS

N. Tokuda, W. J. Yang, J. A. Clark, and H. Merte, Jr.

Abstract

The dynamics of a single bubble moving in a quiescent liquid is analyzed for single- and binary-component systems. The analysis is made for the region in which the bubble dynamics is controlled by the transport of energy and/or mass subject to thermodynamic phase-equilibrium at the bubble interface.

The dynamics of moving bubble in a single-component system is investigated initially. The interfacial temperature remains constant with time for this case. With the application of the boundary layer simplification and approximating the velocity field around the bubble as a uniform flow, two asymptotic solutions of the bubble dynamics for small and large times, are obtained by means of the coordinate perturbation method. The bubble behavior during small times is dominated by diffusion and/or radial convection while at large times it is controlled by diffusion and axial convection. In the analysis, the temperature distribution in the liquid around the bubble is obtained as a function of dimensionless parameters and universal functions. Then the total heat flux over the entire bubble surface is evaluated and related to the interfacial energy balance condition. The resulting equation is integrated to yield the bubble growth or collapse rate. The solutions for small and large times may be joined successfully at an intermediate time. It is disclosed that the dimensionless parameter $\gamma = \sqrt{2K}\ Pe^{1/2}/Ja$ governs the bubble dynamics, where K is a constant, Pe is the Peclet number and Ja is the Jakob number. The results agree very well with experiments.

For binary-component systems, both injection cooling and boiling are treated. The method employed is the extension of that used for the single-component system. Both the interfacial temperature and concentration vary with time.

The dynamics of a moving bubble in injection cooling is governed by the parameters γ and $\beta = Ja/\sqrt{Lu'}$ where Lu' is the Lukomskiy number for gaseous phase.

The dynamics in boiling binary-component is a function of the parameters γ, $\beta_0 = Ja/\sqrt{Lu}\ \rho'/\rho\ \alpha_0-\alpha_1/\alpha_0$ and $\beta_1 = Ja/\sqrt{Lu}\ \rho'/\rho\ X'_\infty-X_\infty/\alpha_0$ in which α_0 and α_1 are the temperature gradients of the phase-equilibrium curves, Lu is the Lukomskiy number for liquid phase, ρ and ρ' are the liquid and gases densities, respectively, and $X'_\infty-X_\infty$ is the relative volatility. The analytical results for the injection cooling case agree well with experiments.

Technical Report No. 2

BOILING OF LIQUID NITROGEN IN REDUCED GRAVITY FIELDS WITH SUBCOOLING

E. W. Lewis, J. A. Clark, and H. Merte, Jr.

Abstract

Pool boiling of liquid nitrogen in a body force field less than standard gravity was studied using a transient calorimeter measurement technique. Experimental variables included: body forces from standard gravity to near-zero; a variety of geometries and orientations of the boiling surface; subcooling from 0°F to 30°F; pressures from 1 to 5 atmospheres; and boiling regimes from film to nucleate, plus free convection. Gravity was varied by using a drop tower and a counterweighted test package. In free fall, the test package achieved a level of less than 0.002 times standard gravity. Heat transfer surfaces included 1/4-, 1/2-, and 1-inch diameter spheres and a 3-inch diameter by 13/16-inch thick disk oriented vertically, horizontally heating up, and horizontally heating down.

Subcooling was achieved by rapid pressurization of the liquid nitrogen; 3 to 5 atmospheres were used, providing maximum subcooling of approximately 20°F and 30°F. Results were obtained in the form of time vs. surface temperature, which were then expressed as heat flux vs. the difference between the test surface temperature and saturated liquid temperature. These results are presented graphically. In addition, high-speed photographs were made showing the film boiling process. These photographs were used to determine vapor film thicknesses for the various geometries. All results were limited to the film-boiling region except for those obtained with the 1-inch diameter sphere, which was used in all boiling regions.

In the film-boiling region, the heat flux on the spheres varied as diameter to the -1/8 power. The heat flux on the disk, within the uncertainty of the measurements, did not exhibit any dependence on the disk orientation, but was approximately 100% higher than the heat flux observed on the spheres with similar liquid conditions. The appearance of the vapor film on the disk as observed in the photographs differed with orientation. The heat flux on the 1/2-inch and 1-inch spheres varied as the 1/3 power of acceleration. The heat flux on the 1/4-inch sphere and the disk varied as the 2/9 power of acceleration. For the 1-inch diameter sphere, the minimum and maximum heat fluxes were proportional to the 1/4 power of acceleration and were increased with subcooling and increased pressure. Nucleate boiling, within the uncertainty of the measurements, was not affected by variations in acceleration, pressure, or subcooling.

Technical Report No. 3

INCIPIENT BOILING OF CRYOGENIC LIQUIDS

K. J. Coeling, J. A. Clark, H. Merte, Jr., and E. R. Lady

Abstract

The purpose of this work was to determine the heat flux and surface superheat necessary to initiate nucleate boiling, i.e., form the initial vapor, on a flat surface heating into a pool of saturated liquid hydrogen. Some incipient boiling data were also obtained with liquid nitrogen, used to check out the system. Natural convection and nucleate boiling heat transfer data were obtained with both liquids when the incipient boiling tests were conducted. The variables investigated are surface material, surface roughness, and orientations. The surface materials used are stainless steel, copper, Teflon, and a special surface consisting of a glass fiber web covered with epoxy cement. The stainless steel and copper surfaces were tested in both a polished and roughened condition. The orientations investigated are horizontal upwards, vertical, and horizontal downwards.

An instrumented test surface was placed in the cryogenic liquid and heated by a dc resistance wire heater. After steady state conditions were established, the heater power and surface superheat were measured and visual observations of the surface made. The visual observations were to determine if vapor was being formed and, if so, the pattern of the boiling. The heater power was then stepped to a new value, steady state conditions established, and new measurements and observations made.

Natural convection and nucleate boiling heat transfer data from surfaces heating upwards and vertically in liquid hydrogen are presented. The range of heat fluxes is from less than 10×10^{-3} watts/cm^2 to 1500×10^{-3} watts/cm^2. For liquid nitrogen, natural convection heat transfer data for surfaces heating upwards and downwards and nucleate boiling heat transfer data for surfaces heating upwards are presented. The range of heat fluxes is from 10×10^{-3} watts/cm^2 to $10{,}000 \times 10^{-3}$ watts/cm^2. The surface superheat and heat flux when the initial observable vapor was formed are reported for 15 combinations of surfaces, liquids and orientations. The surface superheats at the initial vapor point range from almost 0°K for an epoxy coated surface heating upwards in liquid hydrogen to over 6°K for a polished stainless steel surface heating upwards in liquid nitrogen.

During nucleate boiling of liquid hydrogen, the rate of heat transfer at a given surface superheat was as much as 25 times greater from a copper surface than from a stainless steel surface prepared in an identical manner. Over the

range of boiling heat fluxes investigated, the rate of heat transfer from a surface at a given surface superheat was greater when heating vertically than when heating upwards. When boiling liquid hydrogen, the roughest stainless steel surface tested required a larger surface superheat than a smoother stainless steel surface for a given heat flux. The smoothest stainless steel surface required the largest surface superheat. It is postulated that the liquid hydrogen wets the larger surface cavities. The roughest surface has many large cavities on it, so the wetting results in a number of potentially active sites being inactive and the surface superheat at a given heat flux increases.

The surface superheat and heat flux at which the initial vapor was observed to form on a given surface in a given orientation were reproducible to within $\pm 25\%$ of the average values. The initial vapor formation in liquid hydrogen and liquid nitrogen is primarily a function of the superheat and is not a strong function of orientation or heat flux. In general, the lower the surface superheat needed to form the initial vapor on a uniform surface, the lower the surface superheat at a given nucleate boiling heat flux.

Technical Report No. 4

FINITE DIFFERENCE SOLUTION OF STRATIFICATION AND PRESSURE RISE IN CONTAINERS

H. Merte, Jr., J. A. Clark, and H. Z. Barakat

Abstract

The processes of heat and mass transfer interactions between the gas and liquid phases of a single component in cylindrical containers with axial symmetry are considered. In the general formulation attention is given to the cases of external pressurization with and without liquid discharge as well as to the nonvented condition. The governing equations are cast into finite-difference form and numerical computations are carried out for the case of a nonvented container having an imposed head flux, using ideal gas relations for the vapor properties. Of specific interest is the calculation of the pressure-time history of the container under these conditions.

Technical Report No. 5

FINITE DIFFERENCE CALCULATION OF PRESSURE RISE IN SATURN S-IVB FUEL TANK

H. Merte, Jr., C. C. Suh, E. R. Lady, and J. A. Clark

Abstract

The pressure rise of a two-phase system in a closed container subject to an external heat flux is related directly to the temperature of the liquid-vapor interface, which in turn depends on the heat and mass transfer interactions between the liquid, vapor, and container. The problem is formulated here for a cylindrical tank with an axial body force and a symmetrically imposed external heat flux in terms of the transport equations. The temperature and velocity distributions are determined using a finite-difference method, which is coupled with an integral form of the energy equation to determine the pressure rise. The procedure adopted takes into account the possibility of incipient and nucleate boiling.

Numerical computations are carried out for liquid hydrogen in a large, partially filled tank under low gravity. This system models the one orbital experiment conducted to date which provides the only available experimental data. These are the data on pressure rise and system temperature telemetered from a Saturn LH_2 tank orbiting the earth, the AS-203 low gravity orbital experiment. A discussion of the modeling is included.

The numerical computations are carried out for various distributions of heat flux between the liquid and vapor, and with various container wall properties. The outputs of major interest are the pressure rise, and temperature and velocity distributions. Representative plots of the isotherms and streamlines are included.

The computations indicate that even though the container walls constitute an insignificant portion of the total heat capacity, less than 1% that of the liquid and vapor, variation of the wall heat capacity has a significant influence on the pressure rise rate. During a portion of the process, it is found that radial as well as axial stratification exists, with simultaneous evaporation and condensation occurring at various locations on the liquid-vapor interface.

Technical Report No. 6

FILM BOILING ON VERTICAL SURFACES IN TURBULENT REGIME

N. V. Suryanarayana and H. Merte, Jr.,

Abstract

The purpose of this study was to (i) determine the local heat flux values in film boiling in a saturated liquid on a plane vertical surface in the turbulent regime, (ii) extend the region of laminar vapor flow through the use of a drop tower, (iii) gain an understanding of the nature and influence of liquid-vapor interfacial oscillations on heat transfer rates, and (iv) model and analyze the phenomenon of film boiling on a vertical surface to predict heat transfer rates as a function of height and surface superheat.

The variables studied in the determination of the local heat flux values were the height of the heating surface and heater surface superheat in two cryogenic liquids, nitrogen, and hydrogen. To avoid edge effects in a finite plane vertical surface, cylindrical heating surfaces were used. Heat flux values at 11 locations over a total height of 6 in. at four values of surface superheat were determined, employing a transient technique. A warm cylindrical heating surface with thermally insulated instrumented sections was immersed in the cryogenic fluid, inducing film boiling, and the rate of cooling was recorded. From this rate of cooling and properties of the test sections, heat transfer rates were computed.

The region of laminar vapor film was extended by reducing gravity forces in a drop tower. Local heat flux values at six locations in a height of 4 in. were determined for one value of surface superheat each in liquid nitrogen and liquid hydrogen at $a/g \cong 0.008$. Additional heat flux values were obtained under subcooled conditions.

Motion pictures of film boiling on a vertical cylindrical surface in liquid nitrogen were taken at four different heights of the surface and three values of surface superheat. Analyses of these motion pictures indicating the variation of vapor film thickness as a function of time, and the extent of interfacial oscillations, are presented.

Film boiling was modelled on the assumption that the universal velocity profile of Spalding is valid everywhere in the vapor region. It is shown that interfacial oscillations increase heat transfer rates and the effect of such increase is taken into account in the solution of the resulting equations. Solutions are presented based on the effect of such oscillations being constant at all heights and also considering the variation of the extent of interfacial oscillations.

The data presented show an initial decrease in the heat flux with height and a gradual increase after reaching a minimum value. These experimental values show considerable deviation, both quantitatively and qualitatively, from the laminar analysis predictions of heat transfer rates. These departures are explained on the basis of onset of turbulence and interfacial oscillations. The solution to the set of equations taking these effects into account are shown to predict heat transfer rates within $\pm 15\%$ in the turbulent regime. The heat transfer rates under reduced gravity forces show the same behavior as laminar predictions but are consistently higher.

REFERENCES

1. Merte, H., et al., "Finite Difference Calculation of Pressure Rise in Saturn S-IVB Fuel Tank," Technical Report No. 5, Report 07461-39-T, Department of Mechanical Engineering, Heat Transfer Laboratory, The University of Michigan, Contract NAS-8-20228, April, 1969.

2. Coeling, K., et al., "Incipient Boiling of Cryogenic Liquids," Technical Report No. 3, Report 07461-28-T, Department of Mechanical Engineering, Heat Transfer Laboratory, The University of Michigan, Contract NAS-8-20228, December, 1967.

3. Lewis, E., et al., "Boiling of Liquid Nitrogen in Reduced Gravity Fields with Subcooling," Technical Report No. 2, Report 07461-20-T, Department of Mechanical Engineering, Heat Transfer Laboratory, The University of Michigan, Contract NAS-8-20228, May, 1967.

4. Johnson, V. J., "A Compendium of the Properties of Materials at Low Temperature (Part II)," WADD Technical Report 1960.

5. Martin, D. L., "Specific Heat of Copper From 20° to 300°K," Can. J. Phys. 37, 17-24 (1960).

6. Duckerty, S. M., "On the Specific Heat of Copper From 78° to 0°C," Can. J. Res. 9, 84-95, 1933 and 15A, 59-66 (1937).

7. Giaugue, W. F., and Meads, P. F., "The Heat Capacities and Entropies of Aluminum and Copper From 15° to 300°K," J. Am. Chem. Soc. 63, 1897-1901 (1941).

8. Furukawa, G. T., et al., "Critical Analysis of the Heat-Capacity Data of the Literature and Evaluation of Thermodynamic Properties of Copper, Silver and Gold From 0° to 300°K," NSRDS-NBS 18 (1968).

9. Merte, H., and Clark, J. A., "Boiling Heat Transfer with Cryogenic Fluids at Standard, Fractional and Near-Zero Gravity," Trans. ASME, J. Heat Transfer 86C, 351-359 (1964).

10. Noyes, R. C., "An Experimental Study of Sodium Pool Boiling Heat Transfer," Trans. ASME, J. Heat Transfer 85C, 125-131 (1963).

11. Berenson, P. J., "Film Boiling Heat Transfer From a Horizontal Surface," Trans. ASME, J. Heat Transfer 83C, 351-358 (1961).

12. Drayer, D. E., and Timmerhaus, K. D., "An Experimental Investigation of the Individual Boiling and Condensing Heat Transfer Coefficients for

Hydrogen," Advances in Cryogenic Engineering, Vol. 7, Plenum Press, 401-412 (1962).

13. Astruc, J. M., Lacaze, A., and Perroud, P., "Comparison of Heat Transfer to Hydrogen, Deuterium, and Neon Boiling with Free Convection at Atmospheric Pressure," Cryogenics, Vol. 9, No. 4, 248-250, August, 1969.

14. Roubeau, P., "Heat Exchanges in Nitrogen and Hydrogen Boiling Under Pressure," Proceedings of 10th Internation Congress of Refrigeration; Progress in Refrigeration Science and Technology, Vol. I, Edited by M. Jul and A.M.S. Jul, Pergamon Press, 1960.

15. Pomerantz, M. L., "Film Boiling on a Horizontal Tube in Increased Gravity Fields," Trans. ASME, J. Heat Transfer, Vol. 86, No. 2, 213-219, May, 1964.

16. Suryanarayana, et al., "Film Boiling on Vertical Surfaces in Turbulent Regime," Technical Report No. 6, Report 07461-50-T, Department of Mechanical Engineering, Heat Transfer Laboratory, The University of Michigan, Contract NAS-8-20228, September, 1970.

17. Littles, J. W., and Walls, H. A., "Nucleate Boiling of Freon 113 at Reduced Gravity Levels," ASME Paper 70-HT-17. Proceedings of Symposium "The Role of Nucleation in Boiling and Cavitation," ASME Joint Fluid Mechanics and Heat Transfer Conference, Detroit, Michigan, May 25-27, 1970.

18. Sherley, J. E., "Nucleate Boiling Heat Transfer Data for Liquid Hydrogen," Advances in Cryogenic Engineering, Vol. 8, K. D. Timmerhaus, Editor, Plenum Press, 495-500 (1962).

19. Hsu, Y. Y., "On the Size Range of Active Nucleation Cavities on a Heating Surface," Trans. ASME, J. Heat Transfer 84C, 3, 207-216 (1962).

20. Hall, J. A., "The International Temperature Scale," Temperature, Vol. 2, Reinhold Publishing Co., N.Y., 115-139 (1955).

21. McAdams, W. H., "Heat Transmission," 3rd Ed., McGraw-Hill Book Co. (1950).

22. Papell, S. S. and Faber, O. C., Jr., "Zero- and Reduced-Gravity Simulation on a Magnetic-Colloid Pool-Boiling System," NASA TN D-3288, 17 pp., February, 1966.

23. Elrod, W. C., Clark, J. A., Lady, E. R., and Merte, H., "Boiling Heat Transfer Data at Low Heat Flux," Trans. ASME, J. Heat Transfer, Vol. 89, Series C, No. 3, August, 1967, pp. 235-243.

DISTRIBUTION LIST

(One Copy Unless Otherwise Specified)

NASA/Marshall Space Flight Center
Huntsville, Alabama 35812
Attn: Contracting Officer
(A&TS-PR-RS)
Attn: Technical Library
(A&TS-MS-IL)
Attn: Security Office
(A&TS-MS-S)
Attn: Technology Utilization
(A&TS-TU)
Attn: Mr. Dale Burrows
(S&E-ASTN-PJ)
Attn: Dr. J. W. Littles (3)
(S&E-ASTN-PL)
Technical Manager
Attn: Mr. L. Hastings
(S&E-ASTN-PFA)

NASA/Assistant Director for Propulsion
OART, Code RP
Washington, D.C. 20546
Attn: Mr. A. O. Tischler
Attn: Dr. Robert Levine (2)
Attn: Mr. Ward Wilcox

NASA/Lewis Research Center
21000 Brookpark Road
Cleveland, Ohio 44135
Attn: Mr. Irvin Johnsen

Scientific and Technical Information Facility
P. O. Box 5700
Bethesda, Maryland 40014
Attn: NASA Representative, Code CRT

Jet Propulsion Laboratory
Liquid Propulsion Section
4800 Oak Grove Drive
Pasadena, California 91103
Attn: Mr. Robert Rose

NASA/Manned Spacecraft Center
Houston, Texas 77058
Attn: Mr. Cecil Gibson, Code EP2

Mr. Fred O. Briggson
ONR Resident Representative
121 Cooley Building
The University of Michigan
Ann Arbor, Michigan 48105

Mr. K. R. Collins, Assistant Program Manager
Building 2025, Department 9800
Aerojet Liquid Rocket Company
P. O. Box 13222
Sacramento, California 95813

Mr. James E. Halo, Project Engineer
Mail Code AA72
Rocketdyne, North American Rockwell Corporation
6633 Canoga Avenue
Canoga Park, California 91304

Mr. William Cresleine
P. O. Box 2691 - FRDC
Pratt & Whitney Aircraft Division
United Aircraft Corporation
West Palm Beach, Florida 33402

Space Division
North American Rockwell Corporation
12214 Lakewood Boulevard
Downey, California 90241
Attn: Mr. B. Hello, Vice President
Corporate Wide General Manager
Space Shuttle Program

McDonnel Douglas Astronautics Company
P. O. Box 516
St. Louis, Missouri 63166
Attn: Mr. Sherman L. Hislop
Director of Booster/Orbiter Integration

CCSD, Michoud Operation
P. O. Box 29200
New Orleans, Louisiana 70129
Attn: Mr. C. E. Tharrott, Dept. 2760

DISTRIBUTION LIST (Concluded)

Grumman Aerospace Corporation
Plant 25 - Space Shuttle
Bethpage, L.I., New York 11714
Attn: Mr. Fred Raymer

Lockheed Missile and Space Company
P. O. Box 504
Sunnyvale, California 94088
Attn: Mr. John Lloyd, Manager
Alternate Space Shuttle
Concept Study
Dept. G1-51-Building 538

Space Division
North American Rockell Corporation
12214 Lakewood Boulevard
Downey, California 90241
Attn: Mr. Joe Monroe

The Boeing Company
P. O. Box 1470
Huntsville, Alabama 35807
Attn: Maxie Brown (Space Shuttle)